DOI:10.14753/SE.2023.2830

AXONAL PROPERTIES UNDERLYING SIGNAL TRANSMISSION MODULARITY IN THE PRIMATE SOMATOSENSORY CORTEX

PhD thesis

Mohd Yaqub Mir

János Szentágothai Doctoral School of Neurosciences

Semmelweis University

Supervisor: László Négyessy, Ph.D

Official reviewers: Péter Buzás, Ph.D
Gergely Zachar, Ph.D

Head of the Complex Examination Committee: Alán Alpár, DSc

Members of the Complex Examination Committee: Hájos Norbert, Ph.D
Réthelyi Miklós, Ph.D

Budapest

2023

DOI:10.14753/SE.2023.2830

Table of Contents

DOI:10.14753/SE.2023.2830

DOI:10.14753/SE.2023.2830

List of Abbreviations

AAV	Adeno associated virus
ABC	Avidin biotin complex
aIC	Anterior insular cortex
BA	Brodmann area
BA1	Brodmann area 1
BA2	Brodmann area 2
BA3a	Brodmann area 3a
BA3b	Brodmann area 3b
BDA	Biotinylated dextran amine
CS	Central sulcus
cRF	Classical receptive field
D2-D4	Finger d2 to d4 (d: digits)
DCN	Dorsal column nuclei
DRG	Dorsal root ganglion
ECG	Electrocardiogram
ecRF	Extra classical receptive field
EEG	Electroencephalogram
fMRI	functional Magnetic Resonance Imaging
IACUC	Institutional Animal Care and Use Committee
INs	Interneurons
IOS	Intrinsic signal optical imaging
J	Case Joulie
LRGNs	Long range GABAergic neurons
M	Case Maria
M1	Primary motor cortex
ML	Medial-Lateral
Mac	Case Mac
Mo	Case Moh
MD	Mediodorsal thalamus
NIH	National Institutes of Health
NP	No-patch
NiDAB	Nickel-intensified diaminobenzidine

DOI:10.14753/SE.2023.2830

P	Patch
Pe	Case Pecos
PB	Phosphate buffer
PC	Pacinian corpuscle
PCs	Pyramidal cells
PPC	Posterior parietal cortex
RA	Rapidly adapting
RF	Receptive field
RV	Rabies virus
S1	Primary somatosensory cortex
S2	Secondary somatosensory cortex
SA	Slowly adapting
SD	Standard deviation
SN	Salience network
SpO2	Oxygen saturation
TX	TritonX-100
V	Case Vivian
V1	Primary visual cortex
V2	Secondary visual cortex
VIP	Vasoactive intestinal polypeptide
VP	Ventroposterior nucleus
VPL	Ventroposterior lateral nucleus
VPM	Ventroposterior medial nucleus

DOI:10.14753/SE.2023.2830

1. Introduction

1.1. Overview of the primary somatosensory cortex (S1) and the approaches of exploring neuronal circuitries

1.1.1. The primary somatosensory cortex (S1)

In the primary somatosensory cortex (S1) of primates and carnivores (for example monkeys and cats) electrophysiological recordings have shown that BA3b and BA1 contain a separate representation of the body surface (Kaas, 1983). The two representations are parallel and mirrored in somatotopic organisation, so that each runs medially from the tail to the lateral representation of the tongue. Both represented the same skin surfaces along the common boundary and had similar representational sequences in rostral and caudal directions away from the common boundary (Kaas, 1983). BA3b and BA1 are connected mutually in an asymmetric way. Neurons in BA3b project densely to layers III and IV of area 1; BA1 in turn sends a projection back to area 3b, mainly to layer I (Kaas, 1983). This pattern is reminiscent of the hierarchical organisation of these areas with area BA3b serving an important source of information for area 1 via feed-forward connections whereas area 1 sends feedback to BA3b, similar to the pattern of connections between visual cortical areas such as primary visual cortex (V1) and secondary visual cortex (V2) in primates (Kaas, 1983; Ts'o et al., 2001). As might be expected, the representations of the same body parts in BA3b and BA1 are reciprocally connected. Thus, when microelectrode recordings used to identify the representations of digit tips in BA3b and BA1, and injections of different anatomical tracers made at each site, it became clear that neurons representing digit tips in BA1 projected to digit tips in BA3b, and that BA1-digit tip in turn projected to BA3b-digit tip (Figure 1) (Kaas, 1983).

DOI:10.14753/SE.2023.2830

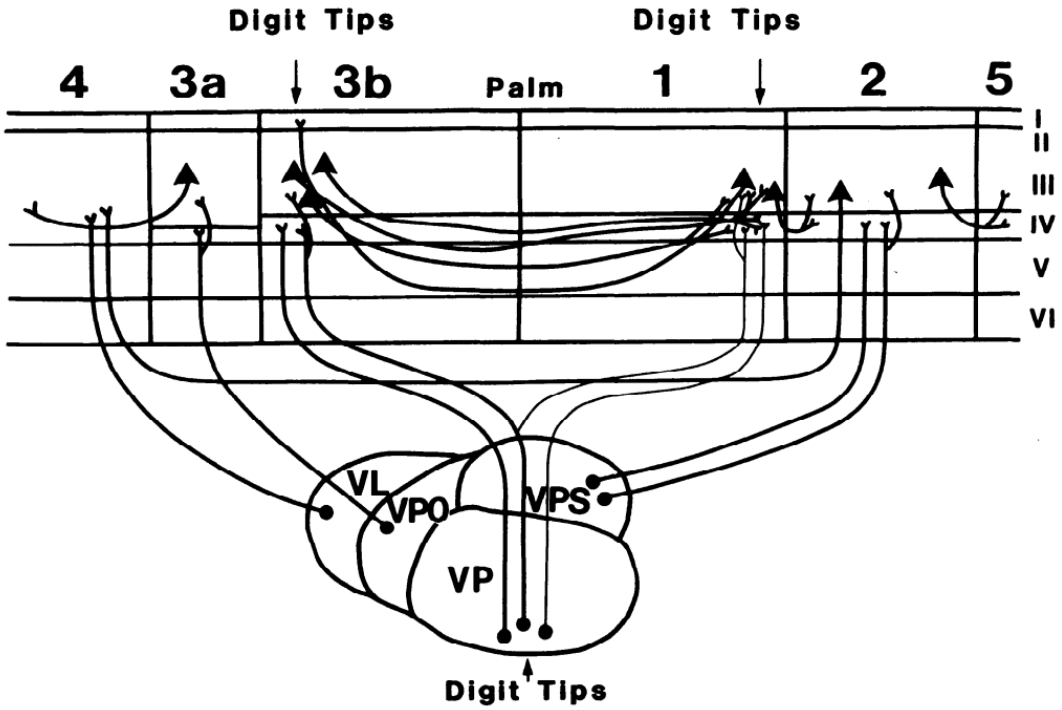

Figure 1. Connections of cortical areas 3a, 3b, 1, and 2 in monkeys.

Areas 3b and 1 receive separate patterns of inputs from a single thalamic nucleus, the ventroposterior (VP) nucleus. There is no generally accepted terminology for the separate thalamic regions projecting to area 3a and area 2. The terms ventroposterior superior (VPS) and ventroposterior oral (VPO) are suggested. Motor cortex divided into rostra1 and caudal representations with somewhat different connections. VL, ventrolateral nucleus; I-VI at right are layers of cortex (adopted from Kaas, 1983).

An important feature of the cerebral cortex is its modular organisation (Szentágothai, 1975). Modules have been defined in various ways, and often the term is used interchangeably with the term cortical column (Kaas, 1993; Krubitzer and Hunt, 2007). The term cortical column was introduced in S1 and refers to the vertical arrangement of neurons with common response properties, such as the location of receptive fields (RFs) in sensory cortices (Mountcastle, 1957, 1997). The best-known example of columnar organisation is the cortical barrel field, a subregion of face representation in S1, which in rodents consists of separate representations of the individual whiskers (Woolsey and Van der Loos, 1970). Similarly, in primates, representations of body parts, including digits, consist of multiple cortical columns (Kaas, 1979; Sur et al., 1983; Mountcastle, 1984) (Figure 2). It is noteworthy that the columns in the somatosensory cortex of primates exhibit different sensitivity to different kinds of tactile stimuli (Kaas et al., 1979).

DOI:10.14753/SE.2023.2830

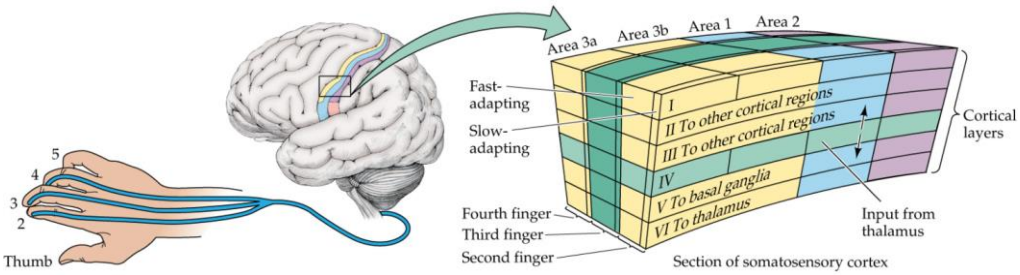

Figure 2. Basic organisational principles of the somatosensory cortex

The part of the somatosensory cortex shown here represents three fingers of the right hand in the different regions of the somatosensory cortex. Brodmann's areas 3a, 3b, 1, and 2 receive their main inputs from different kinds of receptors of the skin (fast and slow adapting, see later). Area 3a receives input from receptors in the muscle spindles. The cortex is organised vertically in columns and horizontally in layers. Input from the thalamus arrives at layer IV, where neurons distribute information up and down layers (adopted from Kaas et al., 1979).

In S1 of non-human primates (NHP), BA3b and BA1 are the first stages of cortical integration of tactile information from the fingers (BA3b: Iwamura 1983a; Chen et al. 2003; Friedman et al. 2008 BA1: Mountcastle and Powell 1959; Sur et al. 1980, 1982, 1985; Iwamura et al. 1983b; Sinclair and Burton 1991). Lateral cortical interactions play an essential role in the integration of sensory information by connecting different sensory representations and cortical columns (Gilbert and Wiesel 1989; Lund et al. 1993; Buzás et al. 2006). However, in S1, the organisation of lateral connectivity is poorly understood. In visual cortex, hierarchical structure plays an important role in the spatial organisation of RFs through the spatial organisation of horizontal connections including ascending (feedforward; FF) and descending (feedback; FB) connections in addition to those intrinsic to an area (Harrison et al. 2007; Bardy et al. 2009; Jeffs et al. 2009). FF connections are the dominant connections in shaping the properties of the classical receptive field (cRF), while FB and intrinsic lateral connections are the dominant connections in shaping the extra classical receptive field (ecRF) properties (Angelucci and Bressloff 2006). Accordingly, different cortical connections have a different lateral or horizontal extent: FF connections are spanning over a smaller cortical area than intrinsic and FB connections, which span over a larger cortical area (Angelucci and Bressloff 2006; Jeffs et al. 2009).

The limited spatial distribution of connections suggests that the interaction of different hierarchies occurs between delimited populations of neurons representing the mesoscopic level of cortical organisation. The functional significance of mesoscale connectivity supported by high-resolution fMRI experiments showing that interactions between visual cortical areas rely on small regions of similar size (Harvey and Dumoulin 2011). In the visual cortex of higher order mammals (cats, monkeys), the clustered distribution of connectivity is well known. V1 and V2 show a modular structure in their intra- and inter-areal connections (Gilbert and Wiesel 1989; Lund et al. 1993; Buzás et al. 2006; Jeffs et al. 2009; Markov et al. 2014; Rockland 2015). It was evident that the neurons forming intra-areal and inter-areal connections showed stronger clustering in V1 than in V2 (Gilbert and Wiesel 1989; Jeffs et al. 2009; Negwer et al. 2017). A similar observation was made in S1 of the squirrel monkey, where retrogradely labelled intra- or inter-areal neurons show a stronger tendency of clustering in BA3b than in BA1 (Pálfi et al, 2018). Remarkably, in primates, anterograde labelling of axons compared to retrograde labelling results in a more distinct and characteristic horizontal pattern that is spatially clustered and forms the so-called patchy organisation or patch domain of axon termination (Rockland and Lund, 1982). In contrast, no-patch domains are formed by long-range lateral projections that terminate in patches and do not exhibit any obvious grouping (Pálfi et al, 2018). In primates, these two domains are present in grey matter in all cortical areas (Lund, et al., 1993; Nicole Voges et al., 2010). However, despite the widespread existence of these two axonal domains across species and cortical areas, their role in signal transduction is unclear. In summary, the population-level connectivity, more specifically the lateral axonal meshwork is essential for understanding the integrative functions of the cortices.

1.1.2. Exploring neuronal connectivity

In our study of the axonal connections in non-human primates (NHP), we applied biotinylated dextran amine tracing, which labels axonal processes with high detail (Lanciego et al., 2012). Biotinylated dextran amine (BDA) is a highly sensitive tracer for anterograde and retrograde pathway studies of the nervous system. BDA can be reliably delivered into the nervous system by iontophoretic or pressure injection and visualized with an avidin-biotinylated (ABC) reaction. For example, high molecular weight BDA (10k) yields sensitive and exquisitely detailed labeling of axons and terminals, whereas low molecular weight BDA (3k) yields sensitive and detailed retrograde labeling of

neuronal cell bodies and dendritic processes. However, in spite of their preferred direction of spread, traditional tracers including BDAs are transported both in the anterograde and retrograde directions (Reiner et al., 2000).

In contrast to BDA and other traditional tracers, recent advancement in the application of neurotropic viruses allows the investigation of the neuronal circuits with unprecedented specificity. The use of a virus as a self-replicating tracer to track brain circuits is known as viral neuronal tracing (Luchicchi et al., 2021). Neurotropic viruses, e.g. rabies (RV) and adeno associated (AAV), which can infect the nervous system, travel among spatially adjacent clusters of neurons through synapses, making it possible to employ them to study functionally related neural networks (Ugolini and Gabriella, 2010; Koyuncu et al., 2013). One of the greatest advantages of viral tracing is its neuronal specificity. With the aid of genetic modifications viruses can be made highly specificity to certain neuronal types, which makes them an effective tool to map specific subcircuits (Saleeba et al., 2019). Viral tracers (AAVs) that remain locked within the targeted cell population are usually replication-deficient. The other vectors (RVs) spread through linked circuits via trans-synaptic travel are always replication-competent. Each class contains vectors that can be used to label selectively in an anterograde or retrograde direction (Boldogköi et al., 2004; Lerner et al., 2016; Jia et al., 2017; Farmer et al., 2019; Saleeba et al., 2019). Neuroscientists widely adopted the recombinant viral vectors that drive the expression of fluorescent “reporter” proteins in transduced neurons because of their directional specificity, the high (in most cases permanent) levels of reporter expression obtained. (Callaway, 2005; Luo et al., 2008; Betley and Sternson, 2011; Nassi et al., 2015). In addition, genetically modified viruses (AAVs) can be used as vectors for modifying neuronal phenotypes for research or clinical purposes. Most notably, viral vectors are essential tools in optogenetic studies of specific neuronal connections (Saleeba et al., 2019).

It was shown that during anterograde tracing, both AAV and BDA labeled the bundles of fibre tracts and surrounding axon branches projecting into the gray matter. However, more axon branches were labeled in the AAV injections as compared with those in the BDA injections. This suggests that AAV exhibits more superior performance in axon tracing in comparison with BDA, and can be applied as a better neural tracer for the morphological study, for example in case of reconstruction of terminal axonal arbors, parent neurons and related neural circuits (Qiu et al., 2002). Another advantage of viral

tracing over traditional molecular tracing is the ease of double or multiple labelling that opens up the possibility of determining close appositions representing probable synaptic contacts (Saleeba et al., 2019, Reiner et al., 2000). However, while viruses are highly compatible with rodent studies, its use in primate studies including tract tracing, is still limited due to species specific difficulties for example widespread axonal loss and neuronal cell death in the macaque brain (Yan et al., 2022). Therefore, another objective of my studies was to investigate the specificity of connections formed by certain types of neurons namely vasoactive intestinal polypeptide expressing interneurons (VIP + INs) in the rodents.

1.2. Neurobiology of tactile perception

1.2.1. Tactile submodalities

The sense of touch and proprioception are relying on mechanotransduction, the processing of mechanical deformations of tissues (skin, muscles, tendons and ligaments) into neural signals (Darian-Smith, 2011). Cutaneous mechanoreceptors signal on contact with objects, while proprioceptors are located in deep tissues including muscles, tendons and ligaments (in the skin as well) to import information about the position and movement of the limbs and the forces they exert (Johnson, 2001). Nerve fibres or sensory afferents innervate the different types of receptors and transmit the tactile and proprioceptive signals to the central nervous system (CNS) (Johnson and Vallbo, 1976). Most tactile and proprioceptive fibres are large and myelinated and therefore exhibit rapid velocity transmission (Johnson, 2001). Different types of cutaneous mechanoreceptors and proprioceptors respond in different ways to mechanical deformation and transmit complementary information about limb state or object features (Mountcastle, 2011). The coupled signals from these receptors provide a detailed neural picture of the state of our body and our immediate environment, including objects (Mountcastle, 2011). Skin mechanoreceptors, which convert skin deformations into electrical signals, are located throughout the body, but their density varies depending on the region of the body. In primates, the hands are the most important receptive body parts and are fundamental for tactile perception (Johansson and Vallbo, 1976).

The conversion of mechanical stimuli into neuronal activity begins with four well-characterised peripheral receptors in the glabrous skin of the hand, two of which occupy the superficial regions of the skin and the other two the deeper tissue (Table 1) (Weber et

al., 2013; Saal and Bensmaia, 2014). The receptors, together with the sensory afferents innervating them, form the psychophysical tactile channels. (Bolanowski et al., 1988). The four psychophysical channels (Pacinian, non-Pacinian I, non-Pacinian II and non-Pacinian III) could be identified by their physiological substrate. Microneurographic recordings from nerves innervating the glabrous skin of the human hand have revealed four groups of low-threshold mechanoreceptive afferents: (a) rapidly adapting (RA); (b) type I slowly adapting (SAI); (c) type II slowly adapting (SAII); and (d) Pacinian (PC) (Johansson and Vallbo, 1979; Vallbo and Johansson, 1984). These channels partially overlap in their absolute sensitivity, so it is likely that supra-threshold stimuli can activate two or more of the channels simultaneously. The perceptual qualities of touch thus may be determined by the combined inputs of four channels (Bolanowski et al., 1988). In addition to different rates of adaptation in the responses to pulse-like mechanical stimuli, the fibre types have other functional properties, which allow them to be divided into four categories. PCs and SAIIs, for example, have large RFs with no clear boundaries, while RAs and SAIs have smaller RFs (Johansson, 1976, 1978). Furthermore, the different fibre types appear to have different capacities to respond to specific frequency ranges of vibrational stimuli, as demonstrated by the tuning properties of isoresponsive contours (Johansson et al., 1982a).

Table 1. Summary of mechanoreceptors and their primary afferents

Afferents	Receptor	Submodality, role in tactile perception
SAI	Merkel cell	Pressure, form, texture
RA	Meissner corpuscle	Flutter, motion
SAII	Ruffini corpuscle	Possibly skin stretch, proprioception
PC	Pacinian corpuscle	High frequency vibration

Superficial mechanoreceptors, the receptors that respond to a light touch on the skin (Figure 3A and B, upper part). These include the Meissner corpuscles with RA responses and the Merkel discs with SA type 1 (SAI) responses (Johansson and Vallbo, 1983). The RA axons that terminate in the Meissner corpuscles are responsible for sensing localized movements along the skin, especially slip mediated by somatosensory feedback when grasping objects. Comparisons of the physiology and human psychophysics of RA afferents show that these receptors are responsible for the ability of humans to perceive low-frequency vibrations, a sensation known as flutter (Talbot et al., 1968). An important function of the RA channel is to adjust grip strength while lifting the object. The RA afferents respond with a brief burst of action potentials when objects move a small

distance in the hand during an early phase of lifting (Westling and Johansson, 1987). In response to the RA afferent activity, the motor system is able to adjust the force level through the spinal reflex until the grasped object stops moving.

The second type of superficial receptors, the Merkel discs, innervated by SA type 1 (SAI) afferents. The SAI pathway is responsible for the perception of shape and texture (Johnson and Hsiao, 1992). Merkel discs are present in high density on the fingers (and around the mouth), in lower density on other glabrous surfaces and in very low density in hairy skin. The density of innervation decreases with age. The SAI afferents show low-threshold and sustained responses to light stimuli. In contrast to the RA afferents, the SAI fibres respond not only to initial indentation of the skin, but also to sustained indentation lasting up to several seconds. The RFs of the individual SAI axons exhibit maximum sensitivity at several points, referred to as hot spots (Phillips and Johnson, 1981). Because the SAI afferents are particularly sensitive to local skin curvature, they respond best to the edges of objects pressed into the skin (Phillips and Johnson, 1981; Burges et al., 1982; Edin and Abbs, 1991).

The deep mechanoreceptors of the skin include two distinct classes, the Pacinian corpuscle and the Ruffini terminals, which produce fast and slow adaptive responses to mechanical stimuli, respectively. (Figure 3A and B, lower part). The Pacinian afferents are extremely sensitive to minute movements of the skin, leading to the perception of high-frequency vibrations. The Pacinian afferents have very large RFs, usually covering several digits and in some cases the entire hand. The sensory axons in the Ruffini corpuscles, called SAII afferents, show responses to lateral movements or stretching of the skin, usually in one direction. Their RFs are large, diffuse and sensitive to limb and finger movements (Burges et al., 1982; Torebjork et al., 1987; Edin and Abbs, 1991).

DOI:10.14753/SE.2023.2830

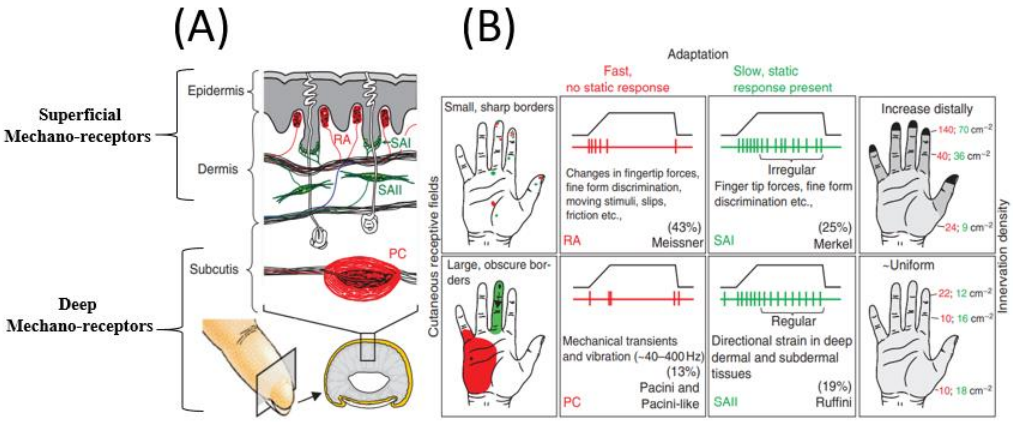

Figure 3. The four classes of cutaneous afferents of the glabrous skin.

(A) Morphology of the different mechanoreceptors and their respective locations in the skin. (B) Adaptation properties and RF size of the four classes of cutaneous afferents. RA (sometimes referred to as fast adapting, particularly for humans) versus SA refers to responses to indentations (transient vs. sustained, respectively). Type I (superficial) versus type II (deep) refers to the size of the RFs, determined in part by the depth of the mechanoreceptors in the skin: Type I fibres have small RFs whereas type II fibres have large ones (adopted from Johansson and Flanagan, 2008).

1.2.2. Central somatosensory pathways

The information from each class of mechanoreceptors reaches a particular group of neurons in the central nervous system (CNS) via parallel ‘labelled lines', resulting in a topographical somatotopic organisation that corresponds to the peripheral arrangement of afferents. The ‘labelled lines’ organisation also results in submodality segregation, in which different types of afferents address different populations of neurons. This is the mechanism by which neurons responsible for different sensations form separate pathways in and through the CNS. Such division begins in the peripheral nerves and continues as the spinal root axons enter the spinal cord (Figure 4) (Brown, 1981; Eric Kandel, 2016). The central afferents of the dorsal root ganglion (DRG) neurons take two distinct routes (Mountcastle, 1984). Focusing only on fine tactile functions, the medium- and large-diameter axons, which, when ignoring pain, transmit fine tactile and proprioceptive signals, respectively, enter various laminae of the grey matter of the dorsal horn and also ascend into the gracile and cuneate fasciculi (the dorsal columns) of the white matter. Axons in the dorsal columns include not only the primary axons of the dorsal root, but

also the postsynaptic axons of the dorsal column (Mountcastle, 1984). By way of the dorsal column, somatosensory input is carried to the gracile and cuneate nuclei (dorsal column nuclei) (DCN) of the lower medulla, where according to the labelled line principle, submodality segregation and somatotopy is maintained. Neurons in the DCN in turn give rise to axons that cross the midline of the medulla and ascend in a bundle of fibres called the medial lemniscus. These terminate in the lateral subdivision of the ventroposterior nucleus (VPL) of the dorsal thalamus (Brown, 1981; Eric Kandel, 2016).

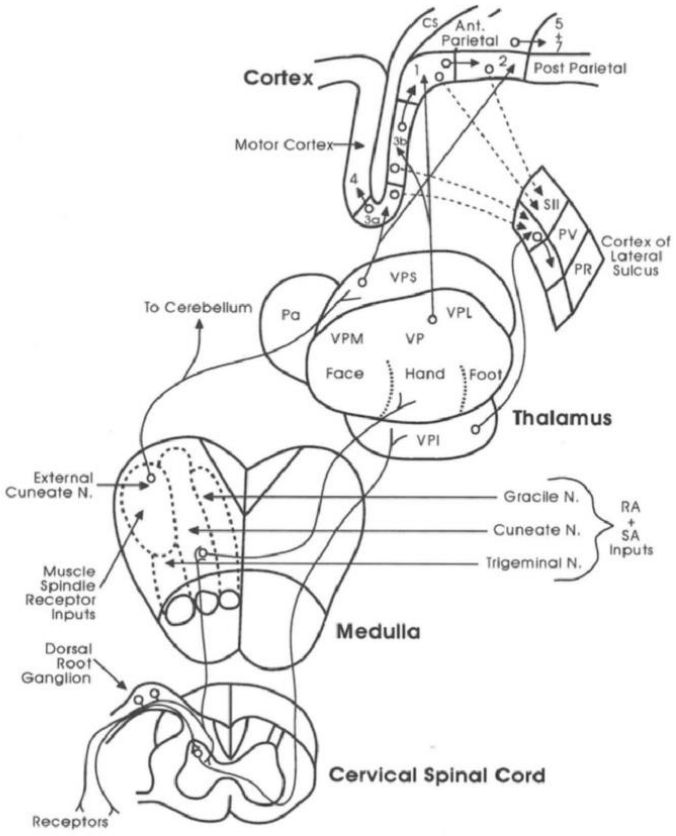

Figure 4. Somatosensory pathways from receptors to the spinal cord, medulla, thalamus and cortex.

Thick sections are shown of the spinal cord and medulla. The drawing of the somatosensory thalamus corresponds to a coronal brain section with medial to the left. Anterior (ant.) parietal cortex is from a parasagittal slice through the central sulcus (CS) in a macaque monkey. The second somatosensory area (S2), the parietal ventral area (PV) and the parietal rostroventral area (PR) form a caudorostral series on the upper bank of the lateral fissure along the lateral border of area 3b. N, nucleus; RA, rapidly adapting cutaneous afferent; SA, slowly adapting cutaneous inputs; VP, the ventroposterior nucleus with ventroposterior medial (VPM) and ventroposterior lateral

(VPL) divisions; VPI, ventroposterior inferior nucleus; VPS, ventroposterior superior nucleus; 3a, 3b, 1, 2, 4, 5 and 7, number of architectonic fields (adopted from Kaas et al., 1993).

The VPL is the principal thalamocortical relay nucleus for fine tactile information. It exhibits somatotopic and submodality specific organisation. Body parts such as a finger are represented by a group of neurons in a cylinder-like shape, which extends through the anteroposterior dimensions of VPL and the ventral posteromedial nucleus (VPM) (Mountcastle and Henneman, 1949, 1952; Rose and Mountcastle, 1959; Jones and Friedman, 1982; Kaas et al., 1984). Somatotopy is organised in the dorsoventral axis of these thalamic nuclei. Each cylinder represents the main region of the endings of axons arising from cells in the somatotopically related part of the main nuclei of the trigeminal nerve or dorsal column. (Mountcastle and Henneman, 1949, 1952). Regarding the segregation of submodalities, RA and SA inputs terminate on different cell groups within the core region of the VPL (Mountcastle and Henneman, 1949). Pacinian inputs and inputs originating from joints and muscles are confined to a shell region on the posterior, rostral, and anterior edges of the nucleus. Individual lemniscal axons arbourize in the sagittal plane to terminate on longitudinal cell clusters in the VPL (Rose and Mountcastle, 1959). Somatotopy and submodality specificity are also maintained in the thalamocortical connections between the VPL and S1 (Jones, 1997).

1.2.3. Primary somatosensory cortex of the primates

1.2.3.1. Areas and anatomical connections of S1

The S1 is located in the posterior bank of the central sulcus (CS) and on the crown of the postcentral gyrus along the anterior border of the parietal lobe. It is traditionally divided into anatomically distinct areas, designated as BA3a, BA3b, BA1 and BA2 (Sanides, 1970 and Jones, 1975; Kaas et al., 1979; Vogt, 1919; Kaas, 1996) (Figure 5A). Each area contains neurons responsive to the mechanical stimuli and each receives direct axonal connections from VPL that provides input originating from the skin of body and face. The precise source of those inputs varies, however, since few thalamic neurons send collaterals to two areas in S1 (Jones, 1983). As a result, the sensory response properties of neurons in one area differ noticeably from those of other areas (Jones, 1975).

In S1 of the primates (e.g. in macaque, squirrel monkeys), the cortical areas perform different functions (Kaas, 1983; Krubitzer and Baldwin, 2017). Neurons in BA3b and

BA1 are responsive to cutaneous inputs, both RA and SA (Kaas, 1983; Krubitzer and Baldwin, 2017). In contrast, BA3a and BA2 respond to deep stimuli, with BA3a being particularly responsive to muscle afferents and BA2 to both cutaneous inputs and muscle afferents (Kaas, 1983; Krubitzer and Baldwin, 2017). In each area, RFs are larger than those displayed by primary sensory axons but are nevertheless specifically RA-like, SA-like or Pacinian-like (Iwamura, 1998; Pack and Bensmaia, 2015).

Further evidence supporting the functional segregation of S1 comes from lesion studies. Lesioning BA3b revealed its crucial role in tactile discrimination based on the shape or texture of stimulus (Carlson, 1980). Removal or inactivation of this area leads to a severe deficit in all aspects of tactile sensibility that translates to a lack of appreciation in the quality or even the existence of tactile stimuli. Lesions of BA1 disrupt performance based on texture but leave intact performance based on the size of object. Lesions in BA2 show the opposite results (Randolph, Semmes, 1974). These findings indicate that BA3b is a conduit for all cutaneous sensibility, BA1 is specialised for the analysis of SAI and RA inputs related to texture perception and the BA2 integrates positional information with edge detection to form an accurate impression of the 3-dimensional shape of an object.

The areas of S1 are strongly connected and show a hierarchical relationship. The interconnectivity shows that BA3b projects to BA1 predominantly via horizontal intracortical fibres, but also projects less densely to BA2 and BA3a (Vogt and Pandya, 1978; Burton and Fabri, 1995), and receives projections from BA3a, BA1, and BA2 (Burton and Fabri, 1995; Coq et al., 2004). BA1 projects primarily to BA2, but is also reciprocally associated with BA3a and BA3b (Jones et al., 1978; Pons and Kaas, 1986; Burton and Fabri, 1995). Finally, BA2 projects mainly to posterior areas (BA5 and BA7), but also has connections to BA1, BA3a, and BA3b (Vogt and Pandya, 1978; Pons and Kaas, 1986). Hence, a strong and sequential outflow of connections from BA3b to BA1 and BA2 (Ruben et al., 2006), then from BA1 to BA2 and finally from BA2 to areas in the posterior parietal cortex (PPC), mainly BA5 and BA7, is observed. As a result, in non-human primates, BA3b has small and relatively simple/homogeneous RFs, while BA1 RFs were larger and more complex (i.e., multi-finger response; Hyvarinen and Poranen, 1978; Iwamura et al., 1980, 1993; Sur, 1980). This complexity of RFs suggests greater convergence of peripheral inputs in BA1 compared to BA3b (Iwamura, 1998; Ruben et al., 2006). Similarly, RFs for neurons in BA2 are typically larger than those in BA1, and

RFs affecting multiple fingers and joints are common. This suggests that the initial cortical processing of tactile discrimination occurs in BA3b, while BA1 is more involved in texture discrimination requiring integration of different aspects of tactile input, and BA2 in size and shape recognition (i.e., even more integrated signal). In contrast, BA3a is mainly dedicated to processing of proprioceptive signals (Jones and Powell, 1969; Phillips et al., 1971).

1.2.3.2. Functional organisation of S1

The most important feature of S1 is its somatotopic organisation, in which adjacent S1 neurons respond to stimulation of adjacent and partially overlapping skin sites on the body (Sur et al., 1980; Sur and Nelson, 1982; Kaas, 1982). (Figure 5B). As a result, S1 comprises four complete maps of the contralateral side of the body, one in each area, with the foot representations near the midline, the face and tongue representations at the lateral end (Kaas, 1996). Although the body maps are complete, they contain many distortions, the most dramatic of which are the greatly enlarged representations of the face and hand, particularly the digits. The fingers and lips regions of the body, which are more densely innervated, occupy more cortical area than less innervated regions such as the proximal arms or the back (Sur et al., 1980). At the same time, neurons receiving afferents from the fingers have much smaller RFs than the neurons with RFs on the back (Sur et al., 1980). The body maps in each S1 area are arranged in a logical order in relation to one another. As a result, the representation of each body part in each area is approximately aligned along the CS and the organisation along the axis perpendicular to the sulcus is also predictable and orderly. For example, proceeding caudally along the axis orthogonal to the CS, RFs in BA3b shift from the digit tips, down the digits, to the palm, where the transition into BA1 occurs. In turn, RFs in BA1 shift back toward the fingertips as one continues to proceed caudally towards BA2. The RFs of BA2 then shift back from the fingertips down the finger as one maintains course (Pons, 1985). The somatotopy in BA2 and BA3a is cruder than that in BA3b and BA1 (Iwamura, 1994)

DOI:10.14753/SE.2023.2830

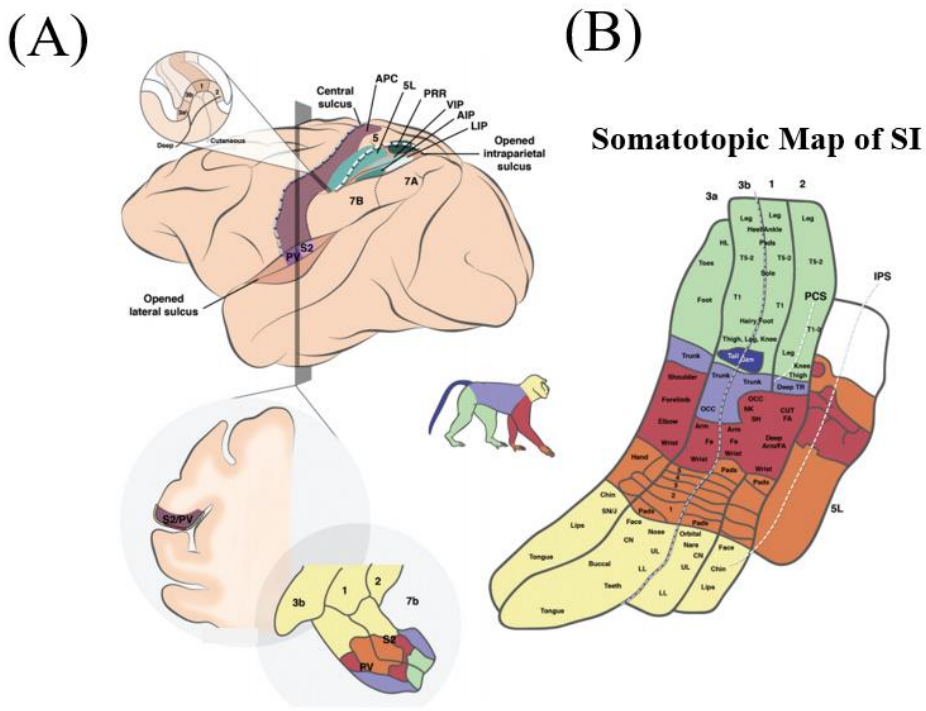

Figure 5. Organisation of somatosensory cortical areas of primates.

(A) A lateral view of the brain showing the different somatosensory areas in the macaque monkey cortex. Inset: Coronal section of the postcentral gyrus at the level of the hand representation, showing the position of the different S1 areas relative to the central and the intraparietal sulci. (B) Detailed view of the somatotopic representation of the body in the four fields of S1 (areas 3a, 3b, 1, and 2) and in area 5L. Somatotopic map: Upper lip (UL); lower lip (LL); chin (CN); snout/jaw (SN/J); digits of the hand (1-5); (cutaneous) forearm ((CUT) FA); occiput (OCC); trunk (TR); toes (T1-5); hind limb (HL) (adopted from Kaas et al., 2011).

In each area of S1, responses to stimuli are recorded for neurons from just below the pial surface of the cortex, in layer II, to just above the white matter, in layer VI (Mountcastle, 1957). A consistent feature of the cortex is the basic similarity in physiological properties displayed by neurons in a radial transverse through the cortex. Cells in layers II-VI along a true radial path in S1 respond to the same stimulus applied to the same part of the body surface (Mountcastle, 1957). This indicates that neurons exhibit place- and the modality-specific responses, which are organised as radial columns (Mountcastle, 1957). In S1 areas, these columns originate from the termination of thalamocortical, intracortical and callosal axons and are carried to all neurons in a column

by radially organised axons that arise from neurons in one layer and terminate up on neurons in another layer (Mountcastle, 1957).

In humans, the basic S1 somatotopic arrangement was found using magnetoencephalogram (MEG) (Baumgartner et al., 1991; Nakamura et al., 1998), electroencephalogram (EEG) (Buchner et al., 1995) and functional magnetic resonance imaging (fMRI). These studies differed in the type of stimulation, the number of fingers stimulated, and the spatial resolution (Villringer et al., 1998; Stippich et al., 1999; Schweizer et al., 2008). The map that was obtained from a few studies showed the complete S1 finger region at a high spatial resolution was quite comparable to that reported by Penfield (Penfield and Boldrey, 1937). The thumb is shown in the position that is the most lateral, anterior, and inferior, and is followed by the remaining fingers sorted along the CS in a manner that goes from superior to medial (Maldjian et al., 1999; Kurth et al., 2000) i.e. similar to non-human primates.

1.3. BA3b and BA1 of the squirrel monkey (*Saimiri sciureus*)

The S1 region of squirrel monkeys (*Saimiri sciureus*) contains four separate representations of the body corresponding to the four classical architectonic fields including BA3a, BA3b, BA1 and BA2 in the primates. Multi-unit microelectrode recordings (Merzenich et al., 1978; Kaas et al., 1981a, b) determined somatotopic organisation of BA3b and BA1. Separate mirror image (whatever skin surface was represented rostrally in BA3b was represented caudally in BA1) cutaneous representation of BA3b and BA1 was postulated (Figure 6). The somatotopic arrangement of the body surface representations in BA3b and BA1 of the squirrel monkey is fundamentally comparable to that of the owl monkey and the macaque monkey (Krishnamurti et al., 1976; Sue et al., 1980a, b; Carlson and welt, 1880). Although minor differences appear as when compared to owl and macaque monkeys, as the representations of some body parts in BA3b and BA1 of squirrel monkeys had the reverse orientation. In squirrel monkeys, the representations of the face, arms, trunk, and legs were all reversed, but the representations of the hands and feet were the same. For example, in owl and macaque monkeys, the dorsal trunk is represented rostrally in BA3b and caudally in BA1 and the ventral trunk is represented at the 3b/l border. In squirrel monkeys, the ventral trunk is represented rostrally in BA3b and caudally in BA1 and the dorsal trunk is represented at the 3b/l border (Nelson et al., 1978; Sur et al., 1982). It is in the orientation of some, but not all, body parts in the two representations that BA3b and BA1 differ in somatotopic

organisation in squirrel monkeys from owl and macaque monkeys (Nelson et al., 1978; Sur et al., 1982). The sequence of representation in BA3b and BA1 proceeded from tail and gluteal skin medially to the oral cavity laterally (Sur et al., 1982) (Figure 6). The sequence demonstrates two important aspects of somatotopic organisation. First, the crudely mirror-image orientations of the two separate representations of BA3b and BA1. The mirror-reversal of somatotopic organisation at the BA3b/BAl border was also noted in other monkeys, and it appears to be a consistent feature of the somatotopy in primates. Second, the RF progression reveals the localization of distinct skin surfaces in the representations with the separate localization of the glabrous and the hairy digit surfaces of the hand in BA3b and caudally in BA1 (Figure 6).

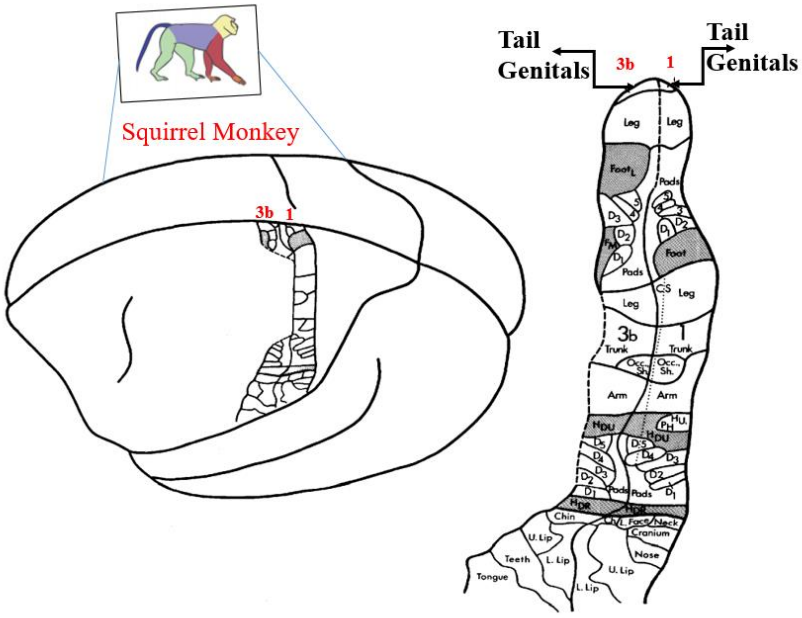

Figure 6. Separate representations of the body surface in BA3b and BA1 of squirrel monkeys.

Location of the representations on a dorsolateral surface view of the brain is on the left. The middle portion of BA3b is deep in the central sulcus. The details of the representation are shown on a flattened view of the surface on the right. Shaded areas correspond to dorsal hairy surfaces of the foot and hand. Dashed line along the rostra1 border of the 3b representation indicates where the precise margin was not determined because the central sulcus limited the spacing of recording sites. Dashed line between BA3b and BA1 indicates where these fields are on the medial wall of the cerebral hemisphere. Dotted

line (CS) marks the central sulcus. D, digits of the hand and foot numbered in order; UL, upper lip; LL, lower lip, Ch, chin; L Face, lateral face; HDr, dorsoradial hand; HDu, doraoulnar hand; Occ, Occiput, Sh, shoulder; Fm, medial dorsal foot; F1, lateral dorsal foot; Leg, hindlimb (adopted from Sur et al., 1982).

1.3.1. Hand representations of BA3b and BA1

The hand is a remarkable tactile organ that gives us the ability to interact with objects with unmatched degree of variety and dexterity (Sainburg et al. 2002; Johansson and Flanagan, 2009). Our ability to grasp and manipulate objects depends not only on complex neural circuits that drive muscles to move the hand but also on neural signals from the hand that provide feedback about the outcome of those movements (Sainburg et al. 2002; Johansson and Flanagan, 2009). People who are deprived of this sensory information have a difficult time doing even the most fundamental actions required in everyday life, such as picking up a coffee cup or using a spoon (Sainburg et al. 2002; Johansson and Flanagan, 2009).

It has been found that the hand is represented in both BA3b and BA1 in the cortex, located just medially to the region that is dedicated to the face (Sur and Nelson, 1982; Kaas, 1982). A representation map was created using electrode penetrations in the hand area of the brain of squirrel monkeys (Figure 7). A large central region of BA3b and BA1 is devoted to the glabrous surface of the hand while the hairy dorsum of the digits and hand is divided into two separate representations in both areas (Sur et al., 1982). The dorsal digits were mostly caudal in BA1 and rostral in BA3b, while the dorsal hand was represented largely near the borders of the areas. Thus, these surfaces were represented in both BA3b and BA1 (Sur and Nelson, 1982; Kaas, 1982).

Representation of the glabrous surface of the hand is indicated by progression of RFs for rostrocaudal rows of recording sites (Figure 7). From these progressions, it is apparent that the digit tips were found rostrally in BA3b and caudally in area BA1. The proximal digit surfaces were more caudal in BA3b and more rostral in BA1 and the representations of the palm form the common border of the two areas. The mediolateral cortical sequence of representation for both areas was from radial to ulnar across the palm and digits (Sur et al., 1982). This was the basic organisation found in other monkeys, although individual variations, especially in the representation of the dorsal hairy surfaces and in the representation of pads, were noted. Moreover, the relative amount of cortex devoted to

various parts of the hand also varied. It is important to conclude that the basic pattern with the digits pointing in opposite directions in BA3b and BA1 is apparently a general property in primates (Nelson, 1980).

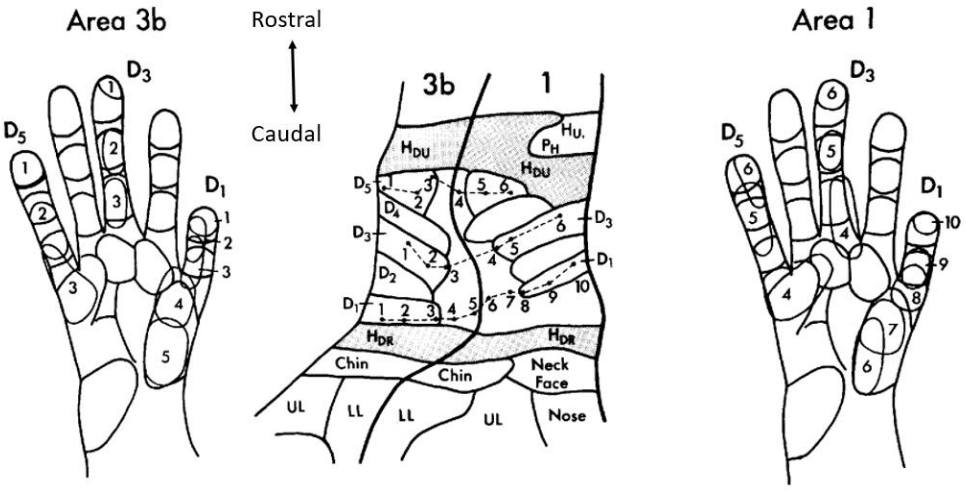

Figure 7. The hand representations in BA3b and BA1.

RFs for three rostrocaudal rows of recording sites are indicated. Cortex devoted to dorsal hairy portions of the digits and hand is shaded and marked H_{DR}, dorsoradial hand, and H_{DU}, dorsoulnar hand. Brain tissue devoted to each digit is outlined; another unlabelled cortex represents the palm. The representation of the hypothenar pad, P_H and adjoining glabrous ulnar hand, $H_{U.}$, was displaced caudomedially in BA1 (adopted from Sur et al., 1982).

1.3.2. Lateral connectivity in BA3b and BA1

Haptic exploration and tactile perception depend fundamentally on the hand and fingers, particularly the distal pads of the fingers. The distal finger pads are distinguished from the rest of the body because these body parts have one of the highest densities of cutaneous receptors (Vallbo and Johansson, 1984). In order to get an understanding of tactile perception, it is crucial to identify the processes that are responsible for integrating the information provided by the distal finger pads in the cerebral cortex.

The classical RFs of BA3b neurons are restricted to individual digit tips, which is in contrast to BA1, where cRF of the neurons often extend more than one digit (Mountcastle and Powell, 1959; Sur et al., 1980, 1982, 1985; Iwamura et al., 1983a, 1993). The larger size also represents evolving complexities of the RF properties in BA1 compared to

BA3b. This is shown by the greater intra- and interdigit integration, higher motion and direction selectivity, and invariant response properties (e.g. velocity, texture, form, speed, and intensity) in BA1 (Iwamura et al., 1983b; Iwamura, 1998; Bensmaia et al., 2008; Pei et al., 2010). Anatomical studies (e.g. BDA tracing) of the brain have shown that the thalamic input to BA1 is weaker than to BA3b, and the majority of the input to BA1 originates from BA3b (Jones et al., 1978; Vogt and Pandya, 1978). All these findings lead to the conclusion that the response properties of neurons in BA1 are defined largely by convergent input from BA3b. However, the role of lateral connectivity has to be taken into consideration before a conclusion is made concerning the integration of tactile information in S1.

Recent research has shown that small injections of neuronal tracers confined to a column-sized region of S1 result in strong reciprocal connections, not only within the injected distal fingertip representation, but also within neighbouring distal fingertip representations in BA3b and BA1 (Négyessy et al., 2013; Ashaber et al., 2014). In contrast, between BA3b and BA1, high-density reciprocal connections are restricted to the homotopic representations of the distal fingertips (Négyessy et al., 2013; Ashaber et al., 2014). Moreover, electrophysiological mapping has revealed the orderly digit topography in BA3b and area BA1 (Figure 8A). Also, optical imaging of cortical activation in response to stimulation of single digit tips has revealed two activation spots, one in BA3b and one in BA1 (response to D2 stimulation shown in Figure 8B) (Friedman et al., 2004, 2008). A focal injection of BDA into BA3b confined to the single digit-tip representation resulted in heavy labelling of cells (orange and yellow) near the injection site in BA3b, as well as patchy label (green and blue) distant from the injection site in the hand area in BA3b (Figure 8C-F). These included adjacent digit representations of distal D1, D3, and D4 within BA3b. A very intense labelling was also observed in BA1, predominantly in the D2/D3 region with more focus in the tip representation zone (Figure 8D-F). The labelling suggests topographically widespread connections from the neighbouring digit locations within BA3b and restricted inputs from BA1 and from largely topographically matched locations. Thus, anatomical connections were characterised by two primary axes of information flow such as broad intra-areal (Figures 8D-F, curved red arrows) and comparatively focused inter-areal connectivity (Figures 8D-F, straight red arrows), which was confirmed by single cell recordings and fMRI experiments (Roe et al, 2013). Furthermore, fMRI and electrophysiological approaches

showed predominant information streams within these two areas, for example, the intra-areal stream integrating information from different fingers and the inter-areal stream integrating information from the same fingers (Roe et al., 2013).

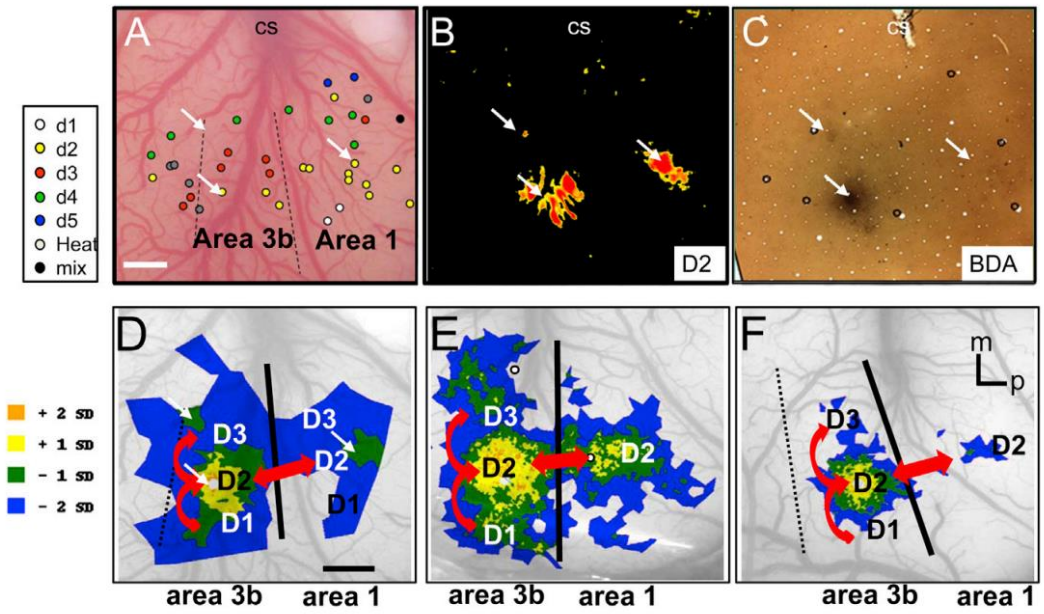

Figure 8. Anatomical connectivity of digits revealed by injections in BA3b

(A) Electrophysiological mapping of the digit region in BA3b and BA1. Same field of view as in (B)–(D). (B) Optical image obtained in response to vibrotactile stimulation of D2, revealing activation in BA3b and BA1 (white arrows). Red pixels, $p < 0.01$. (C) Injection of BDA into the D2 location in BA3b. Arrows indicate sites of strong BDA label in BA3b and BA1, with the lowest arrow pointing to the injection site. The same arrow positions are shown in (A)–(D) for reference. Small circles marking the vessel lumen were used for alignment with the bloodvessel image. (D) Cellular densities resulting from the injection shown in (C). The density colour scale is at left, with high to low density in descending order. (E and F) Second (E) and third (F) cases illustrating BDA-label distribution after injection of the D2 tip in BA3b. Each case reveals a mediolateral intra-areal axis of label and largely digit-matched inter-areal label. For all images: scale bar represents 1 mm; m, medial; p, posterior (adopted from Roe et al., 2013).

Similar to visual cortex, the S1 shows (i) the restricted lateral spread of the feedforward connections forms the connectional basis of the cRF (Favorov and Whitsel, 1988; Angelucci and Bressloff, 2006; Markov et al., 2014), (ii) the greater lateral spread of feedback projection neurons and (iii) the efferent axonal patches which are complemented by the spread of the intrinsic lateral connections into the neighbouring finger

representations, suggesting their role in the formation of the ecRF and more generally in tactile integrative processing in S1 (Angelucci and Bressloff, 2006; Markov et al., 2014; Palfi et al, 2018) (Figure 9).

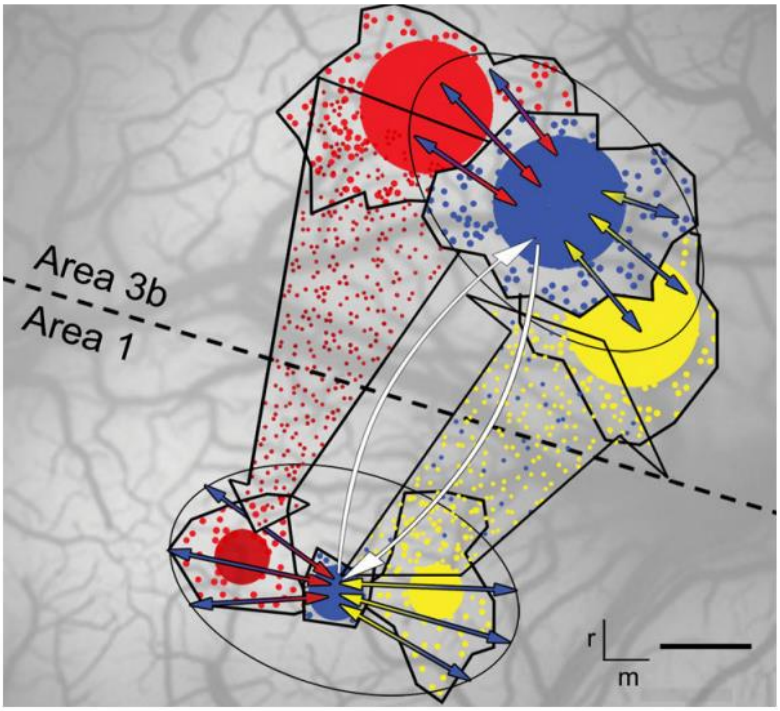

Figure 9. The connectional motif of the columnar circuitry within and between two neighbouring areas in S1.

The schematic summarises the quantitative evidence supports the organisation of the intra- and inter-areal connectivity of a column size cortical domain of area 3b and area 1. Intrinsic connections exhibit a similar, large spread across the finger representations in the two areas (full, coloured arrows within ellipsoids). However, considering both the origin and termination of feedforward connections (large arrow with red dots) are largely convergent and more tightly packed compared to the more divergent and loosely packed distribution of the feedback connections (large arrow with yellow and blue dots). The pattern of dot symbols represents the density and clustering of the projection neurons, which are higher in area 3b than in area 1. Also, due to the different cortical magnification factors (CMFs) (shown by the different size of the outlined regions (OIS-area) which also include the filled circles with different sizes symbolising the different proportion of projection neurons localised within the OIS-area), the lateral spread of connections converges on a larger skin surface in area 1 than in area 3b. White arrows show a reciprocal pathway formed by feedforward and feedback connections, which is

responsible for fast information exchange between homotopic finger representations. The different colours represent connections of different distal finger pad representations. Schematic on the cortical surface of an experimental case is superimposed. Scale bar represents 500 µm. Orientation bars: r: rostral and m: medial (adopted from Palfi at al., 2018).

1.4. Axonal arborization patches of the lateral connections

Pyramidal cells (PCs) represent the majority of neurons in the mammalian cortex (DeFelipe and Farinas, 1992; Markram et al. 2015). In addition, PCs are the projection neurons of the cerebral cortex responsible for long-distance interactions within and between cortical areas (DeFelipe and Jones, 1992). In cerebral cortex (including the neocortex), long-range GABA projections also extend their axons outside of their area of origin, enabling communication between functionally distinct brain regions (Tamamaki and Tomioka, 2010; Caputi et al., 2013; Melzer and Monyer, 2020). However, their role in forming axonal arborization patches is not known. In addition, these cortical long-range GABAergic neurons (LRGNs) comprise a heterogeneous population, showing differences in morphology, intrinsic membrane properties and expression of molecular markers (parvalbumin and calretinin, and neuropeptides like somatostatin (SOM), Neuropeptide Y and cholecystokinin, and enzymes such as the neuronal NO synthase (Pieraut et al.,2014; Yuan et al., 2017; Vaden et al., 2020). Despite such diversity, cortical LRGNs have in common the propensity to target GABAergic neurons, thereby mainly mediating long-range disinhibition (Toth et al., 1997; Melzer et al., 2012; Caputi et al., 2013; Melzer and Monyer, 2020). The axon collaterals of pyramidal neurons (LeVay, 1988) provide horizontally oriented, intracortical projections in the superficial layers of visual, auditory, somatosensory, and motor cortices (Rockland and Lund, 1983; Livingstone and Hubel, 1984; DeFelipe et al., 1986). The projections may spread for extensive distances within a region, or even into adjacent areas forming connections for cortical integration (Rockland and Lund, 1983; Livingstone and Hubel, 1984; DeFelipe et al., 1986). The axon collaterals also give rise to discrete columnar clusters of terminal boutons, which are most prominent in the superficial layers (Figure 10A) (Rockland and Lund, 1983). However, the axonal boutons have been shown to represent synapses, and the pyramidal neurons in layer Va are likely to establish numerous synaptic contacts throughout the course of their axon collaterals (Lübke et al., 2000; Staiger et al., 2002; Lübke and Feldmeyer, 2007). Most notably, such patchy organisation of the lateral

connectivity is present across the different cortical areas including sensory, motor and higher association regions, and appears to be a characteristic feature of the cortical connectivity (Lund et al., 1993; Yoshioka et al., 1996). The patchy lateral connectivity is also known as the “daisy architecture” (Douglas and Martin 2004). As shown by earlier tracing studies, the somatosensory cortex is not an exception and exhibits the clustering of axon terminals (patchy or stripe-like pattern) in layers I-III of S1 and secondary somatosensory cortex (S2) (Rockland and Lund 1982, 1983; Lund et al., 1993) (Figure 10B). It should be noted that the axonal patches are found only in higher order mammals (felines, monkeys) but not in the rodent cerebral cortex.

In the visual cortex, PCs of the superficial cortical layers create a unique network that is characterised by a circular pattern of clusters of synaptic boutons structured around a core of cells, dendrites, and axons (Rockland and Lund 1982). The axons of individual pyramidal neurons form a proximal or a local bouton cluster around the dendritic tree. The distal clusters are made of the "spokes" that branch off from the main axon in different directions (Gilbert and Wiesel 1983; Martin and Whitteridge 1984; Kisvarday and Eysel 1992; Buzás et al. 2006; Binzegger et al., 2007; Martin et al., 2014). Each pyramidal cell axon contributes to only a few of the distal clusters of the daisy. This means that many PCs work together to make the whole daisy.

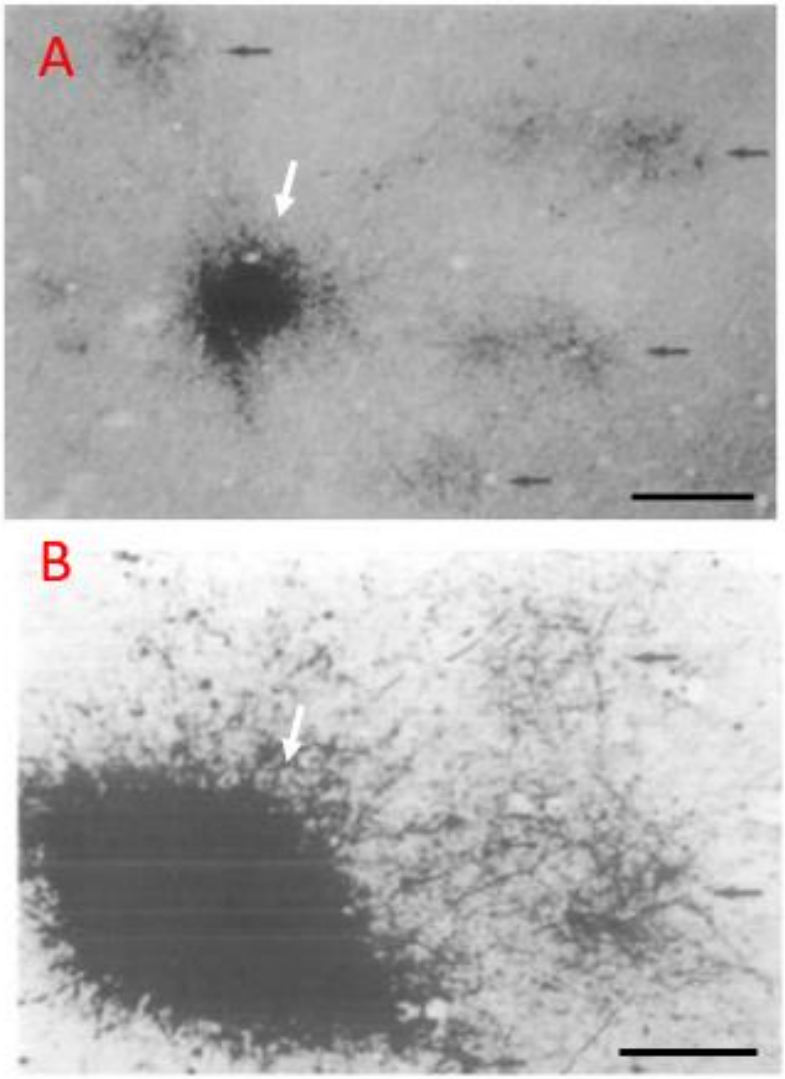

Figure 10. Patch labelling in visual and somatosensory cortical areas

Biocytin injection in visual (A) and somatosensory (B) cortex shows injection site (white arrows) and patchy labelling (black arrows). Scale bar: 200µm (adopted from Lund et al., 1993).

1.4.1. Organisational properties of the patch system

The daisy architecture of axonal connections is the best-known motif in the visual cortex, especially in V1, where focal injections of neural tracers results in a quasi-periodic patchy labelling (Rockland and Lund 1982, 1983; Rockland et al. 1982; Gilbert and Wiesel 1989; Lund et al. 2003) (Figure 11A). These patches are most prominent in the superficial layers where pyramidal neurons give rise to laterally extending intralaminar axons that support the clusters of boutons suggesting that the laminar patches are composed of neuronal clusters (Kisvarday and Eysel 1992; Buzás et al., 2006; Binzegger

et al., 2007; Muir and Douglas 2011). The regular scaling of patch diameter and interpatch distance across many areas and species suggests that patches form a fundamental motif of cortical connections and function (Douglas and Martin 2004; Muir et al. 2011) (Figure 11B). The inter-neighbour distances and angles demonstrate that the patches are forming a hexagonal lattice, which is relatively periodic.

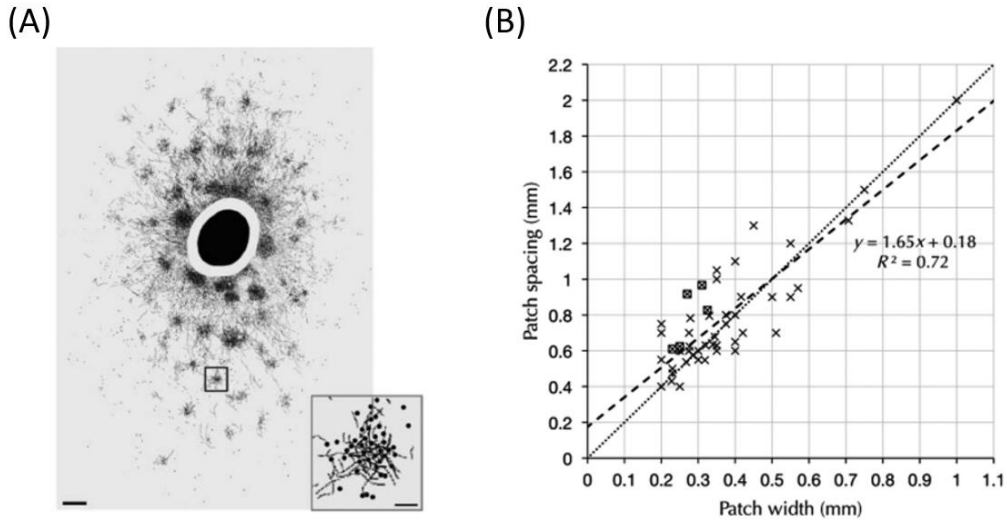

Figure 11. Patchy labelling

(A) Patchy labelling of the terminals in layer II/III in the macaque visual cortex following bulk injection of the tracer cholera toxin B subunit (from Lund et al. 2003). (B) Scaling of interpatch distance with patch diameter observed across various cortical areas and species (from Muir et al. 2011).

Tract tracing using domain-specific microinjections in V1 of non-human primates (NHP) shows that connections between domains have a high degree of specificity (Rockland, 1985; Shmuel et al., 2005). For example, blobs in V1 (responsible for processing surface information such as colour and luminance) are preferentially connected to blobs and interblobs (responsible for processing of orientation information) (Livingstone and Hubel, 1984; Yoshioka et al., 1996). Connections between ocular dominance columns also show an eye-adapted preference (Malach et al., 1993; Yoshioka et al., 1996). These patterns strongly suggest that domain-based connections reflect different functional networks (Sincich and Horton, 2005). Furthermore, in the visual cortex the domains with similar functional preferences (e.g., orientation), are thought to be connected via the distal clusters of axonal branches (Figure 12) (Gilbert and Wiesel,

1989; Bosking et al., 1997; Sincich and Blasdel, 2001). One way to look at the daisy pattern is that it is driven by the functional need to achieve a like-to-like rule of connectivity, perhaps through a fire-together-wire-together mechanism and Hebbian plasticity (Gilbert and Wiesel, 1989).

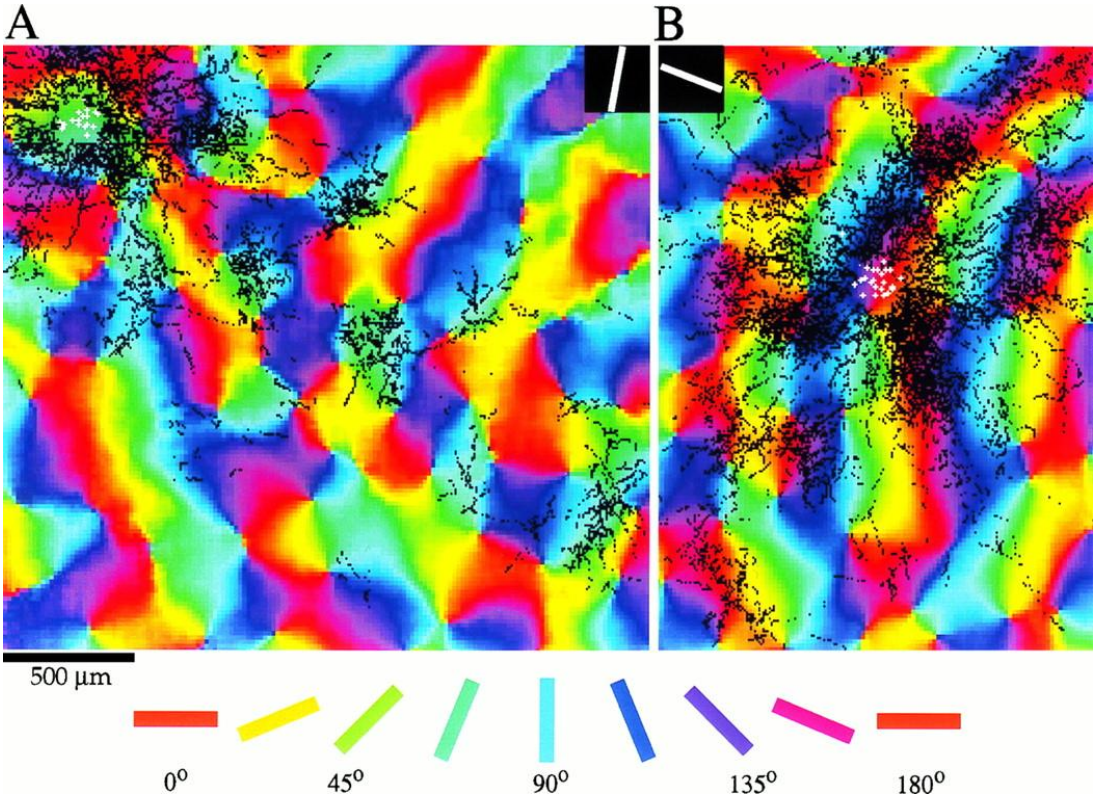

Figure 12. Bouton distributions shown over orientation preference maps

(A) Bouton distribution after an injection into a site with a preferred orientation of 80^0. The white symbols indicate the location of cells that took up the biocytin. Labelled boutons (black symbols) are found at sites with all orientation preferences near the injection site, but preferentially at sites with the same orientation preference as the injection site at longer distances. (B) Same field as shown in A with an orientation preference of 160^0. Colour key and scale bar apply to both figures (adopted from Bosking et al, 1997).

The axonal patches are made of recurrent collaterals of pyramidal neurons bearing high-density bouton clusters (Figure 13) (Buzás et al., 2006; Binzegger et al., 2007; Muir and Douglas, 2011). Patchy labelling becomes evident at a distance from the injection site (Figure 14). The distal clusters connected to the parent soma by linear axonal segments, decorated by numerous boutons can also establish rich connectivity (Figure 14) (Kisvárday et al., 1997; Buzás et al., 2006). The axonal patches continue across adjacent

sections, proving that the intrinsic connections form columns of label throughout the superficial layers (Figure 14) (Stettler et al., 2002). The arrangement of the bouton forming axons within patches and no-patch domains (i.e., outside the patches) is evident from a bird eye view.

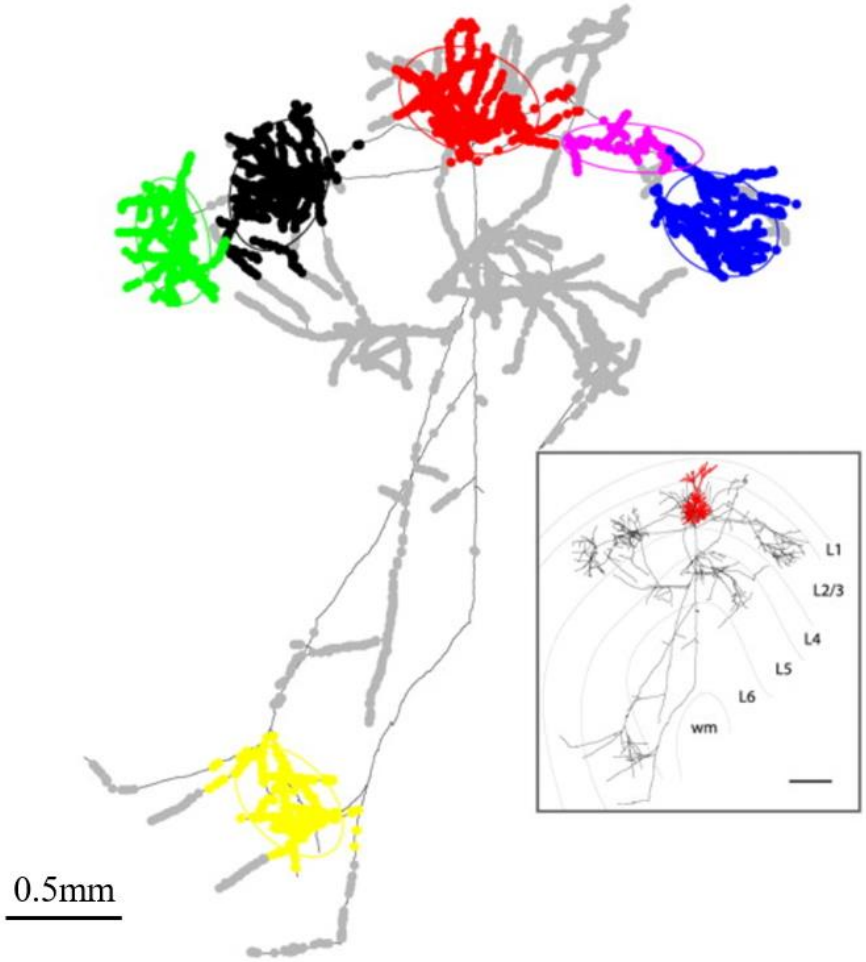

Figure 13. Example of a pyramidal neuron showing bouton clusters

Bouton clouds are from reconstructed pyramidal cells in layers 2/3. The clusters are indicated with different colors (black, red, green, blue and yellow, etc., in order of decreasing bouton number). Colored ellipses indicate the contours of the projected 2-ellipsoids associated with each cluster. Gray dots indicate boutons that are not in a cluster. Insets, Coronal view of the axon (black) and dendrites (red) of each neuron, indicating the position of the neuron in relation to the cortical layers (gray curved lines). (Adopted from Binzegger et al., 2007).

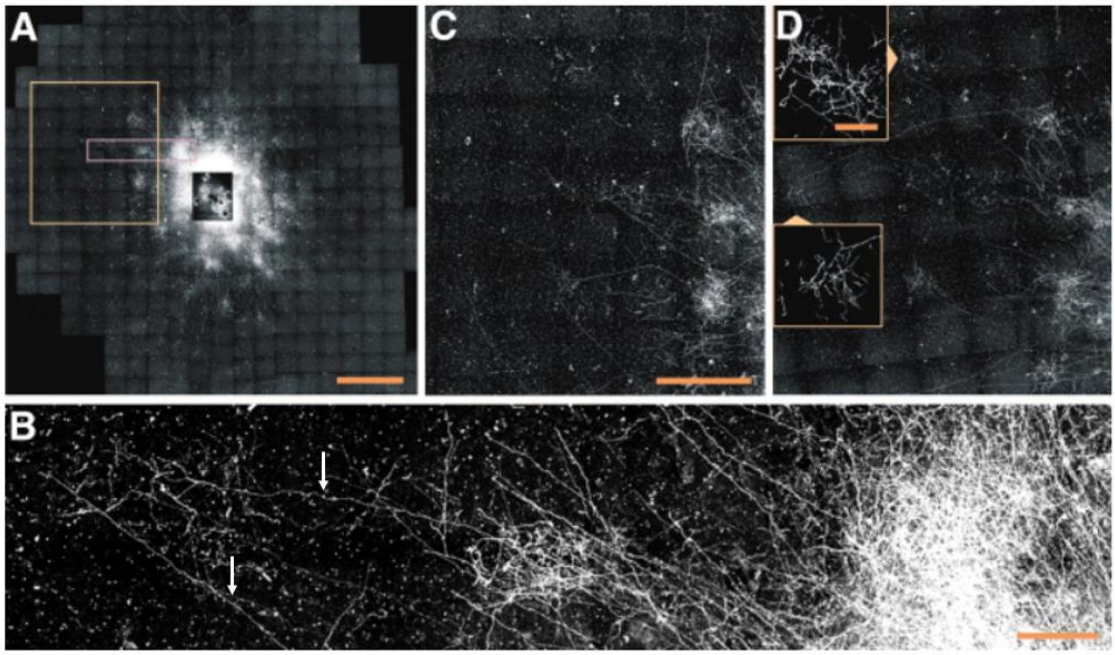

Figure 14. Patch and no-patch domains of horizontal connections in macaque V1

(A) The virus yields strong axonal labelling of horizontal connections, shows dense patches of axons in the superficial layers. (B) The pink-outlined segment in (A), magnified, exhibits patches at multiple distances from the injection site, long-range out patch axons with boutons (white arrows). (C and D) A close-up of the orange-outlined portion of (A) shows patches that are aligned with those in an adjacent section (D), indicating that the intrinsic axons form columns of connectivity in superficial V1. Insets in (D) contain combined axons from the two sections for distal patches (arrowheads) with the background removed. Scale = 1 mm for (A), 500 μm for (C) and (D), and 100 μm for (B) and (D) insets (adopted from Stettler et al., 2002).

At single cell resolution, strong evidence has been found for a more complex connectivity pattern than the like-to-like interconnections by studying the orientation preference of long distance connections (Martin et al., 2014). Superficial PCs did not exclusively form their distal clusters in areas that shared the same orientation preference as that of the parent dendritic tree and the local cluster. Instead, distal clusters were found in a variety of different domains, including orientation domains that had orientation preferences orthogonal to those of the parent dendritic tree (Martin et al., 2014). This architecture seems well suited for contextual processing. In fact, such context dependence of the daisy network is evident at the RF level. By inactivating small regions of V1, the orientation tuning of neurons at distant sites can be shifted (Girardin and Martin, 2009) or broadened and directional selectivity can be lost (Kim and Freeman, 2016). Similarly,

there are many illusions where a straight line appears curved due to the context of the lines. The Hering illusion is a prominent example of these effects, which arguably may be a natural expression of daisy architecture. However, these observations are complementary to the exclusively like-to-like view of connectional architecture and do not deny it. Instead, the evidence suggests that lateral connectivity is biased towards the like-to-like network (Kisvárday, 2016).

Considering inter-areal connections, it is evident from the previous research that connectivity between V1 and V2 is specific (Shmuel et al., 2005). For example, tracer injections in V2 thick/pale stripes produce a distribution of retrogradely labelled V1 cells that fall primarily in the interblobs but also label blobs (feedforward V1-V2 projections). Furthermore, anterograde tracer injections in the V2 orientation domain revealed terminal patch distributions overlying V1 interblobs (feedback V2-V1 projections). The spatially localized pattern of inter-areal connections is reminiscent of the patch-like distribution formed by terminal axonal branches of pyramidal neurons (Shmuel et al., 2005).

In the macaque visual cortex, focal stimulation and optical imaging revealed evoked activations. The activation patterns revealed sparse, focal mesoscale networks with high functional specificity (Hu and Roe, 2022). For example, (i) intra-V2 functional connections connect matching V2 functional stripes (colour projects mainly to colour, orientation projects mainly to orientation (Malach et al., 1994). In addition, V2 stripes were shown to have matching luminance-to-luminance and matching orientation-selection domain connectivity. (ii) Inter-areal connectivity (V1 stimulation): focal stimulation of single interblob locations can result in activation of single V2 orientation-adapted domains, revealing a strong focal projection pattern between single domains in V1 and V2 (Levitt et al., 1994). The stimulation of two nearby interblobs results in activation of the same V2 orientation domain, suggesting that interblobs are involved in highly specific functional integration in V2. (iii) Inter-areal connectivity (V2 stimulation): focal stimulation of a domain within the V2 orientation stripes activates a small array of interblobs in V1, revealing the extent of a V1-V2 network associated with a single V2 domain (Angelucci et al., 2002). The deep-layer stimulation in V2, the main source of feedback to V1, results in patterns resembling known feedback projections. This adds to evidence suggesting that focal electrical stimulation tends to activate orthodromically (Friedman et al., 2020). Furthermore, stimulation of a number of sites along a single electrode track revealed a shifting topography of connectivity, e.g., intra-

areal connectivity is topographically organised at a columnar level (Markov et al., 2014). These results provide a new understanding of the columnar specificity and organisation of local intra-areal and inter-areal connections in the visual cortex of non-human primates (Sincich and Horton, 2005; Federer et al., 2009; Federer et al., 2021). This novel approach to study functional networks at the mesoscale level in vivo reveals the spatial resolution and functional specificity of mesoscale connections in the visual cortex (Sincich and Horton, 2002; Xiao and Felleman, 2004; Sincich et al., 2010). These observations suggest that intra-areal connectivity is topographically organised at a columnar level and the domain-based microcircuits (e.g., intracortical nodal circuits or brain-wide nodal circuits) represent a functional element of the cortical architecture (Hu and Roe, 2022). Such insights further influence circuit models of cortical information processing.

1.4.2. Patchy organisation of S1

In macaque monkeys, wheat germ agglutinin conjugated to horseradish peroxidase (WGA-HRP) tracing in BA3b demonstrated dense, patchy interconnections within and between BA3b and BA1. (Landry and Deschenes 1981, Landry et al., 1987). Later, Lund et al. (1993) using anterograde tracing (e.g., biocytin injections in BA3b and BA1) confirmed the patchy connectivity of S1 intrinsic connections. This showed that the neuronal connections exhibit both a diffuse distribution and a patchy organisation, which may constitute the functional connectivity between adjacent finger representations (Krubitzer and Kaas, 1990; Burton and Fabri, 1995). In S1 of squirrel monkeys, anterograde labelling revealed the existence of (i) bouton forming long-range axonal segments (no-patch domains) and (ii) terminal axon arborizations having dense network of thin fibres with numerous boutons (patch domains) (Négyessy et al., 2013; Ashaber et al., 2014) (Figure 15 and 16).

DOI:10.14753/SE.2023.2830

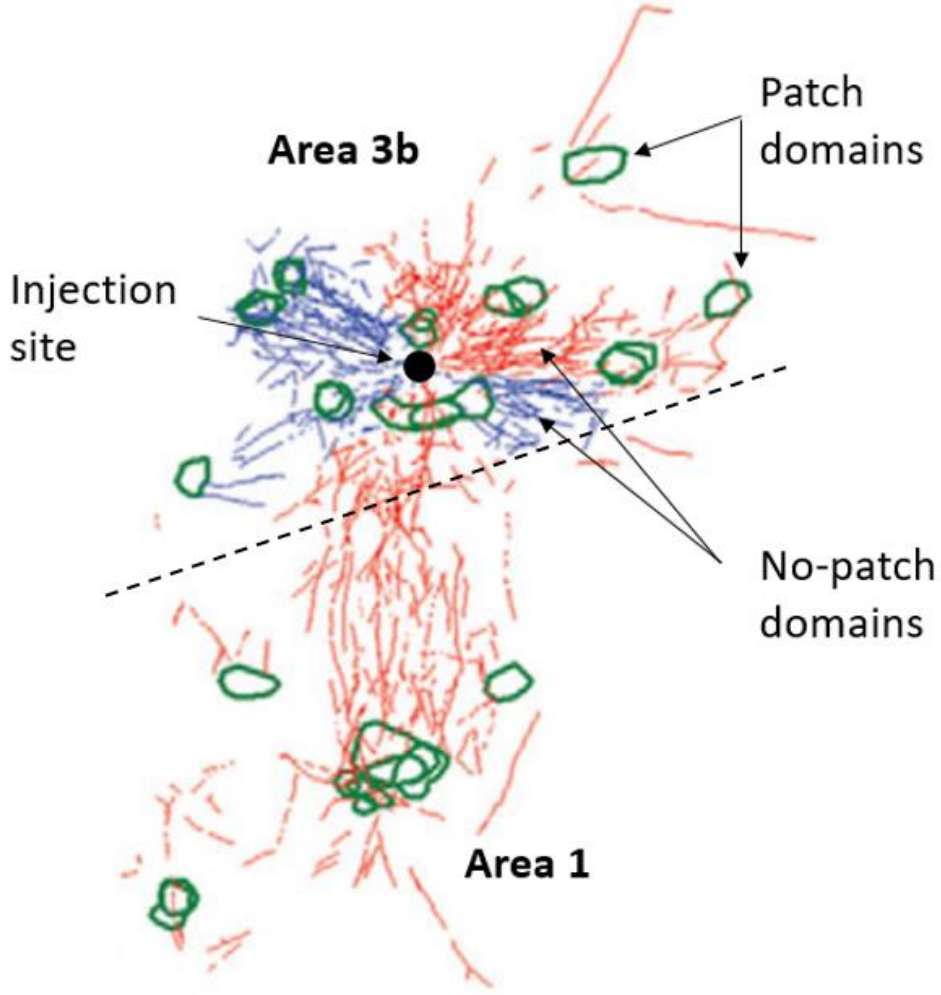

Figure. 15. Horizontal distribution of the anterograde BDA labelling showing patch and no-patch domains in BA3b and BA1

Anterograde labelling is represented by connections intrinsic (blue lines) and extrinsic (red lines) to the hand representation region of area 3b; intrinsic connections mostly course medially and laterally (blue lines), and inter-areal axonal fibres course anteriorly and posteriorly (red lines). Green outlines represent patches of terminal axon arborizations. Fibres crossing the estimated borders of the hand representation of area 3b were defined as long-distance, inter-areal; otherwise, fibres localised within the hand representation were considered intrinsic. Note that patches are connected to the injection site via the bundles of no-patch axons. Note also patches of inter-areal connections. Dashed lines, estimated areal borders. Black dot: injection site. Scale bar = 1 mm (adopted from Négyessy et al., 2013).

DOI:10.14753/SE.2023.2830

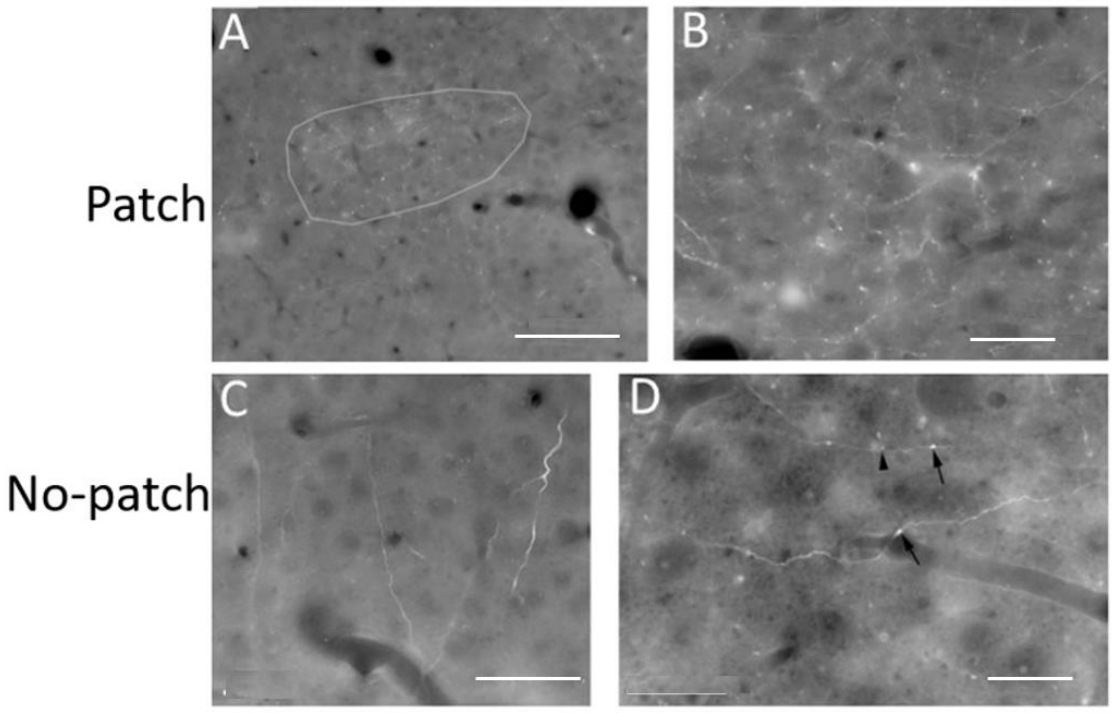

Figure 16. Anterograde BDA labelling of axons in S1

A: Low-resolution image shows the manual demarcation of an anterogradely labelled terminal patch (pale contour). B: Higher magnification shows the appearance of numerous thin fibres and bouton-like structures within another example of a terminal patch. C: A reversed Y-shaped, relatively thick, smooth axonal process running between BA3b and BA1. D: Long-range (out-patch), horizontal axonal fibres decorated by boutons. Arrowheads point to a varicosity giving birth to a bouton with a stalk. Arrows show axonal varicosities. A–D are inverse, darkfield images. Scale bar = 50 µm in A and C, 25 µm in B and D (adopted from Négyessy et al.*, 2013).*

The tactile submodality representation can provide the possible functional explanation for the patchy axonal labelling pattern. For example, in macaque, SA and RA afferents in BA3b are segregated in alternating anteroposterior bands within layer IV, an organisation analogous to that observed in cats (macaque: Sur et al., 1982; cat: Dykes et al., 1980; Dykes and Gabor 1981; Sretavan and Shatz., 1984). The segregation of SA and RA afferents give birth to the functional segregation of two processing streams in the somatosensory cortex (Sur et al., 1982). In line with these observations optical imaging, showed that SA1, RA, and PC input sensitivity is not homogeneously distributed throughout BA3b; instead, preferential activation of each of the three populations yielded a pattern of activation similar to the distribution of orientation columns in V1 (Figure 17)

(Chen et al., 2001). Importantly, however, there was a large degree of overlap between the patterns of activation evoked by the three populations of afferents corroborating previous observations that even SA columns seem to receive RA input (Dykes et al., 1980; Sretavan and Shatz., 1984). Similar results were obtained in BA1 (Friedman et al., 2004). The similarity of submodality representations in S1 to that of V1 puts forward the similar role of patchy connections in these cortical areas. However, the widespread functional responsivity of neurons in S1 raise questions concerning the role of lateral connectivity including the patch and no-patch axonal domains in tactile perception.

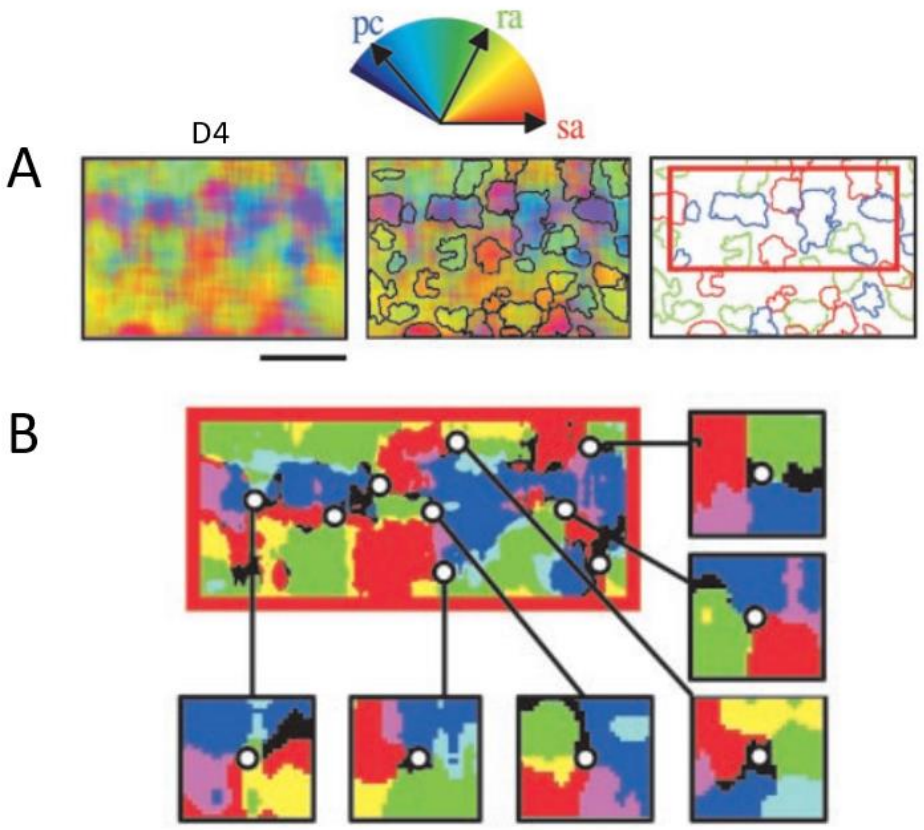

Figure 17. Submodality maps of BA1

Shown above A is the colour-coded vector space. (A) Digit 4 (D4) was stimulated. (Left) Red, green, and blue indicate strong preference for pressure, flutter, and vibration, respectively. (Centre) Vector maps with colour threshold outlines overlain. (Right) Coloured outlines of thresholded colour maps. Outlines were obtained by selecting pixels that exceeded an 80% magnitude threshold and fell within 15° of cardinal SA, RA, or PC vectors. (Scale bar, 1 mm.) Anterior to top, medial to right. (B) Vector map (area indicated by rectangular box in A right) thresholded to six colours. (Inset) Possible

pinwheel centres. Note clockwise and counterclockwise SA (red), RA (green), and PC (blue) rotations. Vector map represents response preference by direction in colour space (e.g., red for pressure, green for flutter, and blue for vibration) and magnitude is encoded by saturation of colour. This method calculates, for each pixel, the relative weight of each response direction and gives a vector value that reflects the overall preferred direction and magnitude (adopted from Friedman et al., 2004).

1.5. Axon morphology

In the cerebral cortex, excitatory neurons are glutamatergic and represent ~70-80% of the neurons in all cortical layers except layer I (Curtis and Watkins, 1960). The major cell type of excitatory neuron population is the pyramidal cells (PCs), although in layer IV spiny stellate and star-pyramidal cells are also commonly present (Gouwens et al., 2019). In contrast to the pyramidal neurons, which are the projection neurons of the cerebral cortex, inhibitory neurons considered local circuit neurons (interneurons) with no obvious axonal projections into white matter (Molyneaux et al., 2007). Studies of Kisvárday et al. (1997, 2000) revealed that the axonal branches of PCs and inhibitory interneurons, most notably basket cells, which form extensive lateral connectivity, exhibit-distinguishing features. The lateral excitatory network is a few times larger in extent than the inhibitory network. The putative excitatory axons had sparsely spaced boutons along their length, the boutons were varicosities or connected to the axon stem via a short stalk. Notably, unlike axons of inhibitory basket neurons, axonal boutons of pyramidal neurons do not make pericellular contacts with other neurons. However, the axons of giant basket cells released bursts of boutons and often established the usual multiple contact pattern resembling a basket with nearby neuronal somata. Basket cell axons are thinner and form smaller boutons than that of pyramidal neurons. In addition, basket cell axons rarely gave off boutons connected via a short stalk with the parent axon.

In the primate cerebral cortex, PC structure is remarkably heterogeneous. The total number of spines (putative excitatory inputs) in the dendritic trees of PCs reveal more than a 30-fold difference between populations of cells sampled in different cortical areas (Elston et al., 2001, 2205a, 2005b). Moreover, there are systematic trends for increasingly more complex phenotypes through a series of functionally related cortical areas. For example, neurons become progressively larger, more branched and more spinous with anterior progression through the dorsal and ventral visual pathways (Elston and Rosa, 1997, 1998, 2000). Furthermore, PCs located in different cortical layers vary considerably

in their connectivity, dendritic morphology and functional properties (Feldmeyer, 2012; Harris and Shepherd, 2015). For example, their axons project to distinct targets. LII/III PCs send axons to both neighboring and distant cortical regions (Fame et al., 2011; Harris and Shepherd, 2015). Presumably, they are important for integrating information across cortical areas and mediating higher order information processing. On the other hand, L5 PCs constitute a major source of cortical outputs to subcortical structures, projecting axons to regions such as the thalamus, the striatum, the midbrain, the pons and the spinal cord (O'Leary and Koester, 1993; Harris and Shepherd, 2015). In addition, PCs in L5 and LII/III differ in cell body size and dendritic arborization. LII/III PCs have smaller somata and more confined dendritic trees compared to L5 PCs (Larkman and Mason, 1990; Feldmeyer, 2012; Rojo et al., 2016).

Structural properties of individual axonal segments are significant determinants of activity propagation, hence neuronal communication. One of the most important morphological parameters regarding the propagation of activity is axon diameter or thickness. It is known that the thicker an axon is the faster the conduction velocity would be (Innocenti et al. 2014). Axon size together with axon length allows computing conduction delays between brain regions (Caminiti et al., 2009, 2013; Innocenti et al. 2014). This enriches the ''connectome'' enterprise significantly by characterising, on morphological grounds, the dynamic properties of neural connections (Innocenti et al. 2014, 2016). In addition to axon thickness, varicosity spacing patterns could also provide information about signal transmission as well as the processes behind synaptogenesis and development — a hypothesis that is important for synaptic plasticity models including varicosity neogenesis (Shepherd et al., 2002). The statistical features of varicosity spacing, most notably probability, density, and distribution reflect basic connectivity principles, which are still under intensive research (Shepherd et al., 2002). Furthermore, variable bouton density can identify specific and non-specific target sites of the projection neurons or the populations of them. The three-dimensional branching pattern of an axon is typically heterogeneous, consisting of spatially distinct regions of intense axonal branching and bouton clustering (Binzegger et al., 2007). For example, patches of a population of nearby neurons have a high bouton density compared to the surrounding zone, and the density distribution, therefore resembles a mountainous landscape where the mountain peaks indicate the regions of high bouton density and the different regions are delineated by low density valleys.

Axon morphology is under the pressure of wiring length minimization (Budd et al., 2010). Related to this constraint, axons of pyramidal neurons are not straight but exhibit a tortuous path, which is thought as the consequence of postsynaptic target selection (Chklovskii et al., 2004; Stepanyants et al., 2004). It was demonstrated using neocortical axonal trees that there is no overall reduction in wire length (material) or path length (conduction delay) (Budd et al., 2010). Instead, their three-dimensional branched architecture represents the trade-off of a modest amount of excess axonal wire to obtain a roughly two-fold gain in overall temporal economy (total axon arbour length based on direct distances between boutons) and three-fold or more gain in temporal precision (the increase in the difference between the conduction times along the different axons) (Kisvárday et al., 1986; Braitenberg and Schuz, 1991; Kisvárday, 1992; Budd et al., 2010). In contrast, the techniques used (e.g. graph optimization algorithm used to measure the degree of optimality of single axons to investigate the neuronal morphology) revealed that wire length minimised arbours would considerably impair the temporal precision of neuronal network communication, whereas path length minimised arbours would demand at least an order of magnitude larger neocortex (Kisvárday et al., 1986; Budd et al., 2010). Specifically, it was shown that axon bifurcations function to preserve the relationship between conduction time and cortical distance, and to tightly regulate the degree of temporal dispersion in transmission of axonal signals (Kisvárday et al., 1986; Budd et al., 2010). It is interesting to note from these axonal tree properties, that the highly interconnected intracortical network architecture, assumed to underlie functional maps, is made to be capable of operating with a high degree of temporal precision (e.g. for coincidence detection) (Kisvárday et al., 1986; Kisvárday, 1992; Kisvárday and Eysel, 1992; Buzás et al., 2001; Buzás et al., 2006; Budd et al., 2010). Analysis of tortuosity of axonal segments provides insight into the temporal properties of signal transmission in the cerebral cortex. Accordingly, tortuosity of axons can also influence signal transmission by increasing the length, i.e. conduction delay of the axons (Chklovskii et al., 2002, Stepanyants et al., 2004; Quan Wen and Chklovskii, 2008). Therefore, a path-finding hypothesis is that in specific patchy target site axons are more tortuous to form more synaptic connections than no-patch target site axons.

In addition to individual axonal properties, the collective nature, i.e. the convergent and divergent characteristics of bouton forming axonal branches, also plays a crucial role in cortical functioning by supporting synchronisation or allowing redundancy (Douglas and Martin, 2007; Muller et al.., 2018). Patches are suitable sites of axonal convergence

(Kisvárday et al., 1986; Buzás et al., 2006, Binzegger et al., 2007). However, the role of the straight, bouton-forming axonal segments of the no-patch cortical domains necessitates further investigations into the role of these two axonal domains in intrinsic and inter-areal connectivity and cortical processing. The connection of the somatosensory areas allowed us to compare feedforward and feedback patch and no-patch domains in addition to intrinsic connections, based on the observation that BA3b and BA1 are hierarchically organized (Kaas, 1983, 2004; Iwamura, 1998; Rossi-Pool et al., 2021).

Based on the observations above, the major goal of the present thesis is to unravel the functionally relevant morphological properties of bouton forming axons within patch domain and no-patch domains in BA3b and BA1 of squirrel monkeys by using tract tracing and quantitative morphological approaches.

2. Objectives

At the mesoscale or population level, cortical connectivity shows a clear structure-function link as shown in S1. The patchy pattern of long-distance cortico-cortical axonal connections formed by a population of nearby pyramidal neurons is well known in the primate cerebral cortex. Similar patchy activation patterns to the distribution of lateral and inter-areal connections are produced by cortical microstimulation in the visual cortex. Further support of the functional relevance of patchy connectivity comes from functional representations i.e. similar to orientation domains in the visual cortex, tactile modalities are mapped in the primate somatosensory cortex in a columnar fashion. The fact that lateral connection is similarly organised throughout the cerebral cortex shows that it is crucial to cortical processing in primates. Recurrent collaterals carrying dense bouton clusters generate pyramidal neuron axonal patches. Linear axonal segments with boutons link these distant clusters to the parent soma. As shown for the primary visual cortex orientation circuitry, patches are not simply arranged by functional preference; rather, there is only a bias in their distribution that favours the development of like-to-like connectivity. Furthermore, bouton-forming linear axonal segments cross varieties of neuronal populations with various response characteristics. Deciphering the processes behind the variety and specificity of neural connections is a crucial aspect of cortical computation. It is unknown how information sent by linear axonal segments outside of the patches and within the axonal patches affects cortical computation. One can get a deeper insight into this question by studying the morphological characteristics of axons relevant to signal transmission including conduction velocity and synaptic integration through single or multiple synapses within and outside of the patches.

The connection of the somatosensory areas BA3b and BA1 allowed us to compare feedforward and feedback patch and no-patch axonal domains in addition to intrinsic connections. Based on the above observations the major goal is to unravel the functionally relevant morphological properties of bouton forming axons within patch domain and no-patch domains in BA3b and BA1 of squirrel monkeys (*Saimiri sciureus*) by using tract tracing and quantitative morphological approaches. We measured individual axonal features regarding tortuosity, bouton spacing and axon thickness as well as collective axonal features indicating convergence or divergence. Multivariate analysis tools were used to determine the role of the variables in pathway-specific properties including patch designation (patch vs. no-patch), intrinsic vs. inter-areal connections, feedforward vs.

feedback inter-areal connections and laminar termination (supra vs. infragranular). Based on the hierarchical relationship of the somatosensory cortical areas, BA3b projections to BA1 were considered as feed-forward connections and the reciprocal way is the feedback.

We hypothesised that

1) Patch designation is the most prevalent organisational feature of axonal morphology in the cerebral cortex and

2) Patches (P) are formed by the convergence of highly tortuous axonal branches with high bouton densities whereas no-patch (NP) axons are less tortuous, and have parallel course and low bouton densities.

3) In addition to BDA tracing, the 3rd objective of my studies was to explore the connectivity of a specific type of neurons namely vasoactive intestinal polypeptide expressing interneurons (VIP + INs) in the anterior insular cortex (aIC) of mice, by using viral tracing.

A note on my role in the studies performed

The experimental part of the primate study was done at Vanderbilt University followed by histology at Semmelweis University. I was not involved in the experimental (animal surgeries and histology) part because I joined the laboratory later on and started my project by reconstructing axonal segments with Neurolucida followed by qualitative and quantitative analysis of already prepared brain sections. However, I performed similar experiments in rodents using viral tracing.

3. Materials and Methods

3.1. Studies of neuronal circuits in primate SI

3.1.1. Tracer injections and tissue processing

Animal care and surgical procedures were performed in compliance with NIH (National Institutes of Health) regulations and with approval of the Institutional Animal Care and Use Committee of Vanderbilt University. Three male (Mac, Mo, Pe) and three female (J, M, V) adult squirrel monkeys (Figure 18) (*Saimiri sciureus*, weighing 600–800grams, 2–9 years old) were used, which were subjects in our prior studies on the connectivity of the distal finger pad representations of BA3b and BA1 (Négyessy et al., 2013; Ashaber et al., 2014, 2020; Pálfi et al., 2016, 2018). Here, we provide a brief description of the experimental procedures (for details, see Négyessy et al., 2013 and Ashaber et al., 2014).

Figure 18. The squirrel monkey (Samiri sciureus) (https://www.shutterstock.com/image-photo/funny-look-sqirrel-monkey-amazonic-rainforest-660745750)

As previously described (Négyessy et al., 2013), each animal was sedated (ketamine, 15 mg/kg, im), placed in a stereotaxic frame, mechanically ventilated with isoflurane anaesthesia and hydrated with lactated ringers via intravenous infusion. Analgesia during surgery was supplied by buprenorphine (0.01 mg/kg, im). Vital signs (peripheral capillary oxygen saturation, heart rate, electrocardiogram (ECG), end-tidal carbon dioxide, respiratory pattern, temperature) were monitored. After a craniotomy (centred at AP 6 mm and ML 15 mm (Gergen and MacLean, 1962)) and durotomy, BA3b and BA1 were located using the CS and blood vessel landmarks. Following electrophysiological

mapping of the hand and finger representations (Figure 19A), intrinsic signal optical imaging (IOS) was used to identify the distal finger pad representations of fingers D2-D4 in BA3b and BA1. Injection of biotinylated dextran amine (BDA, 1:1 mixture of 10% 10K and 10% 3K, Molecular Probes, Inc.) in 0.01 M phosphate buffer (PB, pH 7.4) was then made into a distal finger pad representation in either BA3b or BA1 (Figure 19B) via iontophoresis (3 μA, 7 seconds on/off cycle for 20 minutes) (three cases each). In all cases, the core (≤300 μm in diameter) of the uptake zone of the BDA injection included the upper layers (200-390 μm below the surface), while lower cortical layers were also included into the core (Figure 19C) following BA1 injections (160-800 μm below the surface) (Table 2) (for more details, see Table 1 in Négyessy et al., 2013 and Ashaber et al., 2014). Upon recovery, heat support was provided for the first 12 hr with postoperative analgesia supplied by buprenorphine (0.01 mg/kg, im, twice a day) for 3 days. After a 10- to 20-day survival period, animals were deeply anesthetized before perfusing transcardially with a fixative consisted of 4% paraformaldehyde, 0.1% glutaraldehyde and 0.2% picric acid in 0.1 M PB (pH 7.3). Brains were immediately removed, and the region of interest was then cut from cortex, flattened parallel to the cortical surface and postfixed overnight in 4% paraformaldehyde.

Table 2. Summary of the parameters and morphological appearance of the BDA injections in the six cases J, Mac, V, M, Mo, Pe. Scale μm.

Case	Tip diameter	Injection depth	Core diameter	Core depth	No.of slides	Depth of granular layer
J	15 - 17	350	330	390	3	520
Mac	12	350	260	260	2	520
V	20	350	380	390	2	520
M	30	350 - 750	313	320	1	480
Mo	10	351 - 750	295	160 - 800	2	640
Pe	10	352 - 750	403	161 - 800	2	650

Regularly spaced (at 130–160 μm except case Mac with 270 μm spacing) series of 50 μm thick tangential sections were cut by vibratome sectioning (see Négyessy et al., 2013; Ashaber et al., 2014). A standard Avidin-Biotin Complex (ABC) protocol (Vectastain Elite ABC kit, Vector Laboratories, Inc.) was used to visualise BDA labelling with nickel-intensified diaminobenzidine (NiDAB) (Sigma- Aldrich) as the chromogen. Firstly, the sections were cryoprotected (30% sucrose in PB) and tissue penetration enhanced by freezing thawing. Unbound aldehydes were reduced by borohydride (1% $NaBH_4$ in PB, 30 min), and intrinsic peroxidase activity was blocked by 1% H_2O_2 in PB

(30 min). Sections were then incubated in ABC, 1:200 in PB, 0.1M, pH 7.4) overnight at 4^0C. After the NiDAB reaction, sections were osmicated (1% OsO_4 (Electron Microscopy Sciences) in PB (pH 7.4) containing 5% sucrose for 60 min) and flat embedded in resin (Durcupan ACM, Sigma-Aldrich).

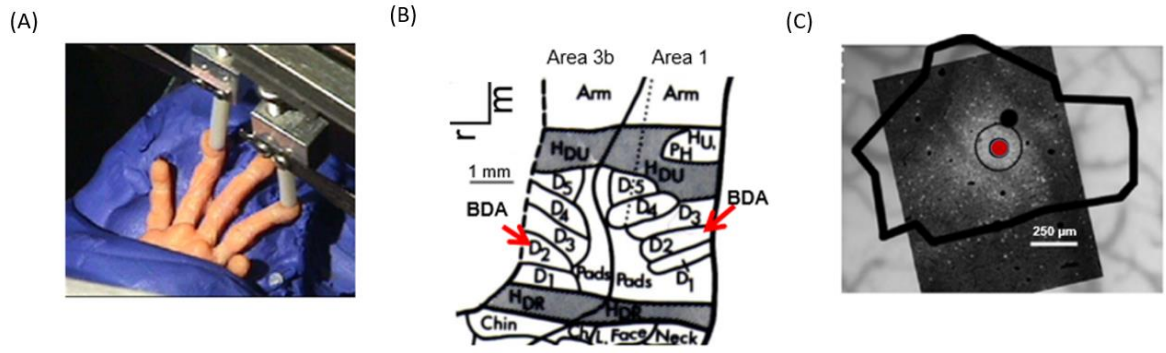

Figure 19. Targeted tracer injections

(A) *Finger stimulation during intrinsic signal optical imaging (IOS) and electrophysiological mapping to identify the injection site.* ***(B)*** *Mirror symmetric somatotopic maps of BA3b and BA1 of the squirrel monkey. Red arrows show the place of the tracer injections into a distal fingerpad representation.* ***(C)*** *Representative image showing the injection site in BA3b. Red dot shows the core region; black outline shows the halo of the injection site. Thick black contour outlines the area of the distal finger pad representation, which was activated in the IOS experiment.*

3.1.2. Identifying the areal borders

Both optical imaging and electrophysiological methods were used to delineate the somatotopic organisation of the hand region of S1. Borders between cortical areas were estimated based on electrophysiological mapping, RF characteristics, and optical imaging. As we were concerned that a high density of electrode penetrations could obstruct the transport of tracers by accidental tissue damage, we performed a limited number of electrode penetrations: a detailed map was made in M (46 penetrations), Mo (20 penetrations) and Pe (40 penetrations), only a few penetrations were used to identify the injection sites in V, and a moderate number of penetrations were made in J. In case M and J, Mo, Mac and Pe clear borders were placed based on optical imaging maps of the distal finger pads in BA3b and BA1; in case V, BA1 did not provide detectable optical signal during the experiment, and the 3b/1 border was placed based primarily on BA3b

activation. Previous studies showed that the optical imaging and electrophysiological maps were matching (Chen et al., 2001, 2003; Friedman et al., 2008).

3.1.3. Alignment of sections

An Olympus xy research microscope and Neurolucida (MicroBrightField Europe, E.K.) were used to made alignment and reconstructions. With a 4x objective mounted on the microscope, which is also used for the Neurolucida reconstruction (i.e. equipped with a motorised stage), sections were scanned with a software written in-house. Using blood vessel shapes and cut edges of the sections, scanned photographs of the 50 μm thick sequence of consecutive sections were aligned with the topmost sections and with each other. Beside, the serial section reconstruction function of Neurolucida was used to reconstruct the distribution of BDA-labelled structures. Finally, the Neurolucida drawings were matched with the images of the scanned sections, resulting in the serial reconstruction being aligned with the cortical surface.

3.1.4. Data collection and analysis

3.1.4.1. Reconstruction of axonal segments

Axonal patches lacking retrogradely labelled somata and spanning the supragranular and infragranular layers (projecting intra-areal and inter-areal in the different cases) (Figure 21) were selected and outlined by using Neurolucida (patch domains). In each patch three BDA-labelled axonal segments were reconstructed in 3D (Figures 21, 22; Tables 4-7). Three labelled axonal segments were also selected in each cortical region between the injection site and the patches and reconstructed (no-patch domains). These no-patch axonal segments were directed towards the patches due to the radial spread of the axons from the injection sites (Figures 21, 22) (Négyessy et al., 2013; Ashaber et al., 2013). The three-dimensional reconstructions of the patch and no-patch axons were made at high detail (100x-oil immersion objective magnification, NA 1.3, pixel size 0.3μ/pixel) allowing the faithful reconstruction of the tortuous path of the axonal segments and the localization of boutons formed by the axons. Most of the boutons were varicosities along axons, only a few terminal-like endings were found (Kisvárday et al., 1997). The two kinds of boutons were not distinguished in the analyses. All reconstructions were made in the grey matter of the injected hemisphere.

3.1.4.2. Measurements and data analysis

Quantitative measures of axonal properties were obtained as follows. Axon length, bouton number and the distances between boutons along an axonal segment were retrieved from Neurolucida's Neuroexplorer. Length was measured from the starting point, where the axon appeared on the top of the section. Inter-bouton interval was defined as the axonal distance to the preceding bouton. For axonal thickness measurements, digital images were captured with 100x objective magnification by a 2-megapixel CCD camera built in the Neurolucida setup. Thickness measurements were made by ImageJ at three different locations taken by chance along an axon and then averaged for each axon separately.

Bouton density, i.e. the number of boutons in a unit length, was calculated for the full length of an axonal segment. The variability of bouton distribution along an axon was characterised by the standard deviation (SD) of the distances between boutons. Bouton clustering was measured by counting the number of boutons that were farther from each other (in terms of inter-bouton intervals) than a separation length along an axon as a function of separation length. Separation length was increased from 1 μm to 150 μm by 1 μm steps. This measurement resulted in a sharp decline of the number of bouton-clusters as the separation length increased, reaching a cluster number of 1 at the full length of the axon. Conversely, the maximum number of clusters i.e., the total number of boutons of an axon, would be counted when the separation length became shorter than the distance between any two boutons. To obtain a single value for bouton clustering for each axon, the data were transformed into a log-linear function and the slope of the fitted line defined clustering. A larger negative value indicated larger clustering propensity of the boutons along the axon. Figure 20A illustrates the measure of bouton clustering after pooling the measures of the patch and no-patch axons.

Tortuosity is a measure of the length of an axon relative to the straight line connecting the endpoints. A caveat in determining tortuosity is that measurements can be sensitive to the length of the axon due to the sharpness of turns. To handle this issue, it was found that making multiple tortuosity measures along the length of an axon revealed length values that allowed for the comparisons of tortuosity of different classes of axons (Stepanyants et al., 2004). To determine the length value that best distinguished between the patch and no-patch axonal segments, we plotted the cumulative change of tortuosity as a function of a fixed 10 μm incremental increase of the axonal length (Figure 20B).

After separately pooling the measures from the patch and no-patch axons, the graphical representation allowed us identifying the first 40-µm segment of the axons (beginning at the start point) as the length where the tortuosity of patch and no-patch axons differed clearly and exhibited low variability (Figure 20B). Consequently, we used as an estimate of the tortuosity of patch and no-patch axons, the tortuosity of the first 40-µm segment.

Directional differences in the projection of axon groups were determined using ImageJ in 2D, ignoring slice depth. Each group was formed by selecting three axons found within the supragranular or infragranular patches, or by selecting three axons outside of the patches to which those axons were directed (Figure 21, 22). The direction was determined in the $0\text{-}180^0$ area relative to a reference line drawn between the injection site and the patches in each section. The ordered projection of individual axons was measured by calculating the difference in the direction of a single fibre's path from its group mean in degrees. A measure of the convergence of boutons (bouton-convergence) was determined in the Neuroexplorer. The mean distance of a bouton of a reconstructed axon segment from the two nearest BDA-labelled boutons of other axons was measured for each patch and no-patch axon.

For the factorial ANOVA we averaged the data obtained from each patch and no-patch axonal segment localised either in the supra- or the infragranular layer in the different categories of the different cases. The sample size (number of means) contributing to each category is summarised in Table 3. Note, because of the lack of infragranular data in case M (see details in the 1st subsection of the Results) the laminar comparisons of patch and no-patch axons had to be omitted as data were available only in two cases with BA1 injections.

Statistical analyses were performed in Statistica (version 13., TIBCO Software Inc. (2018), http://tibco.com.) and MS Excel. Principal Component Analysis (PCA) and stepwise logistic regression were done in Statistica. If not mentioned otherwise, measurements and computations were made in MATLAB and Python.

DOI:10.14753/SE.2023.2830

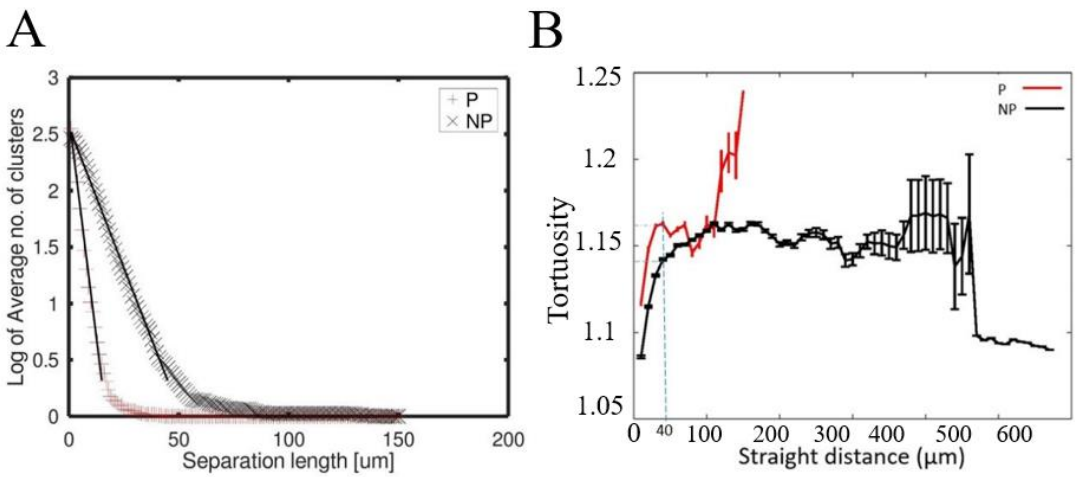

Figure 20. Determination of bouton clustering and tortuosity

(A) *Sharply decreasing number of clusters as a function of increasing axon length. For the population of axon segments from the six cases, the linear fit has a slope of -0.16 (intersection: 2.67) for the patch axons and -0.05 (intersection: 2.57) for the no-patch axons.* ***(B)*** *A sigmoid-like increase of measured tortuosity resulting by an incremental 10µm elongation of the axons from the start to the end point as determined from the population of patch and no-patch axons. Dashed blue lines show tortuosity values at the 40 µm length used in this study. Means and standard errors are shown. P: patch axons, NP: no-patch axons.*

Table 3. Sample size after averaging is shown by anatomical categories. Means of supra- and infragranular layers were obtained in the different cases. Laminar comparisons of P and NP axons have to be omitted due to the small number of cases. BA3b, BA1: injected area, Intra: intra-areal axon, Inter: inter-areal axon, FF: feed-forward axons, FB: feedback axons, supra: supragranular axons, infra: infragranular axons.

Total no	144
BA3b	24
BA1	20
P or NP	22
Intra or Inter	22
FF	12
FB	10
Supra	24
Infra	20
P-Intra or P-Inter	11
NP-Intra or NP-Inter	11

3.2. Studies of neuronal connectivity in rodents

3.2.1. Surgical procedure

Anesthesia was induced with a combination of intraperitoneally injected Ketamine (80 mg/kg; Ketasol, AniMedica) and Xylazine (5 mg/kg; Xylasol, Animedica) and maintained with 2% Sevofluran (SEVOrane). The head was then fixed on a stereotactic frame (Model 1900; Kopf Instruments) and ophthalmic ointment was applied to the eyes to avoid drying. Postoperative pain medication included administration of meloxicam (Metacam, Boehringer Ingelheim; 1 mg/kg subcutaneously). At the end of the experimental procedures, mice were deeply anesthetized with thiopental sodium (150 mg/kg, i.p.) and transcardially perfused with a fixative made of 4% paraformaldehyde, 15% picric acid in 0.1 M phosphate-buffer (PB), pH 7.2–7.4. Brains were cut into 50 μm thick coronal sections using a vibratome (Leica Microsystems VT1000S, Vienna, Austria).

3.2.2. Anterograde viral tracing

VIP-ires-cre mice (N=2) were unilaterally injected with a AAV5.CamKIIa-hChR2(HI34R)-mCherry (This AAV expresses hChR2(H134R)-mCherry driven by a neuron CamKII promoter) (5.1 3 10^12 GC/mL, Addgene #26975) into the mediodorsal thalamus (MD) (coordinates from bregma: AP: -1.58mm; ML: +0.44 mm; DV: -3.20 mm) in a volume of 300 nL. Mice were allowed to recover for 3 weeks before perfusion to ensure adequate viral transduction.

3.2.3. Immunohistochemistry

For the quantification of VIP+ INs, free-floating sections were incubated in primary antibody solution [rabbit antibody against VIP, diluted 1:4000] containing 2% normal goat serum (NGS), 0.3% Triton X-100 (TX) in Tris-buffered saline (TBS-T; pH 7.4) for two days at 6^0C and then in secondary antibody [biotinylated goat anti-rabbit, diluted 1:500] overnight. After washing, sections were incubated in an ABC complex solution (1:100) made up in TBS, followed by diaminobenzidine (DAB) as a chromogen (0.5 mg/mL in TB) and 0.003% H2O2, as the electron donor, for 5 min. The sections were mounted onto gelatin-coated slides, dehydrated in an ascending ethanol series followed by an incubation in butylacetate and cover slipped with Eukitt. Sections immunolabeled for VIP were used to assess the number of VIP + INs (n = 4 mice) by using the Neurolucida software (MBF Bioscience). Borders of the insular cortex (IC) were outlined

with the help of consecutive Nissl stained sections according to a mouse brain atlas (Shi et al, 2008).

4. Results

4.1. Primate studies

4.1.1. Number, distribution and morphology of reconstructed axons and boutons

Our sample of anterogradely labelled axons consisted of 144 3D reconstructed axons forming connections within and between somatosensory BA3b and BA1 after a focal injection of BDA into BA3b (n=3) and BA1 (n=3) in six squirrel monkeys (Figure 21; Tables 6, 7). An equal number of patch and no-patch axons were selected for analysis; however, a larger number of axonal segments were reconstructed following BA3b (n=84) injections compared to BA1 (n=60) injections (Tables 6, 7). This was mainly due to the low number of available axons in case M, where an oblique cut of the sections prevented the reconstruction of infragranular axons with sufficient length (Tables 6, 7, 9). Tables 6 and 7 also show the number of intra-areal and inter-areal axons reconstructed in the supragranular and infragranular layers of the different cases. Sample images of BDA labeling around each injection site and the spacing of bouton varicosities are shown on Figure 22.

Axons formed numerous boutons both within and outside the axonal patches irrespective of the injected area, pathway (intra- vs. inter-areal) or laminar (supra- vs. infragranular) location (Figure 22; Tables 8, 9). Figure 22 shows the Neurolucida reconstructions of the population of patch (red) and no-patch (blue) axons from each of the six cases. Major morphological differences appeared between the patch and no-patch axons concerning their length (distance between the start and end points of the reconstructed segments), direction (how parallel they are), number of boutons and bouton density. We found a larger number of boutons was formed by patch axons compared to no-patch axons (Wilcoxon matched pairs test; $p = 0.001$, Tables 5, 6). This observation was even more compelling when considering that the length of patch axons was significantly shorter than that of the no-patch axons (Wilcoxon matched pairs test; $p < 0.001$, Tables 10, 11). Details of the number of boutons and length of axons as they relate to the different categorization of axons (patch, no-patch, feedforward, feedback, intra- or inter-areal, BA3b or BA1) and cases are summarised in Tables 8-11.

DOI:10.14753/SE.2023.2830

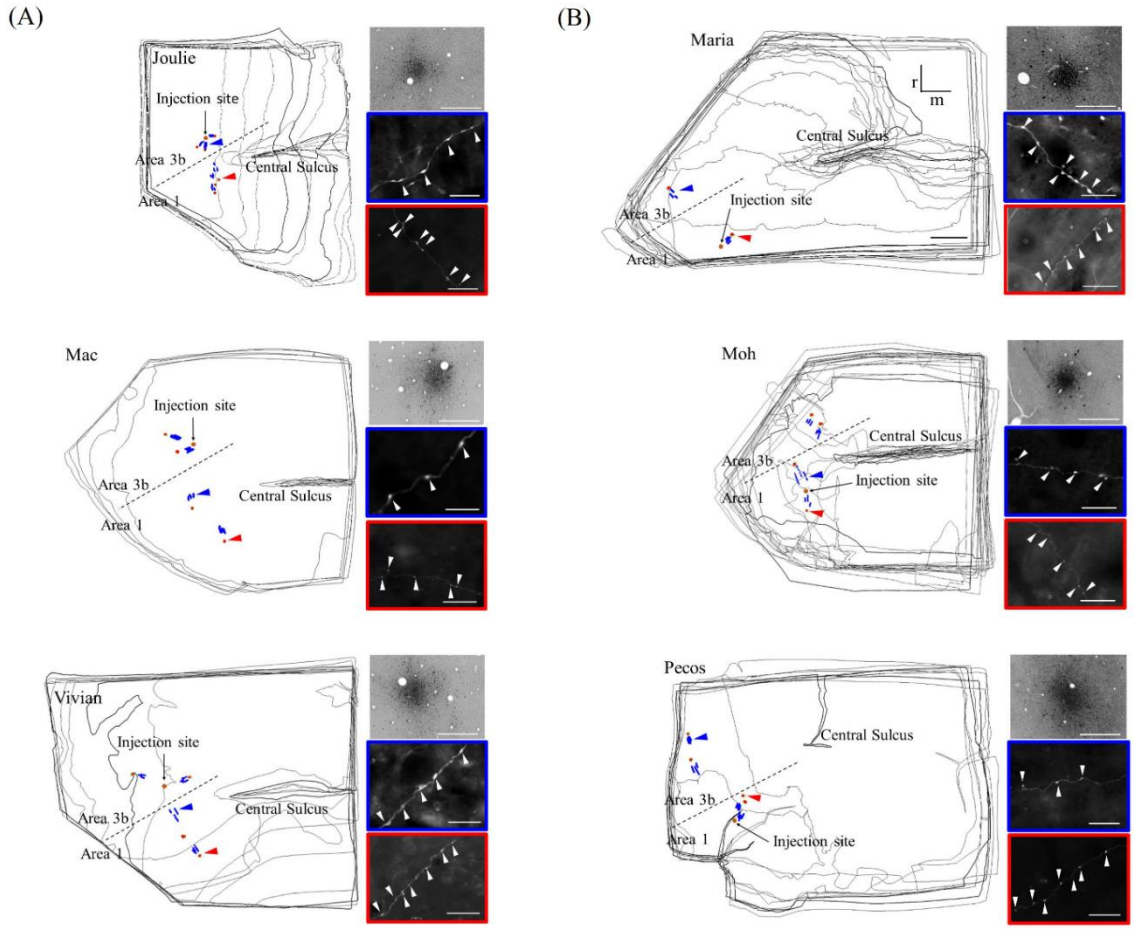

Figure 21. Distribution (left drawings) and light microscopic appearance (right panels) of the reconstructed long distance axonal segments

(A) *BA3b injections,* ***(B)*** *BA1 injections. Distribution of the reconstructed axons are shown on the merged series of sections in the six cases. Anterograde labelling is represented by patch forming axons (red) and no-patch forming axons (blue) in the hand representation region of BA3b and BA1. The name of cases is indicated in the upper left corner. CS: central sulcus, dashed line: border between BA3b and BA1. Orange circle shows the injection site located in the representation of a distal finger pad. The orientation bars on B (case M) apply to all panels; r: rostral, m: medial. Scale bar on B (case M) represents 1 mm, and applies also to the other cases. Right panels: light microscopic images enclosed by a colour border are taken from the sites indicated by the arrowheads of the same colour on the drawings. Top panels show the injection site. Middle and lower panels show, respectively, no-patch axons and patch forming axonal segments with numerous boutons in the form of varicosities (white arrowheads). Scale bar: 25 µm (right, top), 20 µm (right, middle and bottom).*

Table 4. Total number of reconstructed axons labelled by BA3b injection in the different pathways studied. P: patch, NP: no-patch, FF: feed forward, intra: intra-areal, inter: inter-areal, Supra: supragranular; Infra: infragranular.

injected area	BA3b								
	P				NP				
	FF		intra		FF		intra		total
Cases	supra	infra	supra	infra	supra	infra	supra	infra	
J	6	3	6	3	6	3	6	3	36
Mac	3	3	3	3	3	3	3	3	24
V	3	3	3	3	3	3	3	3	24
Supra/Infra	12	9	12	9	12	9	12	9	84
FF/Intra	21		21		21		21		84
P/NP	42				42				84
BA3b	84								84

Table 5. Total number of reconstructed axons labelled by BA1 injection in the different pathways studied. FB: feedback. Other conventions are the same as in Table 4.

injected area	BA1								
	P				NP				
	FB		intra		FB		intra		total
Cases	supra	infra	supra	infra	supra	infra	supra	infra	
M	3	0	3	0	3	0	3	0	12
Mo	3	3	3	3	3	3	3	3	24
P	3	3	3	3	3	3	3	3	24
Supra/Infra	9	6	9	6	9	6	9	6	60
FB/Intra	15		15		15		15		60
P/NP	30				30				60
BA1	60								60

DOI:10.14753/SE.2023.2830

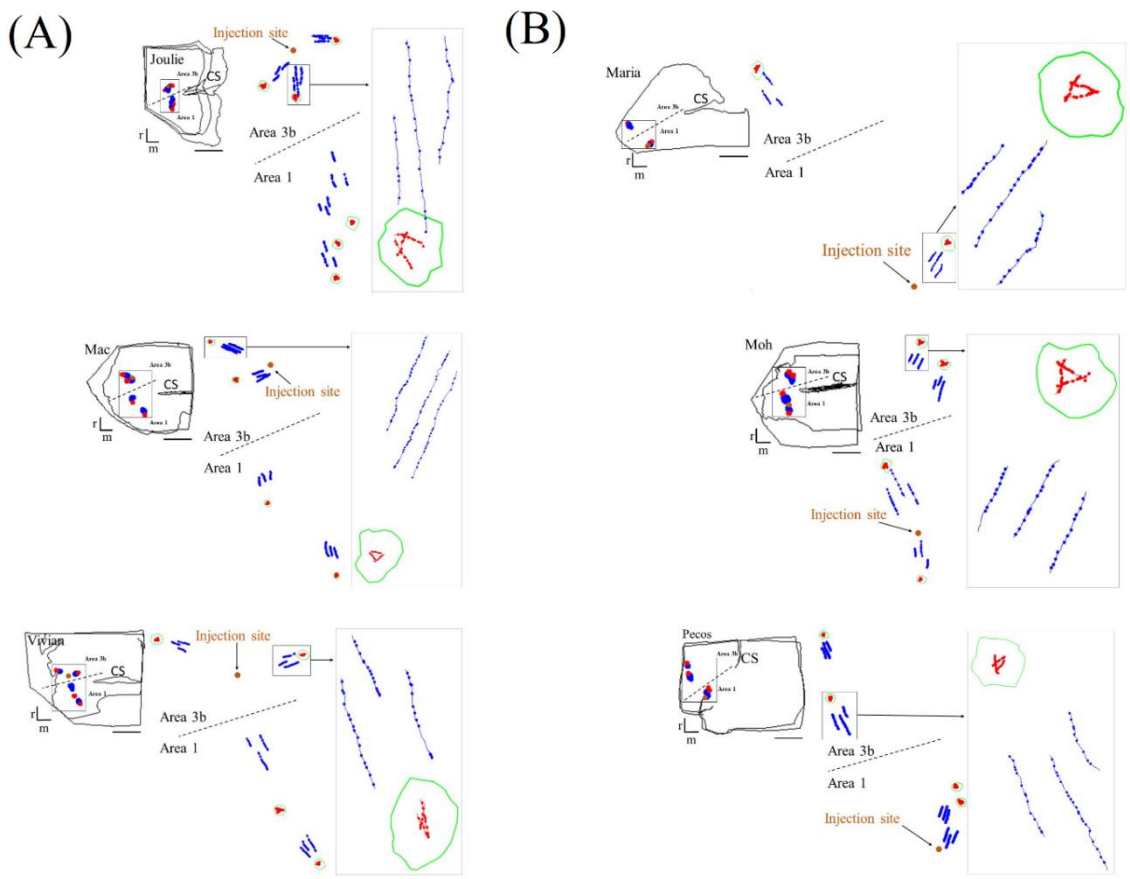

Figure 22. Examples of reconstructions illustrating the morphology of the patch and no-patch axonal segments in the six cases

(A) BA3b injections, ***(B)*** *BA1 injections. For each case: Top left corner: miniature diagram of the section outlines including the reconstructed axons shown at higher magnification in the middle. Middle: enlarged view of the areas (demarcated by the rectangle in the section outlines on left) including the reconstructed axonal segments. Orange dot shows the location of the injection site. Right: high magnification view of the areas outlined by the rectangle (arrow). Note that on the right the high-resolution view is taken from a single section. Axon arborization patches are outlined by green contours. Patch axons and no-patch axons are shown in red and blue, respectively. Boutons formed by the reconstructed axons are marked by dots resulting in the beaded form of the axonal segments. Examples include axons both from the supra- and infragranular layers except case M, where only supragranular axons could be reconstructed. Note the shorter length, highly variable direction and high bouton density of axons within the patch compared to the no-patch axons. Dashed line represents the border between the two areas of the somatosensory cortex. r: rostral, m: medial. Scale bar: 1 mm.*

Table 6. Number of boutons in the different pathways labelled by BA3b injection in the different cases. Conventions are the same as in prior tables.

injected area	BA3b								
	P				NP				
	FF		intra		FF		intra		total
Cases	supra	infra	supra	infra	supra	infra	supra	infra	
J	63	38	65	38	42	18	42	21	327
Mac	37	34	25	57	20	23	58	55	309
V	42	62	20	27	38	26	34	24	273
Supra/Infra	142	134	110	122	100	67	134	100	909
FF/Intra	276		232		167		234		909
P/NP	508				401				909
BA3b	909								909

Table 7. Number of boutons in the different pathways labelled by BA1 injection in the different cases. Conventions are the same as in prior tables.

injected area	BA1								
	P				NP				
	FB		intra		FB		intra		total
Cases	supra	infra	supra	infra	supra	infra	supra	infra	
M	54	0	46	0	31	0	31	0	162
Mo	52	43	21	50	28	36	40	29	299
P	37	43	28	21	41	50	44	25	289
Supra/Infra	143	86	95	71	100	86	115	54	750
FB/Intra	229		166		186		169		750
P/NP	395				355				750
BA1	750								750

Table 8. Length (µm, mean±sd) of the reconstructed axonal segments of the different pathways labelled by BA3b injection. Conventions are the same as in prior tables.

injected area	BA3b				
	P		NP		grand avg±sd
Cases	FF	intra	FF	intra	
J	59.96±12.17	61.21±10.64	123.13±40.86	105.67±31.21	87.49±11.57
Mac	62.25±17.09	108.85±30.39	195.8±64.81	224.63±137.55	147.88±46.71
V	107.6±55.43	85.3±15.64	183.4±41.21	184.88±53.87	140.29±15.93
FF/Intra	76.60±19.33	167.44±8.38	171.73±11.21	125.22±45.42	135.24±14.61
P/NP	122.02±5.47		148.47±17.10		135.24±5.81
BA3b	135.24±5.81				135.24±5.81

Table 9. Length (µm, mean±sd) of the reconstructed axonal segments of the different pathways labelled by BA1 injection. Conventions are the same as in prior tables.

injected area	BA1				
	P		NP		grand avg±sd
Cases	FB	intra	FB	intra	
M	86.06±10.85	70.73±3.21	139.96±19.00	100±25.28	99.19±8.32
Mo	102.45±31.21	114.83±27.30	179.9±35.82	337.98±158.98	183.79±55.30
P	64±11.59	63.76±12.65	291.76±126.65	179.61±52.59	149.78±46.84
FB/Intra	84.17±9.42	83.11±9.91	203.87±47.37	205.86±57.67	144.25±20.44
P/NP	83.64±0.24		204.87±5.15		144.25±2.45
BA1	144.25±2.45				144.25±2.45

4.1.2. Patch and no-patch axonal segments are distinctively different

Only the classification of axons by patch designation (patch or no-patch) showed differences in the distribution of the quantitative properties of the axons (Figures 23, 24). Greater bouton density, convergence, clustering and more consistent bouton spacing were seen in patches than in no-patch segments. Axon measures showed thicker axons for no-patch segments and more similar directionality of axons than patch segments without differences in tortuosity (Figure 23). These morphological distinctions were independent of whether the projections originated from BA1 or BA3b (Figure 24) or whether the axons were intra- or inter-areal or feedback or feedforward projections or whether the segments

were located in supra- or infragranular layers (Figures 25-26). Factorial ANOVA supported these observations. After including categorical variables injection area (BA3b, BA1), patch designation and pathway type (intra- and inter-areal), the factorial analysis resulted in a significant major effect only between patch and no-patch axons and not between interactions (Table 10). Post hoc comparisons resulted in highly significant differences in all variables except for the measure of tortuosity.

Based on these observations, we were interested in determining the relative contribution of the different variables to the patch-like properties of the axons. For this, we utilised principal component analysis (PCA) to account for the variability and stepwise logistic regression to determine predictors of patch designation across the different variables.

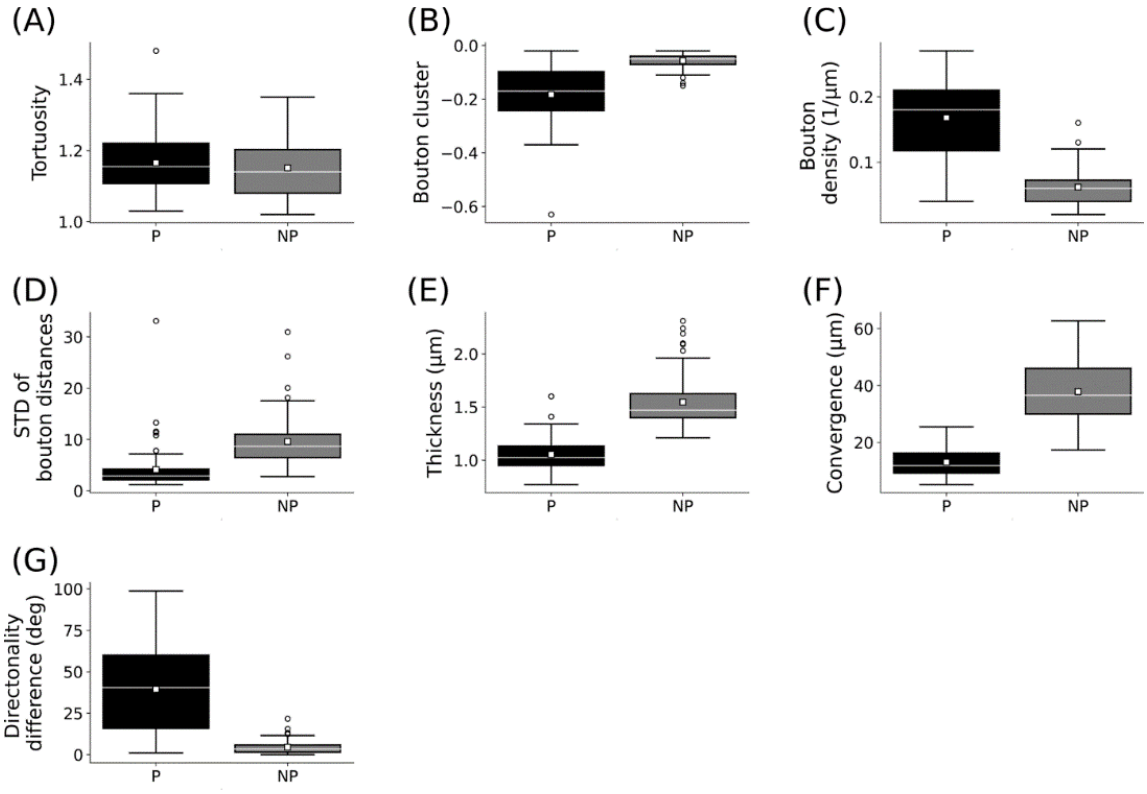

Figure 23. Box plots of measured bouton and axonal characteristics of patch (P: 72) and no-patch (NP: 72) axons

(A) *Tortuosity (the first 40 µm segment of the axons beginning with the starting point),* ***(B)*** *bouton clustering (lower values indicate higher clustering),* ***(C)*** *bouton density,* ***(D)*** *bouton distance std (standard deviation of inter-bouton intervals along the axons),* ***(E)*** *thickness,* ***(F)*** *convergence (or bouton-convergence, the distance of a bouton of a reconstructed axon from the 2 nearest boutons of unconnected axons), and* ***(G)*** *difference*

of directionality of the axonal segments. Here and in the following plots, panels A-E show individual axonal properties and F and G present collective axonal properties. Horizontal line: median, small square: mean, box: 25%-75%, whiskers: non-outlier range, circles outliers representing data > 1.5 x height of the box.

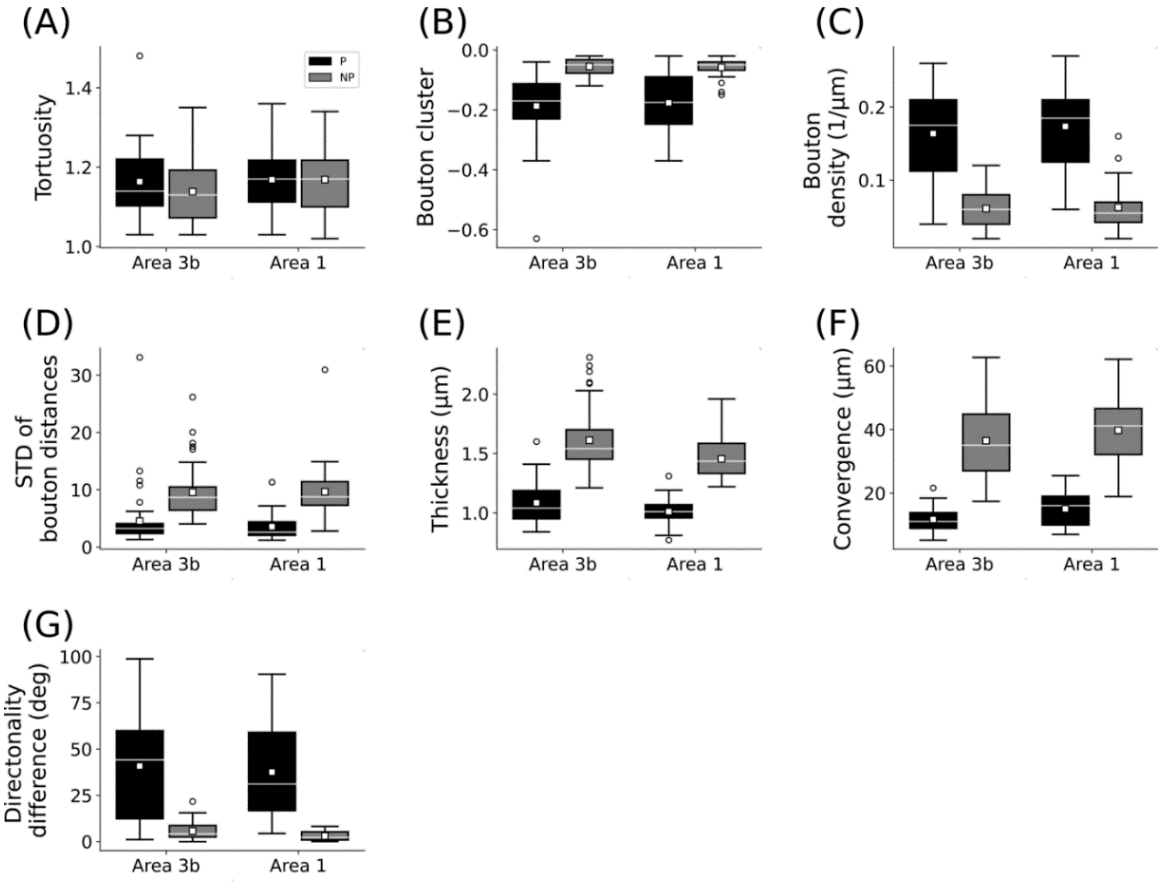

Figure 24. Box plots showing similar characteristics of patch (P) and no-patch (NP) axons following injection of BA3b and BA1. BA3b: n = 42 P, 42 NP axons. BA1: 30 P, and 30 NP axons

(A) *Tortuosity (the first 40 µm segment of the axons beginning with the starting point),* ***(B)*** *Bouton clustering (lower values indicate higher clustering),* ***(C)*** *Bouton density,* ***(D)*** *Bouton distance std (standard deviation of inter-bouton intervals along the axons),* ***(E)*** *Thickness,* ***(F)*** *Convergence (or bouton-convergence, the distance of a bouton of a reconstructed axon from the two nearest boutons of unconnected axons), and* ***(G)*** *Difference of the directionality of the axonal segments. Conventions are the same as in Figure 23.*

DOI:10.14753/SE.2023.2830

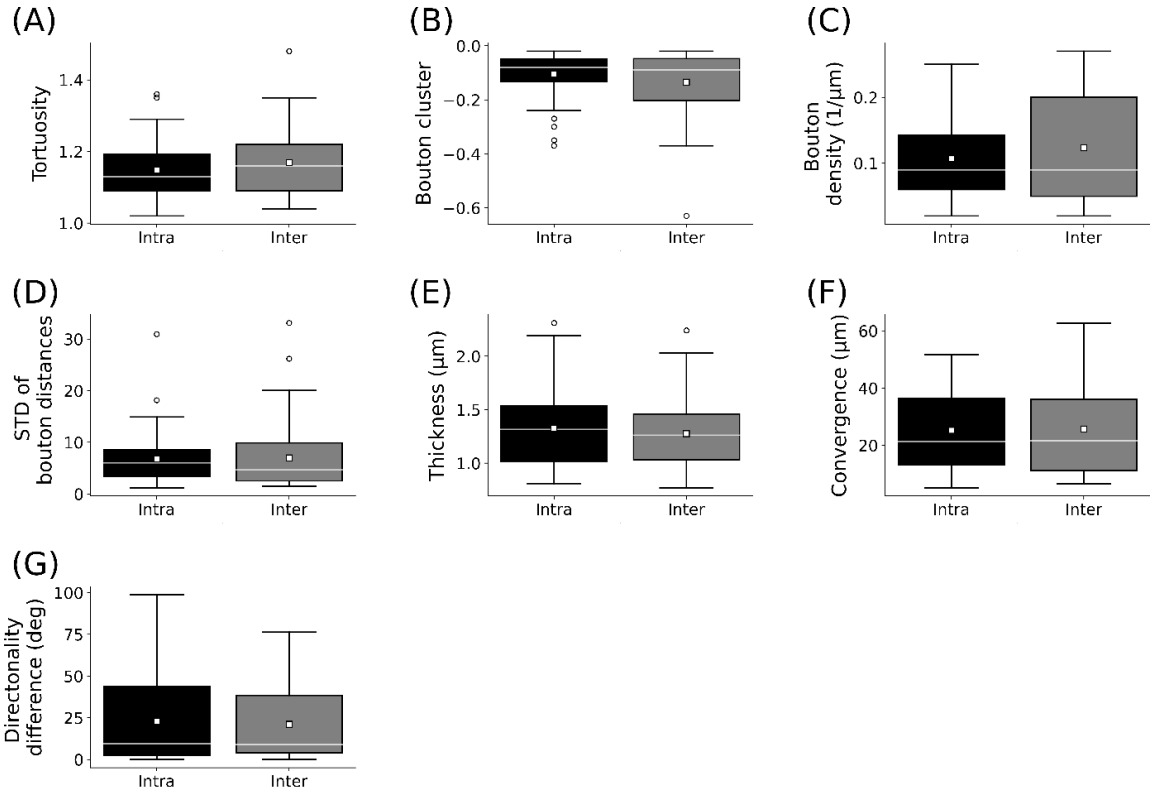

Figure 25. Comparison of variables between the intra-areal and inter-areal axons

(A) *Tortuosity (the first 40 µm segment of the axons beginning with the starting point),* ***(B)*** *Bouton clustering (lower values indicate higher clustering),* ***(C)*** *Bouton density,* ***(D)*** *Bouton distance std (standard deviation of inter-bouton intervals along the axons),* ***(E)*** *Thickness,* ***(F)*** *Convergence (or bouton-convergence, the distance of a bouton of a reconstructed axon from the two nearest boutons of unconnected axons), and* ***(G)*** *Difference of the directionality of the axonal segments. Conventions are the same as in Figure 23.*

DOI:10.14753/SE.2023.2830

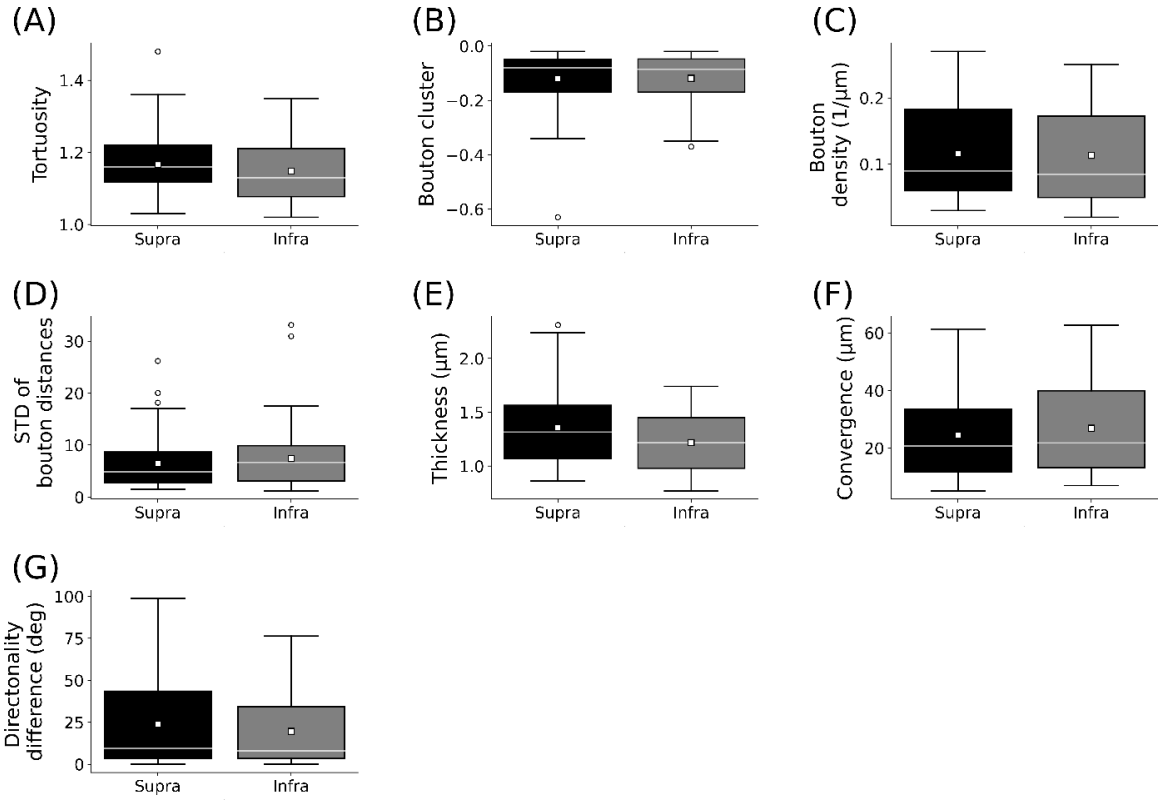

Figure 26. Comparison of variables between the supragranular and infragranular axons

(A) *Tortuosity (the first 40 µm segment of the axons beginning with the starting point),* ***(B)*** *Bouton clustering (lower values indicate higher clustering),* ***(C)*** *Bouton density,* ***(D)*** *Bouton distance std (standard deviation of inter-bouton intervals along the axons),* ***(E)*** *Thickness,* ***(F)*** *Convergence (or bouton-convergence, the distance of a bouton of a reconstructed axon from the two nearest boutons of unconnected axons), and* ***(G)*** *Difference of the directionality of the axonal segments. Conventions are the same as in Figure 23.*

DOI:10.14753/SE.2023.2830

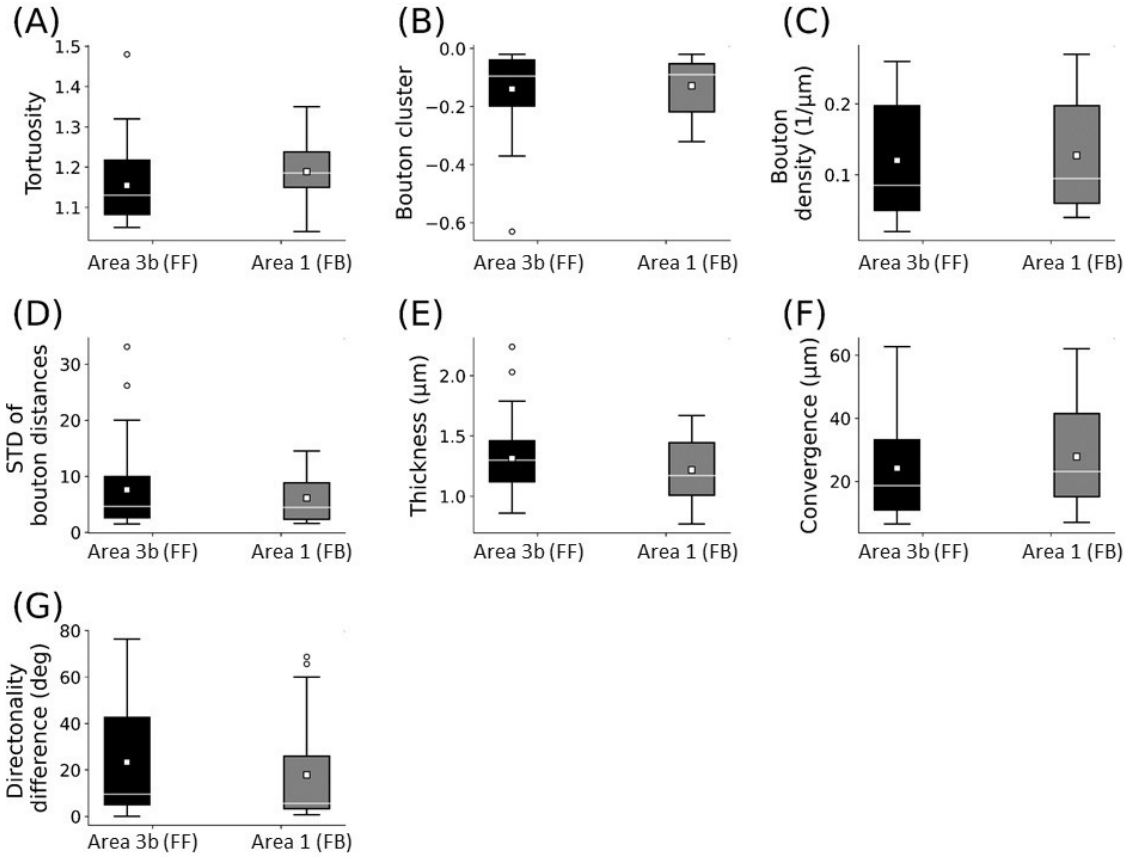

Figure 27. Comparison of variables between the feed-forward (FF) and feed-back (FB) inter-areal axons in BA3b and BA1

(A) *Tortuosity (the first 40 µm segment of the axons beginning with the starting point),* ***(B)*** *Bouton clustering (lower values indicate higher clustering),* ***(C)*** *Bouton density,* ***(D)*** *Bouton distance std (standard deviation of inter-bouton intervals along the axons),* ***(E)*** *Thickness,* ***(F)*** *Convergence (or bouton-convergence, the distance of a bouton of a reconstructed axon from the two nearest boutons of unconnected axons), and* ***(G)*** *Difference of the directionality of the axonal segments. Conventions are the same as in Figure 23.*

DOI:10.14753/SE.2023.2830

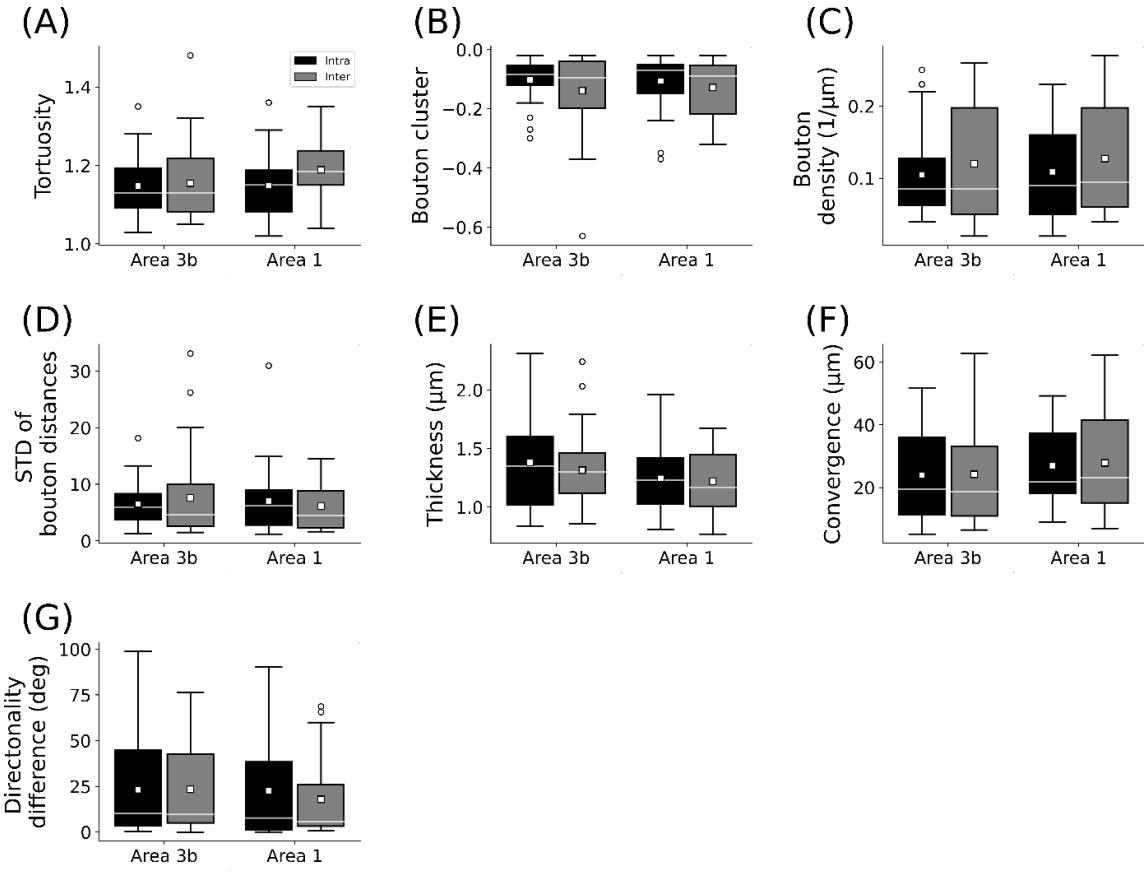

Figure 28. Comparison of variables within and between areas and injection sites: intra-areal and inter-areal axons

(A) *Tortuosity (the first 40 µm segment of the axons beginning with the starting point),* ***(B)*** *Bouton clustering (lower values indicate higher clustering),* ***(C)*** *Bouton density,* ***(D)*** *Bouton distance std (standard deviation of inter-bouton intervals along the axons),* ***(E)*** *Thickness,* ***(F)*** *Convergence (or bouton-convergence, the distance of a bouton of a reconstructed axon from the two nearest boutons of unconnected axons), and* ***(G)*** *Difference of the directionality of the axonal segments. Conventions are the same as in Figure 23.*

4.1.3. Structural properties distinguishing patch and no-patch axons

4.1.3.1. Principal component analysis (PCA)

First, we performed PCA to see the combined effect of the variables as well as their power in distinguishing patch and no-patch segments. Before the analysis, data were normalised such that each variable had zero mean and unit standard deviation. PCA resulted in two significant principal components (PCs) (Figure 29A). However, the two PCs differed greatly as PC1 explained 52% of the variance in contrast to the 15% explained by PC2. Most importantly, in agreement with the results of ANOVA (Table

12), PCA resulted in the clustering of the axons according to their patch designation (Figure 29B). In addition, patch and no-patch axons were grouped by PC1 without additional separation by adding PC2. This observation was in accordance to the different magnitude of variance explained by the two PCs (Figure 29A). Figure 29C shows that all the variables, which exhibited significant differences between the patch and no-patch axons by ANOVA (Table 10), contributed highly to PC1 and had little load on PC2. In contrast, tortuosity had a high load on PC2 and minimally contributed to PC1. Analysis of the importance of the variables by their explained variance in PC1 supported the above observation and showed that bouton-density followed by bouton-convergence had the highest power while tortuosity exhibited almost no importance (Figure 29D).

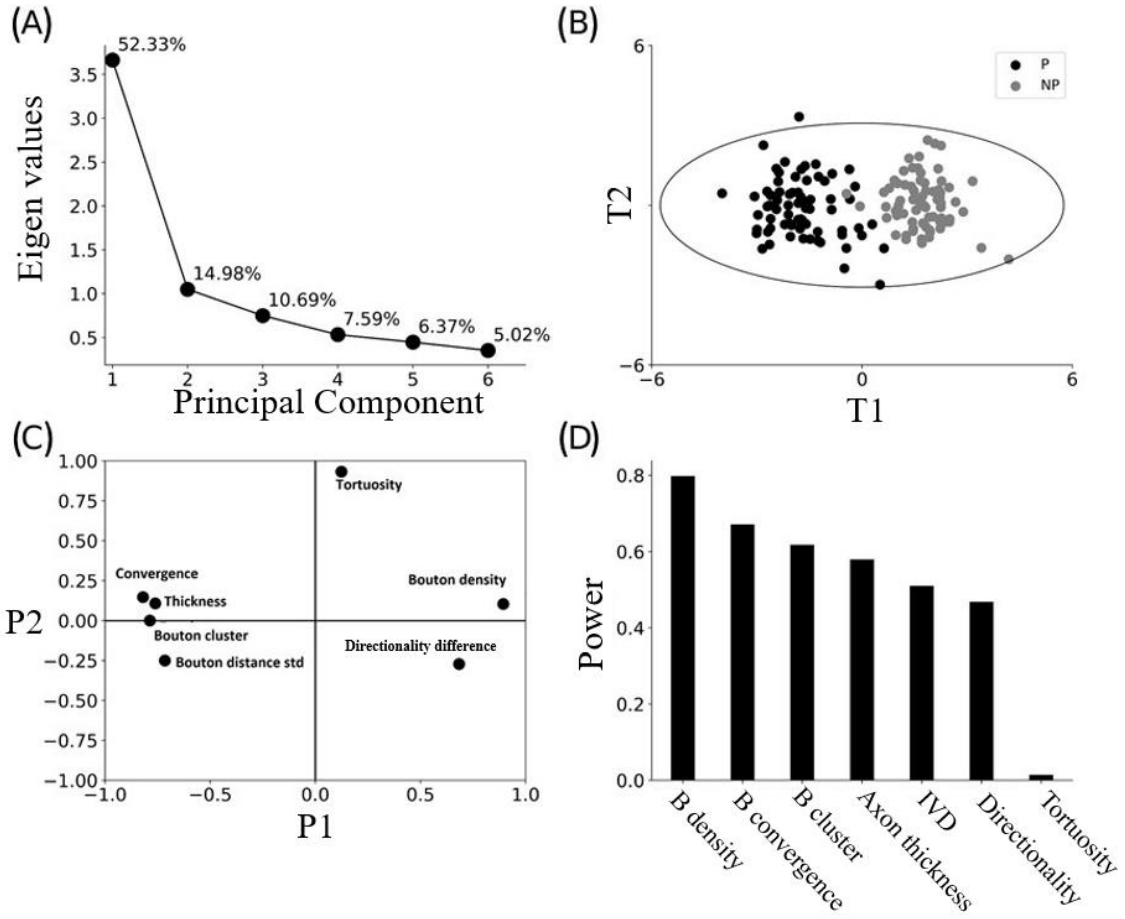

Figure 29. PCA analysis identifies clustering only by patch designation

(A) *Scree plot showing the eigenvalues and the percentage of variance explained by the six principal components.* ***(B)*** *Case-wise analysis shows the tendency of the grouping of patch (P) and no-patch (NP) axons, black and grey circles respectively, along the two principal components. Distribution of the scores (distances of transformed values of the variables from the origin along the PCs) of axons for the first principal component (T1)*

plotted against the scores for the second principal component (T2). Ellipse outlines ±3sd and indicates the presence of a single patch outlier in the dataset. ***(C)*** *Distribution of the loading factors (transformed values showing the contribution of the variable to the PCA model) P1 and P2 for the first and second principal components. The greater a variable is away from zero, the more influence that variable has. A diagonal positioning in opposite quadrants means negative correlation between the variables.* ***(D)*** *The importance of the variables measured by the modelling power, which is defined as the explained standard deviation.*

Table 10. Results of multivariate test of significance by factorial ANOVA (df: 7, 30) and post hoc comparisons (Scheffe test, df: 36). Significant p-value is highlighted by red. Injection-Area: BA3b vs. BA1; Patch Designation: P vs. NP axons; Areal Localization: intra-areal vs. inter-areal axons. Interactions are indicated by the "*" symbol. Other conventions are the same as in prior tables.

ANOVA	F	p values	Scheffe	p values
Injection-Area (IA)	1.09	0.395	Tortuosity	0.672186
Patch Designation (PD)	72.61	0.000	Bouton cluster	2.35E-09
Areal Localization (AL)	0.94	0.490	Bouton density	6.93E-12
IA * PD	0.39	0.899	Bouton distance std	6.93E-07
IA * AL	0.49	0.837	Bouton-convergence	1.03E-14
PD * AL	1.41	0.238	Directionality difference	6.88E-14
IA * PD * AL	0.49	0.831	Thickness	8.20E-13

4.1.3.2. Stepwise logistic regression

To identify the variables that determine patch designation of the axonal segments the best, we applied logistic regression. First, we evaluated marginal effects to select the variables with a significant outcome in the distinction of patch and no-patch axons (Table 11). All variables that exhibited significant differences by ANOVA (Table 10) showed a significant contribution to the regression. The significant variables were then entered into a stepwise model according to model fit statistics (estimation of the constant by minimising fitting error) in the marginal model (Table 12). Bouton-convergence provided the best optimal fit in the regression model and entered first into the model, which resulted in a significant improvement of the classification (Table 13). Interestingly, in marginal models starting among the other six variables only bouton-density exhibited significant contribution to the regression (Table 14). This observation was in close correspondence with the result of the PCA (Figure 29D). Entering bouton-density into the stepwise model with bouton-convergence had the highest predicting power of patch designation of the

axonal segments (Table 13). Subsequent marginal effects showed no significant contribution by any of the remaining five variables in the regression (Table 16). The constants estimated in the two-step model are summarised in Table 14. The sign of the constants shows that bouton-convergence, i.e. the distance of boutons formed by neighbouring, unconnected axonal segments, was positively correlated (indicating larger distances) with the probability of being a no-patch axon whereas bouton-density showed negative correlation with this probability.

The performance of the model was checked by plotting the distribution of the predicted probabilities from the stepwise logistic regression (Figure 30). The full model that included bouton-convergence and bouton-density resulted in only a few erroneous classifications (Figure 30A). Only three no-patch axons (grey bars to the left of the dotted line) were categorised as patch axons; similarly, only three patch axons were misidentified as no-patch axonal segments (Figure 30B and D). As a result, the observed and predicted rates were only slightly different in the full model (Figure 31). Accordingly, the difference between the observed and predicted rates distributed around zero (Figure 31A, B) and the frequencies of occurrence and means of these two rates were nearly identical (Figure 31C, D). Interestingly, a closer look at the distribution of the predicted probabilities showed that bouton-convergence alone was an excellent predictor of patch designation (Figure 31B). In the final model bouton-convergence outperformed bouton-density in detecting patch axons, whereas the opposite was true in recognizing no-patch axons (Figure 31C, D). Overall, bouton-convergence performed better than bouton-density in predicting patch designation by our stepwise logistic regression model. In spite of this, the model showed considerable prediction power and very high accuracy (Figure 32). As shown in Figure 32A, selecting as few as 10% of the axons that were best predicted by the model doubled the ratio of correct predictions to that found in a randomly selected 10%. This advantage of the model against random sampling disappeared only by using larger than 40% of the axons. Also, a 0.99 accuracy was identified by the receiving operating characteristic (ROC) curve (Figure 32B). The sharp rise of the curve indicates that the model (solid line) had a very high true positive rate at a very low level of false positive classification rate. Our model achieved a maximum sensitivity (true positive rate) at a low, approximately 0.2 false positive rate (1-specificity). The best optimal performance resulted in 0.96 (138/144) true positive and 0.04 (6/144) false positive rates (Figure 31A).

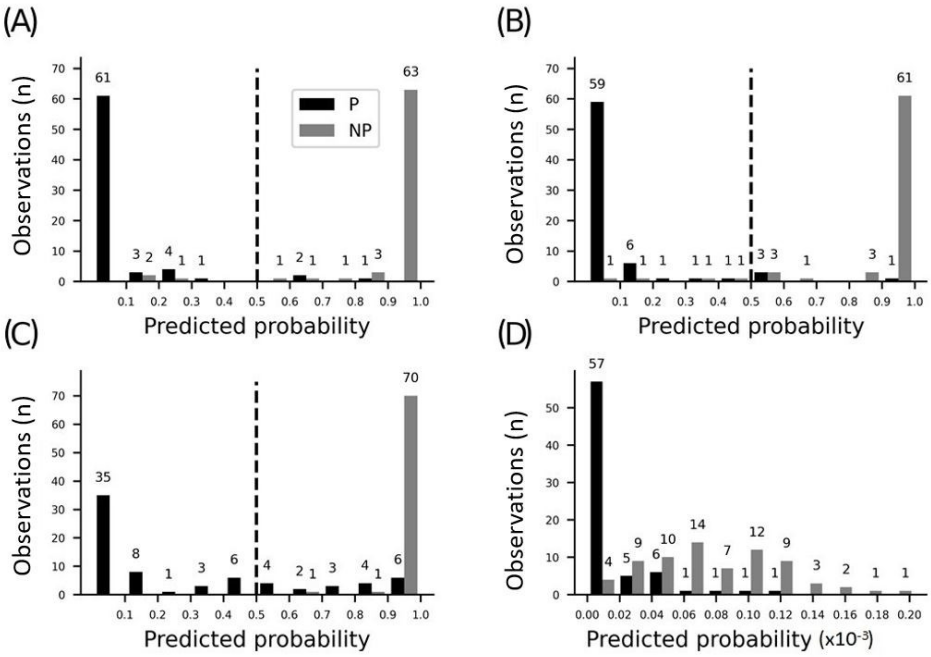

Figure 30. Predicted probabilities of identifying axon types (P vs. NP) in stepwise logistic regression models by applying a threshold of 0.5. Distribution of predicted probabilities:

(A) of the final model with bouton-convergence and bouton-density as the predictor variables; (B) of a model with bouton-convergence as a single predictor variable; (C) contributed by bouton-convergence in the final model; (D) contributed by bouton-density in the final model.

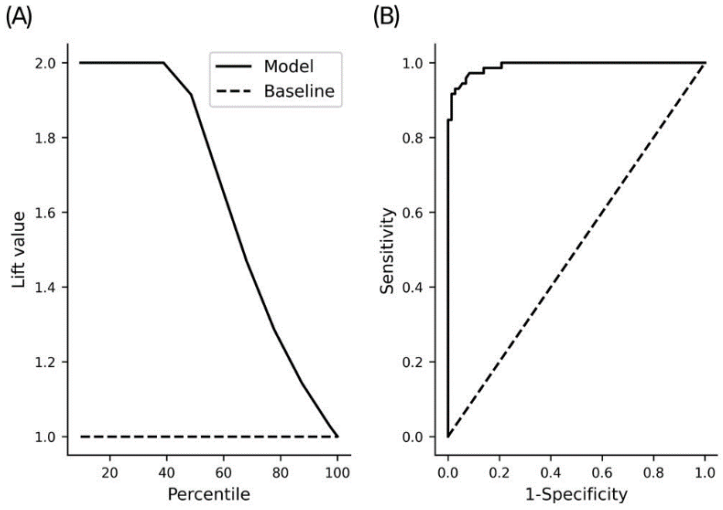

Figure 31. Overall, model performance of the stepwise logistic regression.

*(**A**) The lift chart shows the ratio (lift value) of correct predictions based on deciles (percentile) of the sample (i.e., axons) ordered by decreasing the predicted probability to*

*that of a random sample. At the full sample size (100%), the lift value equals 1. In the final model (solid line) with a threshold value of 0.5 for up to about 40% of the axons, there were two times as many correct predictions as in the case of the same percentage of axons selected randomly (dashed line). In addition, a quick decline in the elevation value after about 40% shows that the inclusion of more axons did not increase the ratio of correct prediction relative to that of a random sample. (**B**) Receiving operating characteristics (ROC) of the model. The area under the ROC curve (0.99) indicates a very high accuracy. The solid line shows the accuracy of the model whereas the dashed line shows the performance if axons were randomly classified. Sensitivity: true positive rate, 1-specificity: false positive rate. A perfect classifier would have a true positive rate of 1 with a false positive rate of 0.*

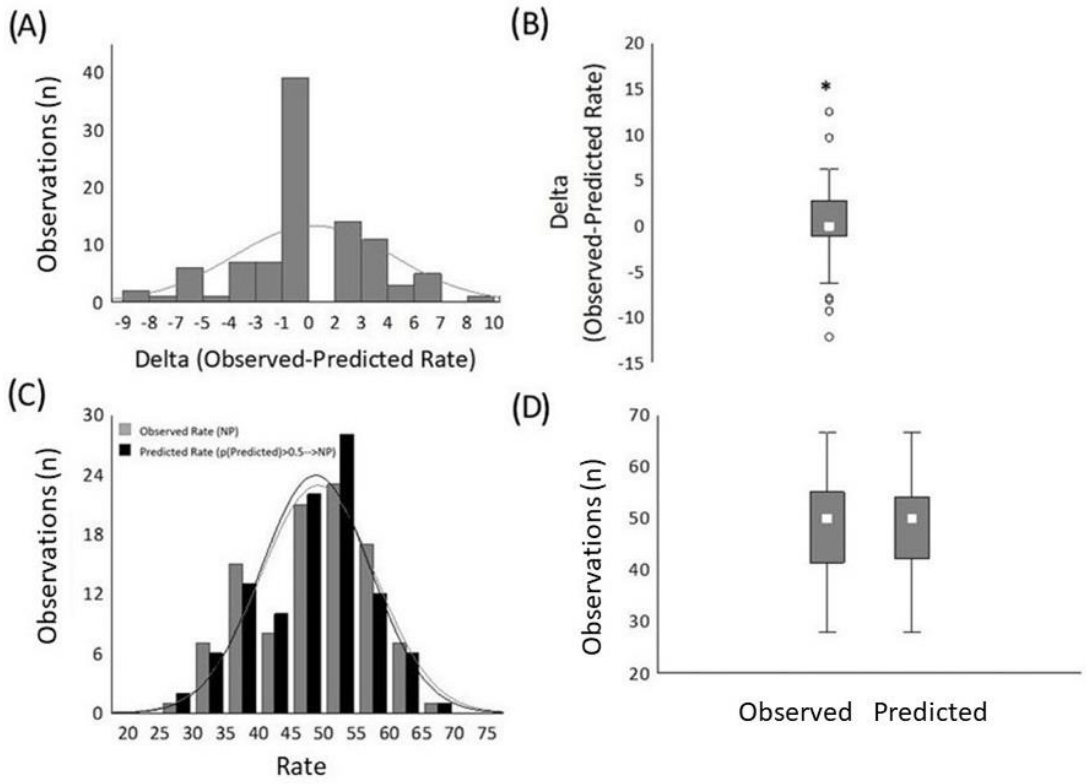

Figure 32. Validation of the stepwise logistic regression by bootstrap (100 replications, 25% holdout and 0.5 probability cut-off threshold)

Distribution (A) and mean +/- std (B) of the observed minus predicted rates in the full model. Distribution (C) and mean +/- std (D) of the observed and predicted rates. Panels A-D show the negligible difference between the observed and predicted rates.

Table 11. Results of marginal model with all seven variables (codes: P = 0, NP = 1). Values showing significant fit are highlighted by red.

Effect	Somers' D	Constant	Pr>Chi2	df
Tortuosity	0.097	-2.139	0.292	1
Bouton cluster	0.847	43.056	5.23E-08	1
Bouton density	0.870	-47.913	1.17E-08	1
Bouton distance std	0.794	0.399	1.05E-08	1
Bouton-convergence	0.982	0.603	7.73E-05	1
Thickness	0.947	16.417	3.97E-08	1
Directionality difference	0.890	-0.256	2.01E-06	1

Table 12. Model fit statistics for the seven variables. AIC: Akaike information criterion, AICC: AIC corrected for small sample size, BIC: Bayesian information criterion, R2: adjusted coefficient of determination.

Marginal Predictors	AIC	AICC	BIC	R2
Tortuosity	202.502	202.587	208.442	0.010
Bouton cluster	101.874	101.959	107.814	0.676
Bouton density	91.959	92.044	97.898	0.719
Bouton distance std	146.747	146.832	152.686	0.435
Bouton-convergence	37.852	37.937	43.791	0.912
Thickness	62.749	62.834	68.688	0.832
Directionality difference	87.049	87.134	92.988	0.740

Table 13. Summary of building the stepwise logistic regression model.

Step No.	Model Variables	df	Wald	Wald p-value	Somers' D	KS statistic	KS p-value
1	Bouton-convergence	1	15,622	7,733E-05	0,982	0,903	6,552E-26
2	Bouton-convergence	1	9,927	0,002	0,989	0,917	1,062E-26
	Bouton density	1	4,308	0,038			

Table 14. Parameter estimates (modelled probability that P/NP = NP) in the final model including the variables that significantly improved the model fit. The p values of bouton-convergence and bouton density correspond to the Wald p-value in Table 12.

Effect	Constant	Standard Error	Wald Stat.	Lower CL 95.0%	Upper CL 95.0%	p
Intercept	-7,993	3,513	5,177	-14,879	-1,108	0,023
Bouton-convergence	0,497	0,158	9,927	0,188	0,806	0,002
Bouton density	-26,612	12,821	4,308	-51,741	-1,482	0,038

Table 15. Marginal table without bouton-convergence.

Effect	Somers' D	Estimate	Pr>Chi2	df
Tortuosity	0.9823	-0.3044	0.9657	1
Bouton cluster	0.9877	12.0204	0.1070	1
Bouton density	0.9888	-26.6115	0.0379	1
Bouton distance std	0.9842	0.1525	0.1719	1
Thickness	0.9996	31.0813	0.1538	1
Directionality difference	0.9985	-0.6328	0.0869	1

Table 16. Marginal table without bouton-convergence and bouton density.

Effect	Somers' D	Estimate	Pr>Chi2	df
Tortuosity	0.9888	3.6100	0.6487	1
Bouton cluster	0.9896	2.9844	0.7651	1
Bouton distance std	0.9904	-0.3575	0.1954	1
Thickness	0.9996	108.5321	0.5725	1
Directionality difference	1.0000	-24.9717	0.4322	1

4.2. Rodent studies

4.2.1 Connections of VIP + INs in anterior insular cortex (aIC)

By means of immunohistochemistry, I investigated the laminar distribution of VIP+ INs across transgenic VIP: Ai9-tdTomato mice insular cortex subdivisions and along its entire rostro-caudal axis. The highest percentage of VIP+ INs was found in cortical layer II/III (Figure 33).

Anterograde viral tracing approach was utilised to identify the projection from mediodorsal thalamus (MD) to VIP+INs of the anterior insular cortex (aIC) (Figure 34 A-D). Figure 34D and E show the bilaminar distribution of thalamocortical afferents. Notably, the distribution of anterograde labelling and VIP+ INs overlapped in the superficial layers. Anterograde tracing identified direct inputs to aIC VIP+ INs from the MD as shown by the close appositions between the anterogradely labelled axons and VIP immunolabelled neurons (Figure 34F). This arrangement supports the synaptic relationship between thalamocortical axons and VIP+ INs. This could be confirmed ontogenetically (data not shown).

DOI:10.14753/SE.2023.2830

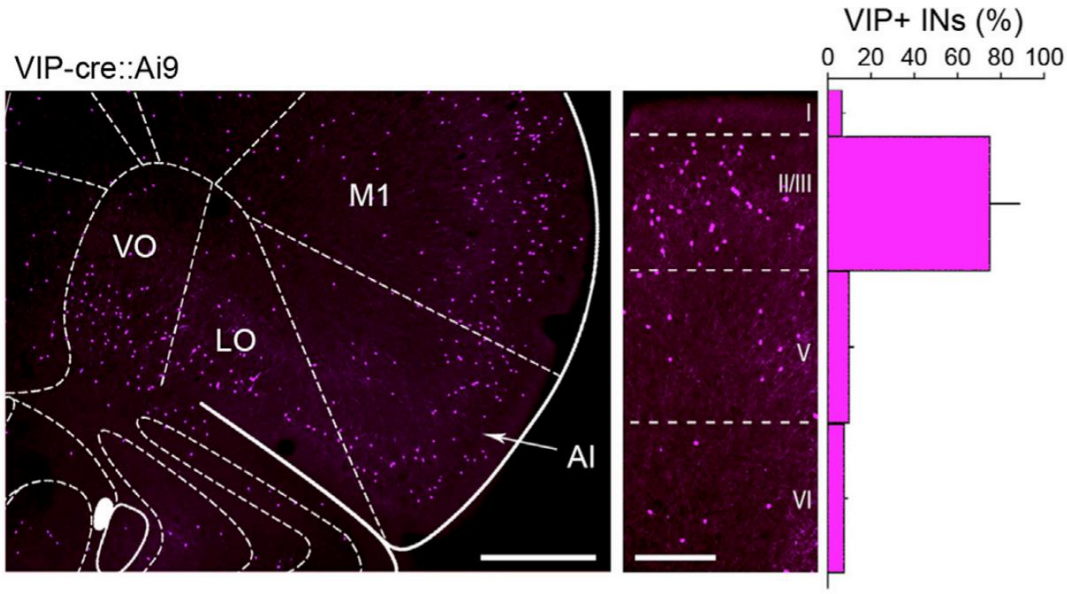

Figure 33. Layer wise distribution of VIP+ INs in insular cortex

Example images of VIP expression throughout the IC in a VIP-ires-cre: Ai9-tdTomato reporter mouse (left and middle panels) and immunohistochemical quantification of VIP+ INs throughout the different cortical layers of the aIC (right panel; N = 3 mice). Scale bars, 500 and 250 mm. Data are shown as mean + SEM.

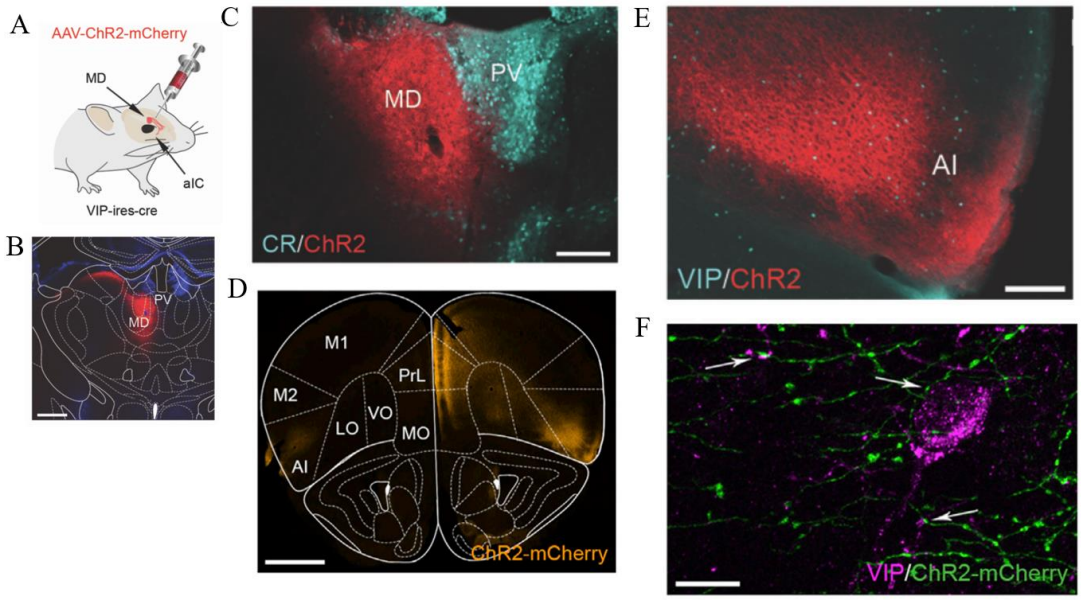

Figure 34. Anterograde tracing

(A) Schematic of the experimental approach used for anterograde tracing from the MD (B) Example image of the histological verification of the injection site of the viral vector AAV-ChR2-mCherry (red) in the MD of a VIP-ires-cre mouse. DAPI was used for histological counterstaining. Scale bar 500 μm (C) Example image of CR (calretinin;

turquoise) and ChR2-mCherry (red) immunolabeling in the thalamus confirming that ChR2-mCherry-expressing neurons are mainly restricted to the MD. Scale bar 200 μm (D) Representative image of ChR2-mCherry immunolabeled axons in the medial prefrontal cortex (mPFC) and aIC originating from the MD. Scale bar, 1 mm.(E) Example image of VIP (turquoise) and ChR2-mCherry (red) immunolabeling in the aIC confirming the high density of MD afferents. Scale bar 200 μm (F) Representative high-magnification image of ChR2-mCherry-labeled axon terminals (green) and VIP immunoreactivity (magenta) in the aIC of a mouse injected with ChR2-mCherry in the MD. Arrows indicate appositions of ChR2-mCherry-labeled boutons onto the soma and dendrites of VIP+ INs. Scale bar, 10 mm.

DOI:10.14753/SE.2023.2830

5. Discussion

5.1. Modular connections of the primate SI

5.1.1. Overview

In this study, we investigated individual (tortuosity, thickness, bouton density, variability of inter-bouton distance and clustering tendency of boutons) and collective (distance of the closest boutons of unconnected axonal segments and directional difference of the axonal segments) morphological variables of bouton forming axonal segments that are relevant to signal transmission and best predict the properties of a patch. We discovered that, with the exception of tortuosity, all of the variables investigated showed substantial differences between axons inside the patches and axons outside the patches. Axons do not differ concerning other attributes such as intrinsic or inter-areal connections including feed-forward and feedback pathways and laminar distribution. Furthermore, we discovered the proximity of boutons of unconnected axonal segments (bouton convergence) as the variable with the highest predictive power of patch identification. In addition to bouton-convergence, bouton density also significantly contributes to the predicting power of patch designation of an axon. Our findings that patches are loci of high synaptic convergence support their role in synchronous cortical activities. As patches are characteristic of the mesoscale connectivity in the cerebral cortex of carnivores and primates, an important finding is that in the different pathways (intrinsic, feed-forward or feedback) and layers (supra- and infragranular) studied axons do not vary their properties; axons differ exclusively by their patch designation. In addition, the patch and no-patch domains of horizontal, long-distance axons exhibit distinguishing morphological properties, which suggest their complementary role in cortical computation and support the modular organisation of cortical interactions.

5.1.2. Limitations

One of the study's methodological drawbacks is that sampling of serial sections does not enable tracing back to the axon's origin. As a result, it is probable that the reconstructed axonal segments are from the same neuron. While this cannot be ruled out, single cell reconstructions demonstrate that cortical spiny neurons' recurrent horizontal axonal branches are directed in diverse rostro-caudal and medio-lateral orientations rather than raising many parallel collaterals (Buzás et al., 2006; Binzegger et al., 2007). Based on this finding, we predict our sample to have only a small number of linear no-patch

axonal segments belonging to the same neuron. However, sampled segments belonging to the same axon arborization within the patches may be higher. Nevertheless, unlike in our sample, where patch axons overlap, distal branches of fully reconstructed neuronal branches frequently ramify in a Y shape and are usually divergent (Buzás et al., 2006; Binzegger et al., 2007). Studies found a high laminar preference for horizontal connections of neurons in distinct layers of the visual cortex (Kisvárday, 2016; Martin et al., 2017). With one exception, we reconstructed patch and no-patch axons from multiple sections with large inter-section gaps (i.e. in widely separated layers) and in distinct horizontal positions in this work, which is reducing the likelihood of sampling axons from the same neuron.

Our approach does not allow the unequivocal identification of the type of the parent neuron of the axonal segments studied. Although, as described in the Introduction, it is known that long-distant horizontal connections are mostly formed by pyramidal neurons, there are transcolumnar and projecting GABAergic neurons that could be labelled anterogradely in our experiments (DeFelipe et al., 2013). Even if this is the case, the number of labelled GABAergic axonal segments forms probably a small fraction of the total number of axonal segments studied. The population of the GABAergic neurons with long distance projection is a subfraction of the total number of GABAergic cells, which form 10-30% of the neurons in the cerebral cortex (DeFelipe et al., 2013). Furthermore, the qualitative and quantitative morphological observations are in agreement with the horizontal distribution of axons of individual PCs. As shown previously, axonal boutons of pyramidal neurons mostly appear in the form of varicosities similar to that found here (Kisvárday et al., 1997). Furthermore, in the visual cortex of cats, single cell labelling revealed that intrinsic horizontal connections of pyramidal neurons consist of linear segments terminating in a rich arborization of short, distal branches (Buzás et al., 2006; Muir and Douglas, 2011). Also in the cat visual cortex, the horizontal pattern of boutons formed by nearby pyramidal neurons is consistent with the distribution of the patch and no-patch domains described here (Kisvárday et al., 1997; Buzás et al., 2006). Together, these observations suggest that our sample consisted of axons originating from pyramidal neurons. Specifically, no-patch axons probably represent the linear segments whereas patch axons can correspond to the terminal arborizations of the horizontal axonal connections.

The chance of including axons labelled by retrograde backfilling of neurons projecting to the injection site that means retrograde labelling would result in the emergence of "secondary" target regions of the injected cortical locus. We cannot rule out this possibility, as complete neuron reconstruction was not achievable in our regularly spaced series. We discovered that reconstructed axons generally ramified toward distant terminal patches, indicating that these axons are propagated away from the injection site. Second, and most importantly, terminal patches accumulated in regions with a high density of retrograde labelling, whereas axonal backfilling would have resulted in the appearance of terminal axonal arborizations in regions without significant retrograde labelling, assuming divergent neuronal connectivity (Négyessy et al., 2013). Our observations about the apparent lack of thalamocortical labelling and secondary labelling of patches formed by neurons after probable backfilling suggest that these factors did not significantly influence our results. Horizontal sectioning may have caused inconsistencies by ignoring the laminar positions of the axonal segments (Pálfi et al., 2018). To avoid inclusion of structures labelled directly by the BDA injection rather than through neuronal transport, labelling inside the core of the injection site, which measured 300 μm in diameter, was omitted from the analysis (Pálfi et al., 2018). In that study, we found a similar laminar preference of connectivity as shown before (Burton and Fabri, 1995). In our samples, the majority of patches and boutons were localized in the supragranular layer (Pálfi et al., 2018), which is consistent with the prevalence of patchy organisation of the horizontal connections in layers II/III (Douglas and Martin 2004; Kisvárday, 2016).

Due to the poor resolution of the digital camera attached to the Neurolucida system, as well as the considerably greater scattering of light through the osmicated and resin embedded sections, our thickness measurements of the axons presumably reflect bigger values than in reality. Consequently, these results are not comparable to those found in the literature (Anderson et al., 2002; Innocenti and Caminiti, 2017; Koestinger et al., 2017). However, the outcomes of the comparisons undertaken in this research would be unaffected by this systematic impact of measurement.

Our qualitative and quantitative morphological observations are in good agreement with the distribution of the lateral horizontal connections of individual PCs. As shown previously, axonal boutons of pyramidal neurons mostly appear in the form of varicosities (Kisvárday et al., 1997). Furthermore, single cell labelling in the visual cortex of cats revealed that intrinsic horizontal connections of pyramidal neurons consist of linear

segments terminating in a rich arborization of short, distal branches (Buzás et al., 2006; Muir and Douglas, 2011). Also in cat visual cortex, the pattern of the horizontal distribution of boutons of a population of closely spaced pyramidal neurons is consistent with that of the patch and no-patch domains described here (Kisvárday et al., 1997; Buzás et al., 2006). Together these observations suggest that our sample consisted of axons originating from pyramidal neurons and that no-patch axons represent the linear segments whereas patch axons correspond to the terminal arborizations of the horizontal axonal connections.

5.1.3. Convergence and divergence of long-distance horizontal connections

Our analyses indicate that the tortuosity of bouton-forming axonal segments of PCs is an invariable property and, therefore, neurons save material and use other strategies in finding their specific targets (Anderson et al., 2002; Budd et al., 2010). We found that all variables related to bouton placement differed significantly between patch and no-patch axons. It should be noted that the coefficient of variation (CV) of inter-bouton intervals observed here is in agreement with the 0.5 reported by Shepherd et al. (2002) and indicates that bouton spacing is neither completely random (CV = 1) nor regular (CV = 0). Our findings support that the sub-random distribution of inter-bouton intervals is a feature of unmyelinated axonal branches in the brain (Hellwig et al., 1994; Shepherd et al., 2002). Even though bouton spacing variability is a constant fraction of the mean spacing along axons, irrespective of the type of neuron or branch order, only boutons on the terminal branches of lateral connections form clusters (Anderson et al., 2002; Shepherd et al., 2002; Binzegger et al., 2007). These observations are corroborated by our findings, which reveal that inside patches, bouton densities are higher, clustering is more common, and inter-bouton intervals are less variable than in no-patch segments. Furthermore, inside the patches, boutons of unconnected axonal segments are substantially closer to one another than outside of patches. In addition, in contrast to the parallel direction of no-patch axons, patch axons are branching in different directions, which increases the possibility of convergence on the same postsynaptic structure. These findings are in line with the observations showing the overlapping distribution of terminal axon arborizations of a population of nearby pyramidal neurons in the cat visual cortex (Kisvárday et al., 1997; Buzás et al., 2006). In agreement with this observation, we corroborated our prior findings in the primate somatosensory cortex by revealing higher

bouton densities inside patches relative to no-patch domains (Négyessy et al., 2013; Ashaber et al., 2014).

Our multivariate data analysis approaches further revealed what makes patch and no-patch domains two fundamentally different cortical sites. We demonstrated using PCA that measured axons only group according to patch designation, without further grouping by other pathway designations or laminar localization, based on the individual and collective variables. A single principal component (PC) explained more than half of the variation in the data. Despite the fact that all factors, with the exception of tortuosity, had a relatively high load on the first PC, the analysis found that bouton density and bouton-convergence had the most differentiating power. We used stepwise logistic regression to determine which of these variables had the best predictive power for patch designation. The model determined bouton-convergence with the strongest prediction power. The model fit was also aided by bouton density, although this parameter had much less predictive potential, as evidenced by the observed probabilities. Overall, these findings suggest that patches are unique cortical sites that may attract axons from a population of adjacent pyramidal neurons, resulting in the formation of bouton clusters by distal terminal arborizations (Buzás et al., 2006; Binzegger et al., 2007). Similar evidence for bouton distributions, obtained by labelling a small population of neurons and pooling single neuron reconstructions, also suggests a highly overlapping distribution of final terminal branches in the cat visual cortex (Kisvárday et al., 1997; Buzás et al., 2006; Martin et al., 2014, 2017).

Apart from bouton spacing, no-patch axons were significantly thicker than patch axons, which is consistent with branching sequence of the axons, since patches are formed by the most distal branches (Buzás et al., 2006; Binzegger et al., 2007). Neural activity can spread at different velocities inside and outside the patches due to the different axon thicknesses. However, given the short length of the distal branches, it is reasonable to assume that larger bouton densities compensate for the slower conduction speed within the patches. Such compensation in conduction velocity would critically depend on the relative diameter between the axon and the bouton, where a larger difference results in a longer lag in signal propagation (Segev and Schneidman, 1999; Alcami and El Hady, 2019). In addition, a bouton density higher than a critical value can result in a nonlinear increase in conduction delay (Segev and Schneidman, 1999). Further uncertainties in conduction speed can be introduced by activity-dependent changes in axon thickness and bouton size (Alcami and El Hady, 2019). How these factors affect the spread of activity

along patch axons remains to be tested. Until these issues are clarified, as a working hypothesis, one can assume similar dynamics in the two bouton-forming axonal domains of the cerebral cortex. In conclusion, the distributed modules of axonal convergence are positioned well to act as sites for the synchronisation of neuronal activity occurring on fast and slower timescales. On the contrary, no-patch axons are better suited to modulate the large-scale dynamics of cortical synchronisation. Because of the functional significance, it is important to know the possible mechanism of patch formation i.e. axonal convergence.

5.1.4. Possible neurobiological mechanisms of patch formation

The neuronal progenitors are genetically predisposed to secrete a variety of morphogens capable of diffusing through the extracellular matrix. These morphogens are transcription factors whose interactions with the genome follow the Gierer-Meinhardt reaction-diffusion dynamics (Turing, 1952; Gierer and Meinhardt, 1972, Bauer et al., 2014). Thus, the precursors of the preplate express a two-dimensional periodic profile of morphogens that provides the basis for clusters of neurons expressing similar profiles. This periodic identity is inherited from the progenitors through their daughter neurons, which migrate radially to form the superficial cortical layers. When these migrating neurons come to rest, they expand lateral axons whose growth cones seek distant target neurons with similar morphogen expression profiles to their own, producing the patchy organisation observed (Bauer et al., 2014).

The selectivity for different molecular markers is probably one of the most important principles in governing patch formation. Pyramidal neurons show a lot of variation in terms of molecular composition (Lodato and Arlotta, 2015; Zeng and Sanes, 2017). Considering the group of component molecules, some degree of neuronal similarity can be dispersed throughout the cortical mantle and result in the diversity of target sites found in the case of no-patch axons. In such a scenario, the strength of molecular similarity can determine the specificity of target sites of a population of cortical neurons. Another likely factor determining the target neurons is the similarity of functional properties with the presynaptic neuron (Kaas, 2012). Our findings suggest that similar rules govern the formation of feedforward, and feedback inter-areal connections as well as the intrinsic connectivity (Négyessy et al., 2013; Ashaber et al., 2014; Pálfi et al., 2018). The perception of how chemical and activity-dependent mechanisms interact in the formation of the different cortical circuits requires further investigation.

Considering also the role of randomness in the formation of synaptic contacts at the target sites (Shepherd et al., 2002), these observations suggest that once a target site is located by chemical and/or activity-dependent cues, synapse forms randomly. A mechanism of this kind is able to assist the local rearrangement of synapse creation (the removal of existing synapses and the growth of new ones) without compromising the functional specificity of the process (importance of large scale).

5.1.5. Functional considerations

In the sensory cortex, feedforward inter-areal input is responsible for activation of "hotspots" (Chen et al., 2003; Friedman et al., 2008) or "imprint" (Chavane et al., 2011) at the population level and the formation of the classical receptive field (RF) of neurons (somatosensory cortex: Favorov and Whitsel, 1988; Chen et al., 2003; Friedman et al., 2008; and the visual cortex: Kisvárday et al., 1997; Angelucci et al., 2017). On the other hand, lateral intra-areal connections are thought to transmit contextual information and are responsible for the configuration of extra-classical RF together with feedback inter-areal connections (Kisvárday, 2016; Angelucci et al., 2017; Chavane et al., 2022). However, how synaptic computations bring the function of these pathways into effect is not completely understood (Douglas and Martin, 2007; Boucsein et al., 2011; Harris and Mrsic-Flogel, 2013; Muller et al., 2018; Rockland, 2018; Chavane et al., 2022). In this study, we made a distinction between the efferents of a population of nearby projection neurons, which is independent of whether the projection pathway is intra-areal, feedforward, or feedback. We found a major difference between patch and no-patch axonal segments. Patches are identified as convergence spots of efferents formed by a population of neighbouring neurons, in contrast to the rather parallel spread of neighbouring no-patch axons. Notably, this distinction applies to all connections studied, specifically intra-areal, feedforward, and feedback ones. Also, patch and no-patch characteristics of the axons are independent of the laminar localization. These observations suggest a fundamental similarity in the computation performed by the different pathways. Considering synaptic connections, the driving functions of the feedforward thalamocortical synaptic boutons are reflected by their structural properties (Négyessy and Goldman-Rakic, 2005; Petrof and Sherman, 2013). However, the ultrastructural characteristics of the cortico-cortical synaptic boutons are more homogenous and support their modulatory role (Ashaber et al., 2020). These electron

microscopy findings provide further hints to the importance of convergence in cortical computation.

The convergence of afferents is recognised as the substrate for increasing the effectiveness of signal transmission through the neuronal network. This recognition is supported by the observation that cortical microstimulation can induce a patchy pattern of activation (Roe et al., 2015; Xu et al., 2019; Friedman et al., 2020). Patches can provide the functional bias found in the case of orientation tuning in the visual cortex (Kisvárday, 2016). In contrast, no-patch axons can diversify the input via conveying contextual information to postsynaptic neurons (Kisvárday, 2016; Chavane et al., 2022). Consequently, neurons with overlapping RFs can significantly shape the response specificity of sensory cortical patches. The functional similarity of the neurons forming the patchy projection argues against the lack of specificity of sensory cortical interactions (Chavane et al., 2022). A possible explanation of the discrepancy between Chavane et al. (2022) and our proposal is that techniques sensitive to subthreshold changes in membrane potential can reveal input diversity provided by non-convergent projections of no-patch axons.

A dynamic stimulus dependence of noise correlations (quantifying the correlation of trial-by-trial variations of response at fixed stimulus attributes) among visual cortical neurons carries information about whether individual neurons respond to the same or distinct objects (Fries et al., 2001; Womelsdorf et al., 2012; Nikolić et al., 2012). This deeply influences the interpretation of mass signals from neurons measured by neuroimaging because it suggests that changes in correlation between the activities of distinct populations may reflect how these populations encode information. However, noise correlations of firing rates may impose limits on the growth of information with population size (Zohary et al., 1994). For example, for neurons with identical tuning curves, the presence of weak positive noise correlations prevents the possibility to improve the accuracy of sensory information encoding by simply averaging the rate of many neurons (correlated noise can only be removed to a limited extent by averaging). The recognition that no-patch regions of a population of neurons probably interact with different functional neuronal populations can explain the formation of cortical circuits that can support both functional specificity and variability. This observation is consistent with the role of patch domains in the emergence of signal correlations (quantifying the correlation of the trial-averaged neural responses across the different stimuli, and thus

quantifying the similarity of stimulus tuning) of the neuronal responses whereas the no-patch domain can contribute to noise correlations (Panzeri et al., 2015; Bányai and Orbán, 2019).

In our previous studies, we explored the direction of information flow within the circuitry of BA3b and BA1 (Wang et al., 2013; Pálfi et al., 2018). The picture that emerged from that data is consistent with the findings of Polack and Contreras (2012) who showed that in the mouse visual cortex information is rapidly forwarded to numerous cortical areas, simultaneously triggering slower serial processing within areas, which can be influenced by the later feedback component in population activity (Semedo et al., 2022). This, in parallel with our findings, suggests that in the regions of the cerebral cortex with terminal arborizations, a higher bouton density coupled with extensive convergence may be responsible for producing a highly effective mode of signalling via neuronal synchronization. Then the output induced by the correlated activity might be rapidly spreading across the parallel long-range axons that are located outside of the patches.

5.2. Connections formed by the VIP + INs of the anterior insular cortex (aIC) in mice

The finding of this particular study supports the participation of VIP+ INs in sensory integration to enable behavioral adaptations. The MD is considered the main salience network (SN) hub within the thalamus (Menon, 2015) and has been shown to modulate the salience of fear-associated cues (Zhou et al., 2021; Lee et al., 2012) as well as social-related behaviors (Zhou et al., 2017; Ferguson and Gao, 2018). Interestingly, MD afferents were also shown to target VIP+ INs in the mPFC (Anastasiades et al., 2021), which raises the possibility for the existence of a conserved bottom-up functional modulation of sensory processing through MD connectivity onto VIP+ INs in these cortical regions.

Regarding viral tracing, it has many advantages including the highly reliable labelling of the axonal processes as shown in my studies. In addition, while in case of BDA the direction of axonal transport (retrograde and anterograde) is rarely exclusive, which complicates circuit analysis, viral tracing provides a unique opportunity to determine the direction of neuronal connections (Noseda et al., 2010; Zhou et al., 2017). Most notably, the close appositions identified by viral tracing between the MD afferents and VIP+INs of aIC were proved to be functional by using optogenetic assessment. There are still

certain limitations of this method. Accordingly, similar to BDAs tracings, anterograde viral tracers (AAV), can be taken up by fibers of passage (Dado et al., 1990; Chen and Aston-Jones, 1995), which can lead to incorrect identification of projections (Schwarz et al., 2015). Also, up to now the application of viral tracing is largely restricted to rodent studies and its applicability is limited in primate studies.

6. Conclusions

In the S1 of the squirrel monkey (*Saimiri sciureus*), anterogradely labelled axonal segments in BA3b and BA1 were reconstructed in three dimensions. Morphological properties of these axonal segments, such as tortuosity, bouton clustering, bouton distances, bouton density, thickness, convergence, and directionality, were quantitatively measured and compared within patch and no-patch domains, intrinsic and inter-areal (FF and FB) connections, and according to laminar localization. Axons exhibited differences only according to the patch classification. We found that except for the tortuosity, which is an invariable property, the distribution of varicosities within the patch and no-patch domains varied substantially. In comparison to no-patch segments, we discovered that bouton densities are larger, clustering is more prevalent, and inter-bouton intervals are less variable within patches. Furthermore, boutons of disconnected axonal segments are much closer to one another within patches than outside patches. The distance between boutons of disconnected axonal segments (bouton-convergence) is found to be the most powerful predictor of patch identity. Aside from bouton convergence, bouton density has a significant influence on predicting accuracy of axon patch identification. Based on the observations and the results, the following conclusions were made:

- The patch and no-patch domains of horizontal, long-distance axons exhibit unique morphological properties. All the variables studied were similar when compared according to pathway or laminar designations (BA3b vs. BA1, intrinsic vs. inter-area, FF vs. FB, supra vs. infra). The patch-like organisation implies the parallel processing via divergence in the no-patch domains, whereas patch domains can promote convergence and functional cortical modularization due to the significantly variable path and higher densities of boutons of the axons.
- Despite the thickness differences of axonal segments in patch and no-patch domains, the neural activity can travel at similar velocities. The distal branches are so short; it is reasonable to assume that the larger bouton densities within the patch domains compensate for slower conduction of speed. Hence, activity may be distributed with similar dynamics throughout the two axonal domains of the cerebral cortex.
- Finally, yet importantly, we proposed that increased bouton density accompanied by extensive convergence could result in a highly efficient way of signal transmission and neuronal synchronization in terminal arborization patches of the

cerebral cortex. In contrast, long-range thick axons outside of patches could subserve quick dissemination of information. The patchy pattern is compatible with cortical circuitry that enables neuronal populations to operate together and boost the effectiveness of signal transmission across the neural network.

- Regarding our 3rd objective, anterograde viral tracing allowed the identification of the selective targeting of VIP+ INs of the aIC by axons from the MD. This finding complements previous observations and suggest that MD modulates PFC functions via VIP+ INs in the rodents.

7. Summary

Axonal patches are distinguished locations at which synaptic connections are made in the cerebral cortex of higher order mammals. Populations of adjacent pyramidal neurons in a topographic fashion form Patches. However, the functional role of these patches is highly debated. Patches are identified as the termination fields of long-distance lateral connections both within and across cortical areas. In addition, axons of pyramidal neurons generate numerous boutons outside of the patches, which further complicate the understanding of the functional significance of patchy termination in the cerebral cortex. To better understand the role of patches in the regulation of signal transmission and synaptic integration, we compared individual and collective morphological features of labelled axons such as tortuosity (length of an axon relative to the straight line connecting the endpoints), bouton clustering (counting the number of boutons that were farther from each other than a separation length along an axon as a function of separation length), bouton density (number of boutons in a unit length), inter-bouton distance (axonal distance to the preceding bouton), thickness (measurements at three different locations along an axon and averaged), bouton-convergence (average distance of a bouton of a reconstructed axonal segment from the two nearest BDA-labelled boutons of other axons) and directional differences (orientation of the axons were determined relative to a reference line) of pyramidal cell axonal segments within and outside the patches of intra-areal, feedforward, and feedback pathways as well as of supragranular and infragranular layers in the circuitry of area 3b and area 1 of the somatosensory cortex of squirrel monkeys, by means of tract tracing. We found that bouton spacing and axonal convergence are significantly different in the patch and no-patch domains. In contrast, tortuosity was identified as an invariant property of the axons. The grouping of axonal segments according to patch formation was validated by principal component analyses showing that the pathway studied or the laminar distribution of the axons did not influence grouping. Convergence and bouton density emerged as the best predictors of patch formation after using stepwise logistic regression. Therefore, Patches promote synchronized neuronal activity, while no-patch domains diversify cortical neuron responses.

For 3rd objective, VIP+ INs in aIC have direct inputs from MD neurons, indicating their role in thalamocortical interactions and sensory processing for behavioral adaptations.

DOI:10.14753/SE.2023.2830

8. Összefoglalás

Az axonális foltok a szinaptikus kapcsolatok létesítésének megkülönböztetett területei a magasabb rendű emlősök agykérgében. Az axon-foltokat szomszédos piramis sejtek populációi alkotják topografikusan rendezett eloszlásban. Az axon-foltok funkcionális szerepe erősen vitatott. A foltok az áreákon belüli és az áreákat összekötő távoli laterális kapcsolatok végződései. A piramissejtek axonjain a foltokon kívül is számos bouton található, ami tovább bonyolítja a foltok funkcionális jelentőségének megértését az agykéregben. Annak érdekében, hogy jobban megértsük az axon foltok szerepét a jelátvitel és a szinaptikus integráció szabályozásában pályajelölést és kvantitatív morfológiai módszereket alkalmaztunk mókusmajmokban, a szomatoszenzoros kérgi área 3b és 1-ben. Piramis sejtek axon-szegmenseinek egyedi és kollektív morfológiai tulajdonságait hasonlítottuk össze a foltokban és azokon kívül áreán belüli és azok közötti felszálló és visszacsatolt összeköttetések, valamint szupragranuláris és infragranuláris rétegek között. Kimutattuk, hogy a boutonok távolságeloszlása és az axonok konvergenciája szignifikánsan különbözik a foltokban és azokon kívül. Ezzel szemben a kanyargósságot az axonok invariáns tulajdonságaként azonosítottuk. Az axonális szegmensek foltképző tulajdonságuk szerinti csoportosítását főkomponens-elemzéssel igazoltuk és kimutattuk, hogy a csoportosítás nem függ a vizsgált pályától vagy az axonok rétegeloszlásától. Léptetéses logisztikus regresszióval bizonyítottuk, hogy a konvergencia és a bouton-sűrűség a foltképző tulajdonság legjobb indikátorai. Ezek az eredmények igazolták hipotézisünket, miszerint a foltok az axonális konvergencia specifikus helyei, amelyek elősegítik a neuronpopulációk szinkronizált aktivitását. A folton kívüli axonok ugyanakkor jelentősen hozzájárulhatnak az idegsejtválaszok diverzitásának kialakításához.

Ezen túlmenően víruskövetéssel demonstráltuk az aIC-ben a VIP+ IN thalamokortikális bemenetét az MD-ból egerekben. Eredményünk alapján feltételezhetjük, hogy a VIP + IN a különböző PFC áreákban központi szerepet játszik a thalamokortikális kölcsönhatásokban, legalábbis rágcsálókban. Az aIC-ben az MD afferentáció a VIP + IN keresztül fontos szerepet játszik a viselkedéses adaptációban.

9. Bibliography

Alcami P, El Hady A. (2019). Axonal Computations. *Frontiers in Cellular Neuroscience*. 13: 413.

Anastasiades P, Collins D, Carter A. (2021). Mediodorsal and ventromedial thalamus engage distinct L1 circuits in the prefrontal cortex. *Neuron*. 109: 314–330.e4

Andersen R, Buneo C. (2002). Intentional Maps in Posterior Parietal Cortex. *Annual Review of Neuroscience*. 25(1): 189-220.

Anderson J, Binzegger T, Douglas R, and Martin K. (2002). Chance or design? Some specific considerations concerning synaptic boutons in cat visual cortex. *Journal of Neurocytology*. 31(3/5): 211-229.

Angelucci A, Bijanzadeh M, Nurminen L, Federer F, Merlin S, Bressloff P. (2017). Circuits and Mechanisms for Surround Modulation in Visual Cortex. *Annual Review of Neurosci*. 40(1): 425-451.

Angelucci A, Bressloff P. (2006). Contribution of feedforward, lateral and feedback connections to the classical receptive field centre and extra-classical receptive field surround of primate V1 neurons. *Progress in Brain Research.* 154: 93-120.

Apkarian A, Shi T. (1994). Squirrel monkey lateral thalamus. I. Somatic nociresponsive neurons and their relation to spinothalamic terminals. *Journal of Neuroscience*. 14: 6779-6795.

Ashaber M, Pálfi E, Friedman R, Palmer C, Jákli B, Chen L, Kántor O, Roe A, Négyessy L. (2014). Connectivity of somatosensory cortical BA1 forms an anatomical substrate for the emergence of multifinger receptive fields and complex feature selectivity in the squirrel monkey (Saimiri sciureus). *Journal of Comparative Neurology*. 522(8): 1769-1785.

Ashaber M, Zalányi L, Pálfi E, Stuber I, Kovács T, Roe A, Friedman R, and Négyessy L. (2020). Synaptic organisation of cortico-cortical communication in primates. *European Journal of Neuroscience*. 52(9): 4037-4056.

Bányai M, Orbán G. (2019). Noise correlations and perceptual inference. *Current Opinion in Neurobiology*. 58: 209-217.

Bardy C, Huang J, Wang C, FitzGibbon T, Dreher B. (2009). 'Top-down' influences of ipsilateral or contralateral postero-temporal visual cortices on the extra-classical receptive fields of neurons in cat's striate cortex. *Neuroscience*. 158(2): 951–968.

Bauer R, Zubler F, Hauri A, Muir D, Douglas R. (2014). Developmental origin of patchy axonal connectivity in the neocortex: a computational model. *Cereb. Cortex* 24(2): 487-500.

Baumgartner C, Doppelbauer A, Sutherling W, Lindinger G, Levesque M, Aull S, Zeitlhofer J, Deecke L. (1993). Somatotopy of human hand somatosensory cortex as studied in scalp EEG. *Electroencephalography and Clinical Neurophysiology/Evoked Potentials Section*. 88(4). 271–279.

Bengtsson F, Brasselet R, Johansson R, Arleo A, Jörntell H. (2013). Integration of Sensory Quanta in Cuneate Nucleus Neurons in Vivo. *PLOS One*. 8(2): e56630.

Bentivoglio M, Rustioni A. (1986). Corticospinal neurons with branching axons to the dorsal column nuclei in the monkey. *The Journal of Comparative Neurology*. 253(2): 260-276.

Betley J, Sternson S. (2011). Adeno-Associated Viral Vectors for Mapping, Monitoring, and Manipulating Neural Circuits. *Human Gene Therapy*. *22*(6): 669–677.

Binzegger T, Douglas R, Martin K. (2007). Stereotypical Bouton Clustering of Individual Neurons in Cat Primary Visual Cortex. *Journal of Neuroscience*. 27(45): 12242-12254.

Bishop G, Chang H, Kitai S. (1982). Morphological and physiological properties of neostriatal neurons: An intracellular horseradish peroxidase study in the rat. *Neuroscience*. *7*(1): 179–191.

Bolanowski S, Gescheider G, Verrillo R, Checkosky C. (1988). Four channels mediate the mechanical aspects of touch. *The Journal of the Acoustical Society of America*. *84*(5): 1680–1694.

Boldogköi Z, Sík A, Dénes Á, Reichart A, Toldi J, Gerendai I, Kovács K, Palkovits M. (2004). Novel tracing paradigms—genetically engineered herpesviruses as tools for mapping functional circuits within the CNS: Present status and future prospects. *Progress in Neurobiology*. *72*(6): 417–445.

Bolz J, Hübener M, Kehrer I, Novak N. (1991). Structural Organisation and Development of Identified Projection Neurons in Primary Visual Cortex. In P. Bagnoli & W. Hodos (Eds.), *The Changing Visual System* (pp. 233–246). Springer US.

Bosking W, Zhang Y, Schofield B, Fitzpatrick D. (1997). Orientation Selectivity and the Arrangement of Horizontal Connections in Tree Shrew Striate Cortex. *The Journal of Neuroscience*. *17*(6): 2112–2127.

Boucsein C, Nawrot M, Schnepel P, Aertsen A. (2011). Beyond the cortical column: abundance and physiology of horizontal connections imply a strong role for inputs from the surround. *Frontiers in Neuroscience*. 5: 32.

Braitenberg V, Schüz A. (1998). *Cortex: Statistics and geometry of neuronal connectivity* (2nd thoroughly rev. ed). Springer.

Brodmann K. (1909). Vergleichende Lokalisationsiehre der Grosshirnrinde in ihren Prinzipien Dargestellt auf Grund des Zellenbaues. Barth.

Brown A. (1981). *Organisation in the Spinal Cord*. Springer London.

Buchner H, Adams L, Müller A, Ludwig I, Knepper A, Thron A, Niemann K, Scherg M. (1995). Somatotopy of human hand somatosensory cortex revealed by dipole source analysis of early somatosensory evoked potentials and 3D-NMR tomography. *Electroencephalography and Clinical Neurophysiology/Evoked Potentials Section*. 96(2): 121–134.

Budd J, Kovács K, Ferecskó A, Buzás P, Eysel U, Kisvárday Z. (2010). Neocortical axon arbours trade-off material and conduction delay conservation. *PLoS Computational Biology*. 6(3): e1000711.

Burgess P, Wei J, Clark, F, Simon J. (1982). Signaling of Kinesthetic Information by Peripheral Sensory Receptors. *Annual Review of Neuroscience*. 5(1): 171-188.

Burton H, Fabri M. (1995). Ipsilateral intracortical connections of physiologically defined cutaneous representations in BA3b and BA1 of macaque monkeys: Projections in the vicinity of the central sulcus. *The Journal of Comparative Neurology*. 355(4): 508-538.

Bushnell M, Duncan G. (1987). Mechanical response properties of ventroposterior medial thalamic neurons in the alert monkey. *Experimental Brain Research*. 67: 4-7.

Buzás P, Kovács K, Ferecskó A, Budd J, Eysel U, Kisvárday Z. (2006). Model-based analysis of excitatory lateral connections in the visual cortex. *The Journal of Comparative Neurology*. 499(6): 861-881.

Callaway E, Katz L. (1990). Emergence and refinement of clustered horizontal connections in cat striate cortex. *The Journal of Neuroscience*. 10(4): 1134-1153.

Callaway E. (2008). Transneuronal circuit tracing with neurotropic viruses. *Current Opinion in Neurobiology*. *18*(6): 617–623.

Caminiti R, Ghaziri H, Galuske R, Hof P, Innocenti G. (2009). Evolution amplified processing with temporally dispersed slow neuronal connectivity in primates. *Proceedings of the National Academy of Sciences*. 106(46): 19551–19556.

Caputi A, Melzer S, Michael M, Monyer H. (2013). The long and short of GABAergic neurons. *Current Opinion in Neurobiology*. 23(2): 179–186.

Carlson M, Welt C. (1980). Somatic sensory cortex of the prosimian primate Galago crassicaudatus: Organisation of mechanoreceptive input from the hand in relation to cytoarchitecture. *The Journal of Comparative Neurology*. 189(2): 249-271.

Carlson M. (1980). Characteristics of sensory deficits following lesions of Brodmann area1 and 2 in the postcentral gyrus of Macaca mulatta. *Brain Research*. 204(2): 424-430.

Case L, Laubacher C, Olausson H, Wang B, Spagnolo P, Bushnell M. (2016). Encoding of Touch Intensity but Not Pleasantness in Human Primary Somatosensory Cortex. *Journal of Neuroscience*. 36(21): 5850-5860.

Catania K, and Kaas J. (1995). Organisation of the somatosensory cortex of the star-nosed mole. *The Journal of Comparative Neurology*. 351(4): 549-567.

Chavane F, Perrinet L, Rankin J. (2022). Revisiting horizontal connectivity rules in V1: from like-to-like towards like-to-all. *Brain Structure and Function*. 10.1007/s00429-022-02455-4.

Chavane F, Sharon D, Jancke D, Marre O, Frégnac Y, Grinvald A. (2011). Lateral Spread of Orientation Selectivity in V1 is controlled by Intracortical Cooperativity. *Frontiers in Systems Neuroscience.* 5: 4.

Cheema S, Whitsel B, Rustioni A. (1983). The Corticocuneate Pathway in the Cat: Relations among Terminal Distribution Patterns, Cytoarchitecture, and Single Neuron Functional Properties. *Somatosensory Research*. 1(2): 169-205.

Chen L, Friedman R, Ramsden B, LaMotte R, Roe A. (2001). Fine-Scale Organisation of SI (BA3b) in the Squirrel Monkey Revealed with Intrinsic Optical Imaging. *Journal of Neurophysiology*. 86(6): 3011-3029.

Chen L, Friedman R, Roe A. (2003). Optical Imaging of a Tactile Illusion in BA3b of the Primary Somatosensory Cortex. *Science*. 302(5646): 881-885.

Chen L, Friedman R, Roe A. (2009). Area-specific representation of mechanical nociceptive stimuli within SI cortex of squirrel monkeys. *Pain.* 141(3): 258-268.

Chen S, Aston-Jones G. (1995). Evidence that cholera toxin B subunit (CTb) can be avidly taken up and transported by fibers of passage. *Brain Research*. *674*(1): 107–111.

Chklovskii, D. B. (2004). Synaptic Connectivity and Neuronal Morphology. *Neuron*. 43(5): 609–617.

Craig A. (2006). Retrograde analyses of spinothalamic projections in the macaque monkey: Input to ventral posterior nuclei. *Journal of Comparative Neurology*. 499: 965-978.

Curtis D, Watkins, J. (1960). The excitation and depression of spinal neurones by structurally related amino acids. *Journal of Neurochemistry*. 6(2): 117–141.

Dado R, Burstein R, Cliffer K, Giesler G. (1990). Evidence that Fluoro-Gold can be transported avidly through fibers of passage. *Brain Research*. *533*(2): 329–333.

Darian-Smith C, Darian-Smith I, Burman K, Ratcliffe N. (1993). Ipsilateral cortical projections to areas 3a, 3b, and 4 in the macaque monkey. *The Journal of Comparative Neurology*. 335(2): 200-213.

Darian-Smith I. (2011). Chapter 17, the sense of touch: Performance and peripheral neural processes. *Comprehensive Physiology*. pp: 1-50

Debowy D, Ghosh S, Gardner E, Ro J, (2001). Comparison of neuronal firing rates in somatosensory and posterior parietal cortex during prehension. *Experimental Brain Research*, 137(3-4): 269-291.

DeFelipe J, Conley M, Jones E. (1986). Long-range focal collateralization of axons arising from corticocortical cells in monkey sensory-motor cortex. *The Journal of Neuroscience*. 6(12): 3749–3766.

DeFelipe J, Fariñas I. (1992). The pyramidal neuron of the cerebral cortex: Morphological and chemical characteristics of the synaptic inputs. *Progress in Neurobiology*. 39(6): 563–607.

DeFelipe J, Jones E. (1992). Santiago Ramón y Cajal and methods in neurohistology. *Trends in Neurosciences*. 15(7): 237–246.

DeFelipe J, López-Cruz P, Benavides-Piccione R, Bielza C, Larrañaga P, Anderson S, Burkhalter A, Cauli B, Fairén A, Feldmeyer D, Fishell G, Fitzpatrick D, Freund T, González-Burgos G, Hestrin S, Hill S, Hof P, Huang J, Jones E, … Ascoli G. (2013). New insights into the classification and nomenclature of cortical GABAergic interneurons. *Nature Reviews Neuroscience*. 14(3): 202–216.

Delhaye B, Long K, Bensmaia S. (2018). Neural Basis of Touch and Proprioception in Primate Cortex. *Comparative Physiology*. 8(4): 1575-1602.

DiCarlo J, Johnson K, Hsiao S. (1998). Structure of Receptive Fields in BA3b of Primary Somatosensory Cortex in the Alert Monkey. *The Journal of Neuroscience*. 18(7): 2626-2645.

Douglas R, Martin K. (2007). Mapping the matrix: the ways of neocortex. *Neuron* 56(2): 226-238.

Douglas R, Martin, K. (2004). Neuronal circuits of the neocortex. *Annual Review of Neuroscience*. 27(1): 419-451.

Dragger U; Hubel D. (1975). Physiology of visual cells in mouse superior colliculus and correlation with somatosensory and auditory input. *Nature.* 253(5488): 203–204.

Dykes R, Gabor A. (1981). Magnification functions and receptive field sequences for submodality-specific bands in SI cortex of cats. *The Journal of Comparative Neurology*. 202(4): 597–620.

Dykes R, Rasmusson D, Hoeltzell P. (1980). Organisation of primary somatosensory cortex in the cat. *Journal of Neurophysiology*. *43*(6): 1527–1546.

Dykes R, Rasmusson D, Sretavan D, Rehman N. (1982). Submodality segregation and receptive-field sequences in cuneate, gracile, and external cuneate nuclei of the cat. *Journal of Neurophysiology*. 47: 389-416.

Edin B, Abbs J. (1991). Finger movement responses of cutaneous mechanoreceptors in the dorsal skin of the human hand. *Journal of Neurophysiology*. 65(3): 657-670.

Elston G, Benavides-Piccione R, DeFelipe J. (2001). The pyramidal cell in cognition: a comparative study in human and monkey. *Jounal of Neuroscience*. (21): RC163.

Elston G, Benavides-Piccione R, DeFelipe J. (2005a). A study of pyramidal cell structure in the cingulate cortex of the macaque monkey with comparative notes on inferotemporal and primary visual cortex. *Cerebral Cortex.* (15): 64–73.

Elston G, Elston A, Casagrande V, Kaas J. (2005b). Areal specialization in pyramidal cell structure in the visual cortex of the tree shrew: a new twist revealed in the evolution of cortical circuitry. *Experimental Brain Research*. (163): 13–20.

Elston G, Rosa, M. (1997). The occipitoparietal pathway of the macaque monkey: comparison of pyramidal cell morphology in layer III of functionally related cortical visual areas. *Cerebral Cortex.* (7): 432–452.

Elston G, Rosa, M. (2000). Pyramidal cells, patches, and cortical columns: a comparative study of infragranular neurons in TEO, TE, and the superior temporal polysensory area of the macaque monkey. *Journal of Neuroscience*. (20): RC117.

Elston, Rosa M. (1998). Morphological variation of layer III pyramidal neurones in the occipitotemporal pathway of the macaque monkey visual cortex. *Cerebral Cortex*. (8): 278–294.

Fang P, Jain N, Kaas J. (2002). Few intrinsic connections cross the hand-face border of BA3b of New World monkeys. *The Journal of Comparative Neurology*. 454(3): 310-319.

Farmer D, Pracejus N, Dempsey B, Turner A, Bokiniec P, Paton J, Pickering A, Burguet J, Andrey P, Goodchild A, McAllen R, McMullan S. (2019). On the presence and functional significance of sympathetic premotor neurons with collateralized spinal axons in the rat. *The Journal of Physiology*. *597*(13): 3407–3423.

Favorov O, Whitsel B. (1988). Spatial organisation of the peripheral input to BA1 cell columns. I. The detection of 'segregates'. *Brain Research*. 13(1): 25-42.

Federer F, Ichida J, Jeffs J, Schiessl I, McLoughlin N, Angelucci A. (2009). Four projection streams from primate V1 to the cytochrome oxidase stripes of V2. *J. Neurosci*. 29: 15455–15471.

Federer F, Taafua S, Merlin S, Hassanpour M, Angelucci A. (2021). Stream-specific feedback inputs to the primate primary visual cortex. *Nat. Commun*. 12: 228

Feldmeyer D. (2012). Excitatory neuronal connectivity in the barrel cortex. Frontiers in *Neuroanatomy*. 6.

Ferguson B, Gao W. (2018). Thalamic Control of Cognition and Social Behavior Via Regulation of Gamma-Aminobutyric Acidergic Signaling and Excitation/Inhibition Balance in the Medial Prefrontal Cortex. *Biological Psychiatry*. *83*(8): 657–669.

Ferraina S, Bianchi L. (1994). Posterior parietal cortex: functional properties of neurons in area 5 during an instructed-delay reaching task within different parts of space. *Experimental Brain Research*. 99(1):175-178

Fitzgerald P, Lane J, Thakur P, Hsiao S. (2006). Receptive Field (RF) Properties of the Macaque Second Somatosensory Cortex: RF Size, Shape, and Somatotopic Organisation. *Journal of Neuroscience*. 26(24): 6485-6495.

Friedman D, Jones E. (1981). Thalamic input to areas 3a and 2 in monkeys. *Journal of Neurophysiology*. 45(1): 59-85.

Friedman D, Murray E, O'Neill J, Mishkin M. (1986). Cortical connections of the somatosensory fields of the lateral sulcus of macaques: Evidence for a corticolimbic pathway for touch. *The Journal of Comparative Neurology*. 252(3): 323-347.

Friedman R, Chen L, Roe A. (2004). Modality maps within primate somatosensory cortex. Proceedings of the National Academy of Sciences. 101(34): 12724-12729.

Friedman R, Chen L, Roe A. (2008). Responses of BA3b and BA1 in Anesthetized Squirrel Monkeys to Single- and Dual-Site Stimulation of the Digits. *Journal of Neurophysiology*. 100(6): 3185-3196.

Friedman R, Morone K, Gharbawie O, Roe A. (2020) Mapping mesoscale cortical connectivity in monkey sensorimotor cortex with optical imaging and microstimulation. *Journal of Comparative Neurology*. 528(17):3095-3107.

Fries P, Neuenschwander S, Engel A, Goebel R, Singer W. (2001). Rapid feature selective neuronal synchronization through correlated latency shifting. *Nature Neuroscience*. 4(2): 194–200.

Fyffe R, Cheema S, Rustioni A. (1986). Intracellular staining study of the feline cuneate nucleus. I. Terminal patterns of primary afferent fibres. *Journal of Neurophysiology*. 56: 1268-1283.

Gardner EP. (2010). Dorsal and ventral streams in the sense of touch. *Senses*: *A Comprehensive Reference*. 6: 233-258.

Gergen J, MacLean P. (1962). A Stereotaxic Atlas of the Squirrel Monkey's Brain (Saimiri Sciureus). Washington, DC: United States Government Printing Office. *Arch. Neurol.* 9(1):104.

Gierer A, Meinhardt H. (1972). A theory of biological pattern formation. *Kybernetik*. 12(1): 30–39.

Gilbert C, Wiesel T. (1989). Columnar specificity of intrinsic horizontal and corticocortical connections in cat visual cortex. *The Journal of Neuroscience*. 9(7): 2432-2442.

Girardin C, Martin K. (2009). Inactivation of lateral connections in cat area 17. *European Journal of Neuroscience*. 29(10): 2092–2102.

Gouwens N, Sorensen S, Berg J, Lee C, Jarsky T, Ting J, Sunkin S, Feng D, Anastassiou C, Barkan E, Bickley K, Blesie N, Braun T, Brouner K, Budzillo A, Caldejon S, Casper T, Castelli D, Chong P, … Koch C. (2019). Classification of electrophysiological and morphological neuron types in the mouse visual cortex. *Nature Neuroscience*. 22(7). 1182–1195.

Grossberg S. (2003). Laminar Development of Receptive Fields, Maps and Columns in Visual Cortex: The Coordinating Role of the Subplate. *Cerebral Cortex*. 13(8): 852-863.

Harris K, Mrsic-Flogel T. (2013). Cortical connectivity and sensory coding. *Nature* 503(7474): 51-58.

Harris K, Shepherd G. (2015). The neocortical circuit: Themes and variations. Nature *Neuroscience.* 18(2): 170–181.

Harrison L, Stephan K., Rees G, Friston K. (2007). Extra-classical receptive field effects measured in striate cortex with fMRI. *NeuroImage*. 34(3), 1199–1208.

Harting Glendenning K; Diamond I; Hall W. (1973). Evolution of the primate visual system Anterograde degeneration studies of the tecto-pulvinar system. *American Journal of Biological Anthropology*. 38(2): 383–392.

Harvey B, Dumoulin, S. (2011). The Relationship between Cortical Magnification Factor and Population Receptive Field Size in Human Visual Cortex: Constancies in Cortical Architecture. *Journal of Neuroscience*. 31(38): 13604–13612.

Hayward V, Terekhov A, Wong S, Geborek P, Bengtsson F, Jörntell H. (2014). Spatio-temporal skin strain distributions evoke low variability spike responses in cuneate neurons. *Journal of The Royal Society Interface*. 11(93): 20131015.

Hellwig B, Schüz A, Aertsen A. (1994). Synapses on axon collaterals of pyramidal cells are spaced at random intervals: A Golgi study in the mouse cerebral cortex. *Biological Cybernetics*. 71(1): 1–12.

Hu J, Roe A. (2022). Functionally specific and sparse domain-based micro-networks in monkey V1 and V2. *Current Biology*. 32(13): 2797-2809.e3.

Huffman K, Krubitzer L. (2001). Thalamo-cortical connections of areas 3a and M1 in marmoset monkeys. *The Journal of Comparative Neurology*. 435(3): 291-310.

Hummelsheim H, Wiesendanger R, Wiesendanger M, Bianchetti M. (1985). The projection of low-threshold muscle afferents of the forelimb to the main and external cuneate nuclei of the monkey. *Neuroscience*. 16: 979-987.

Humphrey L; Norton T. (1980). Topographic organisation of the orientation column system in the striate cortex of the tree shrew Deoxyglucose mapping. *Journal of Comparative Neurology*. 192(3): 549–566.

Hyvärinen J, Poranen A. (1978). Receptive field integration and submodality convergence in the hand area of the post-central gyrus of the alert monkey. *The Journal of Physiology*. 283(1): 539-556.

Iggo A, Andres K. (1982). Morphology of cutaneous receptors. *Annual revision of neuroscience*. 5: 1-32

Innocenti G, Caminiti R. (2017). Axon diameter relates to synaptic bouton size: structural properties define computationally different types of cortical connections in primates. *Brain Structure and Function*. 222(3): 1169-1177.

Innocenti G. (2017). Network causality, axonal computations, and Poffenberger. *Experimental Brain Research*. 235(8): 2349-2357.

Iwamura Y, Iriki A, Tanaka M. (1994). Bilateral hand representation in the postcentral somatosensory cortex. *Nature*. 369(6481): 554-556.

Iwamura Y, Tanaka M, Sakamoto M, Hikosaka O, (1983). Converging patterns of finger representation and complex response properties of neurons in BA1 of the first somatosensory cortex of the conscious monkey. *Experimental Brain Research*. 51(3).

Iwamura Y, Tanaka M, Sakamoto M, Hikosaka O. (1985). Diversity in receptive field properties of vertical neuronal arrays in the crown of the postcentral gyrus of the conscious monkey. *Experimental Brain Research*. 58(2).

Iwamura Y. (1998). Hierarchical somatosensory processing. *Current Opinion in Neurobiology*. 8(4): 522-528.

Jain N, Florence S, Kaas J. (1998). Reorganization of Somatosensory Cortex after Nerve and Spinal Cord Injury. *Physiology*. 13(3): 143-149.

Jain N. (1998). A histologically visible representation of the fingers and palm in primate BA3b and its immutability following long-term differentiations. *Cerebral Cortex*. 8(3): 227-236.

Jeannerod M, Arbib M, Rizzolatti G, Sakata H. (1995). Grasping objects: the cortical mechanisms of visuomotor transformation. *Trends in Neurosciences*. 18(7): 314-320.

Jeffs J, Ichida J, Federer F, Angelucci A. (2009). Anatomical Evidence for Classical and Extra-classical Receptive Field Completion Across the Discontinuous Horizontal Meridian Representation of Primate Area V2. *Cerebral Cortex*. 19(4): 963–981.

Johansson R, Flanagan J. (2009). Coding and use of tactile signals from the fingertips in object manipulation tasks. *Nature Reviews Neuroscience*. 10(5): 345-359.

Johansson R, Vallbo A. (1979a). Tactile sensibility in the human hand: relative and absolute densities of four types of mechanoreceptive units in glabrous skin. *The Journal of Physiology*. 286(1): 283-300.

Johansson R, Vallbo A. (1979b). Detection of tactile stimuli. Thresholds of afferent units related to psychophysical thresholds in the human hand. *The Journal of Physiology*. 297(1): 405-422.

Johansson R, Vallbo A. (1983). Tactile sensory coding in the glabrous skin of the human hand. *Trends in Neurosciences*. 6: 27-32.

Johansson RS, Flanagan JR (2008). Somatosensation, *the Senses*: A Comprehensive Reference. San Diego Academic Press. 6: 67-86.

Johnson K, Hsiao S. (1992). Tactual form and texture perception. Annual *Review of Neuroscience*. 15: 227-250

Johnson K. (2001). The roles and functions of cutaneous mechanoreceptors. *Current Opinion in Neurobiology*. 11(4): 455-461.

Jones E, Coulter J, Hendry S. (1978). Intracortical connectivity of architectonic fields in the somatic sensory, motor and parietal cortex of monkeys. *The Journal of Comparative Neurology*. 181(2): 291-347.

Jones E, Friedman D. (1982). Projection pattern of functional components of thalamic ventrobasal complex on monkey somatosensory cortex. *Journal of Neurophysiology*. 48(2): 521-544.

Jones E. (1975). Lamination and differential distribution of thalamic afferents within the sensory-motor cortex of the squirrel monkey. *The Journal of Comparative Neurology*. 160(2): 167-203.

Jones E. (1983). Lack of collateral thalamocortical projections to fields of the first somatic sensory cortex in monkeys. *Experimental Brain Research*. 52(3): 375-384.

Jörntell H, Bengtsson F, Geborek P, Spanne A, Terekhov A, Hayward V. (2014). Segregation of Tactile Input Features in Neurons of the Cuneate Nucleus. *Neuron*. 83(6): 1444-1452.

Kaas J. (1983). What, if anything, is SI? Organisation of first somatosensory area of cortex. *Physiological Reviews*. 63(1): 206-231.

Kaas J. (1993). The functional organisation of somatosensory cortex in primates. *Annals of Anatomy - Anatomischer Anzeiger*. 175(6): 509–518.

Kaas J. (2004). Evolution of somatosensory and motor cortex in primates. *The Anatomical Record*. 281 (1): 1148-1156.kaas

Kaas J., Gharbawie O, Stepniewska I. (2011). The Organisation and Evolution of Dorsal Stream Multisensory Motor Pathways in Primates. *Frontiers in Neuroanatomy*. 5: 34

Kaas JH, Nelson JR, Sur M, Menenich MM. (1981a). Organisation of somatosensory cortex in primates. *The Organisation of the Cerebral Cortex*. Boston, MIT Press. pp: 237-261.

Kaas JH, Nelson JR, Sur M, Menenich MM. (1981b). Multiple representations of the body in the postcentral somatosensory cortex of primates. *Multiple Somatic Areas*. New Jersey. Vol.1. Humana Press. pp: 2945.

Kaas JH. (2000). The reorganization of somatosensory and motor cortex after peripheral nerve or spinal cord injury in primates. *Prog Brain Res*. 128: 173-179.

Kandel E. (2016). *Reductionism in Art and Brain Science: Bridging the Two Cultures*. Columbia University Press.

Kanold P. (2004). Transient microcircuits formed by Subplate neurons and their role in functional development of thalamocortical connections. *NeuroReport*. 15(14): 2149-2153.

Kim S, Gomez-Ramirez M, Thakur P, Hsiao S. (2015). Multimodal Interactions between Proprioceptive and Cutaneous Signals in Primary Somatosensory Cortex. *Neuron*. 86(2): 555-566.

Kim T, Freeman R. (2016). Direction selectivity of neurons in the visual cortex is non-linear and lamina-dependent. *European Journal of Neuroscience*. 43(10): 1389–1399.

Kisvárday Z, Crook J, Buzás P, Eysel U. (2000). Combined physiological-anatomical approaches to study lateral inhibition. *Journal of Neuroscience Methods*. 103(1): 91–106.

Kisvárday Z, Eysel U. (1992). Cellular organisation of reciprocal patchy networks in layer III of cat visual cortex (BA1 7). *Neuroscience*. 46(2): 275-286.

Kisvárday Z, Martin K, Freund T, Maglóczky Zs, Whitteridge D, Somogyi P. (1986). Synaptic targets of HRP-filled layer III pyramidal cells in the cat striate cortex. *Experimental Brain Research*. 64(3): 541–552.

Kisvárday Z, Tóth E, Rausch M, Eysel U. (1997). Orientation-specific relationship between populations of excitatory and inhibitory lateral connections in the visual cortex of the cat. *Cerebral Cortex* 7: 605-618.

Kisvarday Z. (1997). Orientation-specific relationship between populations of excitatory and inhibitory lateral connections in the visual cortex of the cat. *Cerebral Cortex*. 7(7): 605–618.

Kisvárday Z. (2016). Topography of Excitatory Cortico-cortical Connections in Three Main Tiers of the Visual Cortex: Functional Implications of the Patchy Horizontal Network. In Axons and Brain Architecture, ed. Rockland K.S., Academic Press, Pages 135-158. ISBN 9780128013939.

Koestinger, G., Martin, K., Roth, S., and Rusch, E. S. (2017). Synaptic connections formed by patchy projections of pyramidal cells in the superficial layers of cat visual cortex. *Brain Structure and Function*. 222: 3025-3042.

Koyuncu O, Hogue I, Enquist L. (2013). Virus Infections in the Nervous System. *Cell Host & Microbe. 13*(4). 379–393.

Krishnamurti A, Sanides F, Welker W. (1976). Microelectrode Mapping of Modality-Specific Somatic Sensory Cerebral Neocortex in Slow Loris. Brain, *Behavior and Evolution*. 13(4): 267-283.

Krubitzer L, Huffman K, Disbrow E, Recanzone G. (2004). Organisation of area 3a in macaque monkeys: Contributions to the cortical phenotype. *The Journal of Comparative Neurology*. 471(1): 97-111.

Krubitzer L, Kaas J. (1990). The organisation and connections of somatosensory cortex in marmosets. *The Journal of Neuroscience*. 10(3): 952-974.

Krubitzer L, Kaas J. (1992). The somatosensory thalamus of monkeys: Cortical connections and a redefinition of nuclei in marmosets. *The Journal of Comparative Neurology*. 319(1): 123-140.

Krubitzer LA, Baldwin MKL. (2017). Revisiting Kaas and colleagues-The homunculus: The discovery of multiple representations within the “primary” somatosensory cortex. *Revisiting the Classic Studies in Behavioral Neuroscience*. Los Angeles. Chapter 4. pp: 33-54

Krubitzer LA, Hunt DL. (2007). Captured in the Net of Space and Time: Understanding Cortical Field Evolution. *Evolution of Nervous System*. pp: 49-72.

Kurth R, Villringer K, Curio G, Wolf K, Krause T, Repenthin J, Schwiemann J, Deuchert M, Villringer A. (2000). FMRI shows multiple somatotopic digit representations in human primary somatosensory cortex. *Neuroreport*. 11(7). 1487–1491.

Lacquaniti F, Guigon E, Bianchi L, Ferraina S, Caminiti R. (1995). Representing Spatial Information for Limb Movement: Role of Area 5 in the Monkey. *Cerebral Cortex*. 5(5): 391-409.

Landry P, Deschênes M. (1981). Intracortical arbourizations and receptive fields of identified ventrobasal thalamocortical afferents to the primary somatic sensory cortex in the cat: Ventrobasal afferents to S1 in the cat. *Journal of Comparative Neurology*. 199(3): 345–371.

Lanciego J, Luquin N, Obeso J. (2012). Functional Neuroanatomy of the Basal Ganglia. Cold Spring Harbor Perspectives in Medicine. 2(12): a009621–a009621.

Landry P, Diadori P, Leclerc S, Dykes R. (1987). Morphological and electrophysiological characteristics of somatosensory thalamocortical axons studied with intra-axonal staining and recording in the cat. *Experimental Brain Research*. *65*(2).

Larkman A, Mason A. (1990). Correlations between morphology and electrophysiology of pyramidal neurons in slices of rat visual cortex. I. Establishment of cell classes. The *Journal of Neuroscience*. 10(5): 1407–1414.

László N. (2010). Overlap of connections of fingertip representations in the somatosensory cortex of the squirrel monkey. *Frontiers in Neuroscience*. 4.

Lee S, Ahmed T, Lee S, Kim H, Choi S, Kim D, Kim S, Cho J, Shin H. (2012). Bidirectional modulation of fear extinction by mediodorsal thalamic firing in mice. *Nature Neuroscience*. *15*(2): 308–314.

Leinonen L. (1980). Functional properties of neurons in the posterior part of area 7 in awake monkey. *Acta Physiologica Scandinavica*. 108(3): 301-308.

Lerner T, Ye L, Deisseroth K. (2016). Communication in Neural Circuits: Tools, Opportunities, and Challenges. *Cell*. *164*(6): 1136–1150.

LeVay S. (1988). Chapter 14: The patchy intrinsic projections of visual cortex. In *Progress in Brain Research* (Vol. 75, pp. 147–161). Elsevier.

Levitt J, Yoshioka T, Lund J. (1994). Intrinsic cortical connections in macaque visual area V2: evidence for interaction between different functional streams. J. Comp. Neurol. 342: 551–570.

Li H, Fukuda M, Tanifuji M, Rockland K. (2003). Intrinsic collaterals of layer 6 meynert cells and functional columns in primate v1. *Neuroscience*. 120(4): 1061-1069.

Li J, Liu T, Dong Y, Kondoh K, Lu Z. (2019). Trans-synaptic Neural Circuit-Tracing with Neurotropic Viruses. *Neuroscience Bulletin*. *35*(5): 909–920

Liets L, Olshausen B, Wang G, Chalupa L. (2003). Spontaneous Activity of Morphologically Identified Ganglion Cells in the Developing Ferret Retina. *The Journal of Neuroscience*. 23(19): 7343-7350.

Lipton M, Liszewski M, O'Connell M, Mills A, Smiley J, Branch C, Isler J, Schroeder C. (2010). Interactions within the Hand Representation in Primary Somatosensory Cortex of Primates. *Journal of Neuroscience*. 30(47): 15895-15903.

Livingstone M, Hubel D. (1984). Anatomy and physiology of a colour system in the primate visual cortex. *The Journal of Neuroscience*. 4(1): 309–356.

Livingstone M, Hubel D. (1984). Specificity of intrinsic connections in primate primary visual cortex. *The Journal of Neuroscience*. 4(11): 2830–2835.

Lodato S, Arlotta P. (2015). Generating neuronal diversity in the mammalian cerebral cortex. *Cell and Developmental Biology*. 31: 699-720

Luchicchi A, Pattij T, Viaña J, de Kloet S, Marchant N. (2021). Tracing goes viral: Viruses that introduce expression of fluorescent proteins in chemically-specific neurons. *Journal of Neuroscience Methods*. *348*: 109004.

Luhmann H, Milln L, Singer W. (1986). Development of horizontal intrinsic connections in cat striate cortex. *Experimental Brain Research*. 63(2).

Lund J, Yoshioka T, Levitt J. (1993). Comparison of intrinsic connectivity in different areas of macaque monkey cerebral cortex. *Cerebral Cortex* 3, 148-162.

Lund J. (2003). Anatomical Substrates for Functional Columns in Macaque Monkey Primary Visual Cortex. *Cerebral Cortex*. 13(1): 15-24.

Luo L, Callaway E, Svoboda K. (2008). Genetic Dissection of Neural Circuits. *Neuron*. *57*(5): 634–660.

Lübke J, Egger V, Sakmann B, Feldmeyer D. (2000). Columnar Organisation of Dendrites and Axons of Single and Synaptically Coupled Excitatory Spiny Neurons in Layer 4 of the Rat Barrel Cortex. *The Journal of Neuroscience*. 20(14): 5300–5311.

Lübke J, Feldmeyer D. (2007). Excitatory signal flow and connectivity in a cortical column: Focus on barrel cortex. *Brain Structure and Function*. 212(1): 3–17.

Makous J, Friedman R, & Vierck C. (1996). Effects of a dorsal column lesion on temporal processing within the somatosensory system of primates. *Experimental Brain Research*. 112(2): 253-267.

Malach R, Amir Y, Harel M, Grinvald A. (1994). Relationship between intrinsic connections and functional architecture revealed by optical imaging and in vivo targeted biocytin injections in primate striate cortex. *Proceedings of the National Academy of Sciences*. 90(22): 10469-10473.

Maldjian J, Gottschalk A, Patel R, Detre J, Alsop D. (1999). The Sensory Somatotopic Map of the Human Hand Demonstrated at 4 Tesla. *NeuroImage*. 10(1): 55–62.

Manger P, Woods T, Muñoz A, Jones E. (1997). Hand/Face Border as a Limiting Boundary in the Body Representation in Monkey Somatosensory Cortex. *The Journal of Neuroscience*. 17(16): 6338-6351.

Markov N, Vezoli J, Chameau P, Falchier A, Quilodran R, Huissoud C, Lamy C, Misery P, Giroud, P, Ullman S, Barone P, Dehay C, Knoblauch K, Kennedy H. (2014). Anatomy of hierarchy: Feedforward and feedback pathways in macaque visual cortex. *Journal of Comparative Neurology*. 522(1): 225–259.

Markram H, Muller E, Ramaswamy S, Reimann M, Abdellah M, Sanchez, C, Ailamaki A, Alonso-Nanclares L, Antille N, Arsever S, Kahou G, Berger T, Bilgili A, Buncic N, Chalimourda A, Chindemi G, Courcol J, Delalondre F, Delattre V, … Schürmann F. (2015). Reconstruction and Simulation of Neocortical Microcircuitry. *Cell*. 163(2): 456–492.

Marshall W, Woolsey C, Bard P. (1937). Cortical Representation of Tactile Sensibility as Indicated by Cortical Potentials. *Science*. 85(2207): 388-390.

Martin K, Roth S, Rusch E. (2017). A biological blueprint for the axons of superficial layer pyramidal cells in cat primary visual cortex. *Brain Struct. Funct*. 222(8): 3407-3430.

Martin K, Whitteridge D. (1984). Form, function and intracortical projections of spiny neurones in the striate visual cortex of the cat. *The Journal of Physiology*. 353(1). 463–504.

Martin K, Whitteridge D. (1984). The relationship of receptive field properties to the dendritic shape of neurones in the cat striate cortex. *The Journal of Physiology*. 356(1): 291–302.

Martin, K, Roth S, Rusch E. (2014). Superficial layer pyramidal cells communicate heterogeneously between multiple functional domains of cat primary visual cortex. *Nature Communications*. 5(1): 5252.

Matsubara J, Chase R, Thejomayen M. (1996). Comparative morphology of three types of projection-identified pyramidal neurons in the superficial layers of cat visual cortex. *The Journal of Comparative Neurology*. 366(1): 93–108.

Megías M, Emri Z, Freund T, Gulyás A. (2001). Total number and distribution of inhibitory and excitatory synapses on hippocampal CA1 pyramidal cells. *Neuroscience*. 102(3): 527–540.

Melzer S, Monyer H. (2020). Diversity and function of corticopetal and corticofugal GABAergic projection neurons. *Nature Reviews Neuroscience*. 21(9): 499–515.

Menon V. (2015). Salience network. In Brain Mapping, A.W. Toga, ed. (Academic Press).

Merzenich M, Kaas J, Sur M, Lin C. (1978). Double representation of the body surface within cytoarchitectonic area3b and area1 in “S1” in the owl monkey (aotus trivirgatus). *The Journal of Comparative Neurology*. 181(1): 41-73.

Merzenich M, Kaas J, Wall J, Nelson R, Sur M, Felleman D. (1983). Topographic reorganization of somatosensory cortical BA3b and BA1 in adult monkeys following restricted differentiation. *Neuroscience*. 8(1): 33-55.

Merzenich M, Nelson R, Kaas J, Stryker M, Jenkins W, Zook J, Cynader M, Schoppmann A. (1987). Variability in hand surface representations in BA3b and BA1 in adult owl and squirrel monkeys. *The Journal of Comparative Neurology*. 258(2): 281-296.

Merzenich M, Nelson R, Stryker M, Cynader M, Schoppmann A, Zook J. (1984). Somatosensory cortical map changes following digit amputation in adult monkeys. *The Journal of Comparative Neurology*. 224(4): 591-605.

Mishkin M. (1979). Analogous neural models for tactual and visual learning. *Neuropsychologia*. 17(2): 139-151

Mitchison G, Crick F. (1982). Long axons within the striate cortex: their distribution, orientation, and patterns of connection. *Proceedings of the National Academy of Sciences*. 79(11): 3661-3665.

Molyneaux B, Arlotta P, Menezes J, Macklis J. (2007). Neuronal subtype specification in the cerebral cortex. *Nature Reviews Neuroscience*. 8(6): 427–437.

Mountcastle V. (1984). Neural Mechanisms in Somesthesis: Recent Progress and Future Problems. In C. von Euler, O. Franzén, U. Lindblom, & D. Ottoson (Eds.), *Somatosensory Mechanisms* (pp. 3–16). Palgrave Macmillan UK

Mountcastle V. (1997). The columnar organisation of the neocortex. *Brain*. 120(4): 701–722.

Mountcastle VB. (2011). Central nervous mechanisms in mechanoreceptive sensibility. *Comprehensive Physiology*. pp: 33-89.

Muir D, Da Costa N, Girardin C, Naaman S, Omer D, Ruesch E, Grinvald A, Douglas R. (2011). Embedding of Cortical Representations by the Superficial Patch System. *Cerebral Cortex*. 21(10): 2244-2260.

Muir D, Douglas R. (2010). From Neural Arbors to Daisies. *Cerebral Cortex*. 21(5): 1118-1133.

Muller L, Chavane F, Reynolds J, Sejnowski T. (2018). Cortical travelling waves: mechanisms and computational principles. *Nature Reviews Neuroscience.* 21(5): 255-268.

Nakamura A, Yamada T, Goto A, Kato T, Ito K, Abe Y, Kachi T, Kakigi R. (1998). Somatosensory Homunculus as Drawn by MEG. *NeuroImage*. 7(4): 377–386.

Nassi J, Cepko C, Born R, Beier K. (2015). Neuroanatomy goes viral! *Frontiers in Neuroanatomy*. *9*:80

Negwer C, Ille S, Hauck T, Sollmann N, Maurer S, Kirschke J, Ringel F, Meyer B, Krieg S. (2017). Visualization of subcortical language pathways by diffusion tensor imaging fibre tracking based on rTMS language mapping. *Brain Imaging and Behavior*. 11(3): 899–914.

Négyessy L, Gál V, Farkas T, Toldi J. (2000). Cross-modal plasticity of the corticothalamic circuits in rats enucleated on the first postnatal day. *European Journal of Neuroscience*. 12(5): 1654-1668.

Négyessy L, Goldman-Rakic P. (2005). Morphometric characterization of synapses in the primate prefrontal cortex formed by afferents from the mediodorsal thalamic nucleus. *Exp. Brain Res*. 164(2): 148-154.

Négyessy L, Pálfi E, Ashaber M, Palmer C, Jákli B, Friedman R, Chen L, Roe A. (2013). Intrinsic horizontal connections process global tactile features in the primary somatosensory cortex: Neuroanatomical evidence. *Journal of Comparative Neurology*. 521(12): 2798-2817.

Nelson R, Sur M, Felleman D, Kaas J. (1980). Representations of the body surface in postcentral parietal cortex of Macaca Fascicularis. *The Journal of Comparative Neurology*. 192(4): 611-643.

Nikolić D, Mureşan R, Feng W, Singer W. (2012). Scaled correlation analysis: A better way to compute a cross-correlogram: Scaled correlation analysis. *European Journal of Neuroscience*. 35(5): 742–762.

Niu J, Ding L, Li J, Kim H, Liu J, Li H. (2013). Modality-Based Organisation of Ascending Somatosensory Axons in the Direct Dorsal Column Pathway. *Journal of Neuroscience*. 33(45): 17691-17709.

Noseda R, Kainz V, Jakubowski M, Gooley J, Saper C, Digre K, Burstein R. (2010). A neural mechanism for exacerbation of headache by light. *Nature Neuroscience*. *13*(2): 239–245.

O'Leary D, Koester S. (1993). Development of projection neuron types, axon pathways, and patterned connections of the mammalian cortex. *Neuron*. 10(6): 991–1006.

Pack C, Bensmaia S. (2015). Seeing and Feeling Motion: Canonical Computations in Vision and Touch. *PLOS Biology*. 13(9): e1002271.

Padberg J, Cerkevich C, Engle J, Rajan A, Recanzone G, Kaas J, Krubitzer L. (2009). Thalamocortical Connections of Parietal Somatosensory Cortical Fields in Macaque Monkeys Are Highly Divergent and Convergent. *Cerebral Cortex*. 19(9): 2038-2064.

Pálfi E, Zalányi L, Ashaber M, Palmer C, Kántor O, Roe A, Friedman R, Négyessy L. (2018). Connectivity of neuronal populations within and between areas of primate somatosensory cortex. *Brain structure and function.* 223(6): 2949-2971.

Panzeri S, Macke J, Gross J, Kayser C. (2015). Neural population coding: combining insights from microscopic and mass signals. *Trends in Cognitive Sciences.* 19(3): 162-72.

Pei Y, Denchev P, Hsiao S, Craig J, Bensmaia S. (2009). Convergence of Submodality-Specific Input onto Neurons in Primary Somatosensory Cortex. *Journal of Neurophysiology*. 102(3): 1843-1853.

Penfield W, Boldrey E. (1937). Somatic motor and sensory representations in the cerebral cortex of man as studied by electrical stimulation. *Brain*. vol. 60: 389-443

Petrof I, Sherman, S. (2013). Functional significance of synaptic terminal size in glutamatergic sensory pathways in thalamus and cortex. *Journal of Neurophysiology*. 591(13): 3125-3131.

Phillips J, Johnson K. (1981). Tactile spatial resolution: II. Neural representation of bars edges and gratings in monkey afferents. *Journal of Neurophysiology*. 46: 1192-1203.

Pieraut S, Gounko N, Sando R, Dang W, Rebboah E, Panda S, Madisen L, Zeng H, Maximov A. (2014). Experience-dependent remodeling of basket cell networks in the dentate gyrus. *Neuron*. 84(1): 107–122.

Polack P, Contreras D. (2012). Long-range parallel processing and local recurrent activity in the visual cortex of the mouse. *Journal of Neuroscience*. 32(32): 11120-11131.

Pollock, David M. (2011). Neural Basis of Touch and Proprioception in Primate Cortex. *Comprehensive Physiology*. 8(4): 1575–1602.

Pons T, Garraghty P, Cusick C, Kaas J., 1985. The Somatotopic organisation of area 2 in macaque monkeys. *The Journal of Comparative Neurology*. 241(4): 445-466.

Price D. (1986). The postnatal development of clustered intrinsic connections in BA1 8 of the visual cortex in kittens. *Developmental Brain Research*. 24(1-2): 31-38.

Purves D, Riddle D. (1992). Iterated patterns of brain circuitry (how the cortex gets its spots). *Trends in Neuroscience*. 15(10): 362-368.

Qi H, Gharbawie O, Wong P, Kaas J. (2011). Cell-poor septa separate representations of digits in the ventroposterior nucleus of the thalamus in monkeys and prosimian Galagos. *Journal of Comparative Neurology*. 519: 738-758.

Qi H, Kaas J. (2004). Myelin stains reveal an anatomical framework for the representation of the digits in somatosensory BA3b of macaque monkeys. *The Journal of Comparative Neurology*. 477(2): 172-187.

Qiu L, Zhang B, Gao Z. (2022). Lighting Up Neural Circuits by Viral Tracing. *Neuroscience Bulletin*. *38*(11): 1383–1396.

Ramos-Prats A, Paradiso E, Castaldi F, Sadeghi M, Mir M, Hörtnagl H, Göbel G, Ferraguti F. (2022). VIP-expressing interneurons in the anterior insular cortex contribute to sensory processing to regulate adaptive behavior. *Cell Reports*. *39*(9): 110893.

Randolph M, Semmes J. (1974). Behavioral consequences of selective subtotal ablations in the postcentral gyrus of Macaca mulatta. *Brain Research*. 70(1): 55-70.

Rasmussen A, Peyton W. (1948). The course and termination of the medial lemniscus in man. *The Journal of Comparative Neurology*. 88(3): 411-424.

Rathelot J, Strick P. (2006). Muscle representation in the macaque motor cortex: An anatomical perspective. *Proceedings of the National Academy of Sciences*. 103(21): 8257-8262.

Ratzlaff E, Grinvald, A. (1991). A tandem-lens epifluorescence microscope: Hundred-fold brightness advantage for wide-field imaging. *Journal of Neuroscience Methods*. 36(2-3): 127-137.

Reed J, Pouget P, Qi H, Zhou Z, Bernard M, Burish M, Haitas J, Bonds A, Kaas J. (2008). Widespread spatial integration in primary somatosensory cortex. *Proceedings of the National Academy of Sciences*. 105(29): 10233-10237.

Reiner A, Veenman C, Medina L, Jiao Y, Del Mar N, Honig M. (2000). Pathway tracing using biotinylated dextran amines. *Journal of Neuroscience Methods*. *103*(1): 23–37.

Remple M, Reed J, Stepniewska I, Kaas J. (2006). Organisation of front parietal cortex in the tree shrew. I. Architecture, microelectrode maps, and corticospinal connections. *The Journal of Comparative Neurology*. 497(1): 133-154.

Rockland K, Knutson T. (2000). Feedback connections from area MT of the squirrel monkey to areas V1 and V2. *The Journal of Comparative Neurology*. 425(3): 345-368.

Rockland K, Knutson T. (2001). Axon collaterals of meynert cells diverge over large portions of area V1 in the macaque monkey. *The Journal of Comparative Neurology*. 441(2): 134-147.

Rockland K, Lund J. (1982). Widespread periodic intrinsic connections in the tree shrew visual cortex. *Science*. 215(4539): 1532-1534.

Rockland K, Lund J. (1983). Intrinsic laminar lattice connections in primate visual cortex. The *Journal of Comparative Neurology*. 216(3): 303-318.

Rockland K. (2018). Axon Collaterals and Brain States. *Frontiers in Systems Neuroscience*. 12: 32.

Rockland K. (2020). What we can learn from the complex architecture of single axons. *Brain Structure and Function.* 225(4): 1327-1347.

Roe A, Chernov M, Friedman R, Chen G. (2015). In Vivo Mapping of Cortical Columnar Networks in the Monkey with Focal Electrical and Optical Stimulation. *Frontiers in Neuroanatomy*. 9: 135.

Roe A. (2019). Columnar connectome: toward a mathematics of brain function. *Network Neuroscience.* 3(3): 779-791.

Rossi-Pool R, Zainos A, Alvarez M, Parra S, Zizumbo J, Romo R. (2021). Invariant timescale hierarchy across the cortical somatosensory network. *Proceedings of the National Academy of Sciences.* 118(3): e2021843118.

Ruben J, Dally M, Bailey M, Smith R, McLean C, Fedele P. (2006). Cerebral radiation necrosis: Incidence, outcomes, and risk factors with emphasis on radiation parameters and chemotherapy. *International Journal of Radiation Oncology Biology Physics*. 65(2): 499-508.

Ruthazer E, Stryker M. (1996). The Role of Activity in the Development of Long-Range Horizontal Connections in BA1 7 of the Ferret. *The Journal of Neuroscience*. 16(22): 7253-7269.

Saal H, Bensmaia S. (2014). Touch is a team effort: interplay of submodalities in cutaneous sensibility. *Trends in Neurosciences*. 37(12): 689-697.

Sainburg R. (2002). Evidence for a dynamic-dominance hypothesis of handedness. *Experimental Brain Research*. 142(2): 241–258.

Sakata H, Takaoka Y, Kawarasaki A, Shibutani H. (1973). Somatosensory properties of neurons in the superior parietal cortex (area 5) of the rhesus monkey. *Brain Research*. 64: 85-102.

Saleeba C, Dempsey B, Le S, Goodchild A, McMullan S. (2019). A Student's Guide to Neural Circuit Tracing. *Frontiers in Neuroscience. 13*: 897.

Sanides F. (1968). The architecture of the cortical taste nerve areas in squirrel monkey (Saimiri sciureus) and their relationships to insular, sensorimotor and prefrontal regions. *Brain Research*. 8(1): 97-124.

Sanides F. (1970). Functional architecture of motor and sensory cortices in primates in light of a new concept of neocortical evolution. *The Primate Brain*. New York: Appleton Century-Crofts. Vol (1) pp: 137-298.

Sathian K. (2016). Analysis of haptic information in the cerebral cortex. *Journal of Neurophysiology*. 116(4): 1795-1806.

Schwarz L, Miyamichi K, Gao X, Beier K, Weissbourd B, DeLoach K, Ren J, Ibanes S, Malenka R, Kremer E, Luo L. (2015). Viral-genetic tracing of the input–output organization of a central noradrenaline circuit. *Nature*. *524*(7563): 88–92.

Schweizer R, Voit D, Frahm J. (2008). Finger representations in human primary somatosensory cortex as revealed by high-resolution functional MRI of tactile stimulation. *NeuroImage*. 42(1), 28-35.

Seelke A, Padberg J, Disbrow E, Purnell S, Recanzone G, Krubitzer L. (2011). Topographic Maps within Brodmann Area 5 of Macaque Monkeys. *Cerebral Cortex*. 22(8): 1834-1850.

Segev I, Schneidman E. (1999). Axons as computing devices: basic insights gained from models. *Journal of Physiology*. 93(4): 263-270.

Semedo, Jasper A, Zandvakili A, Krishna A, Aschner A, Machens C, Kohn A, Yu B. (2022). Feedforward and feedback interactions between visual cortical areas use different population activity patterns. *Nature Communications.* 13: 1099.

Shepherd G, Raastad M, Andersen P. (2002). General and variable features of varicosity spacing along unmyelinated axons in the hippocampus and cerebellum. *Proceedings of the National Academy of Sciences*. 99(9): 6340-6345.

Shi J, Franklin J, Yelinek J, Ebersberger I, Warren G, He C. (2008). Centrin4 coordinates cell and nuclear division in *T. brucei*. *Journal of Cell Science*. *121*(18): 3062–3070.

Shmuel A. (2005). Retinotopic Axis Specificity and Selective Clustering of Feedback Projections from V2 to V1 in the Owl Monkey. *Journal of Neuroscience*. 25(8): 2117–2131.

Sincich L, Blasdel G. (2001). Oriented Axon Projections in Primary Visual Cortex of the Monkey. *The Journal of Neuroscience*. 21(12): 4416–4426.

Sincich L, Horton J. (2005). THE CIRCUITRY OF V1 AND V2: Integration of Colour, Form, and Motion. *Annual Review of Neuroscience*. 28(1). 303–326.

Sincich L, Jocson C, Horton J. (2010). V1 interpatch projections to v2 thick stripes and pale stripes. *J. Neurosci*. 30: 6963–6974.

Sinclair R, Burton, H. (1991). Tactile Discrimination of Gratings: Psychophysical and Neural Correlates in Human and Monkey. *Somatosensory & Motor Research*. 8(3), 241–248.

Smith M, Deacon P. (1984). Topographical anatomy of the posterior columns of the spinal cord in man. *Brain*. 107(3): 671-698.

Snyder L, Batista A, Andersen R. (1997). Coding of intention in the posterior parietal cortex. *Nature*. 386(6621): 167-170.

Somogyi P, Tamás G, Lujan R, Buhl E. (1998). Salient features of synaptic organisation in the cerebral cortex. *Brain Research Reviews*. 26(2/3) 113-135.

Sreepathi H, Ferraguti F. (2012). Subpopulations of neurokinin 1 receptor-expressing neurons in the rat lateral amygdala display a differential pattern of innervation from distinct glutamatergic afferents. *Neuroscience*. *203*: 59–77.

Sretavan D, Shatz C. (1984). Prenatal development of individual retinogeniculate axons during the period of segregation. *Nature*. 308(5962): 845–848.

Sripati A. (2006). Spatiotemporal Receptive Fields of Peripheral Afferents and Cortical BA3b and BA1 Neurons in the Primate Somatosensory System. *Journal of Neuroscience*. 26(7): 2101-2114.

Staiger J, Schubert D, Zuschratter W, Kötter R, Luhmann H, Karl Zilles. (2002). Innervation of interneurons immunoreactive for VIP by intrinsically bursting pyramidal cells and fast-spiking interneurons in infragranular layers of juvenile rat neocortex: Local connectivity in barrel cortex. *European Journal of Neuroscience*. 16(1): 11–20.

Stepanyants A, Tamás G, Chklovskii D. (2004) Class-specific features of neuronal wiring. *Neuron*. 43(2): 251-259.

Stettler D, Das A, Bennett J, Gilbert C. (2002). Lateral Connectivity and Contextual Interactions in Macaque Primary Visual Cortex. *Neuron*. 36(4). 739–750.

Stippich C, Hofmann R, Kapfer D, Hempel E, Heiland S, Jansen O, Sartor K. (1999). Somatotopic mapping of the human primary somatosensory cortex by fully automated tactile stimulation using functional magnetic resonance imaging. *Neuroscience Letters*. 277(1): 25–28.

Sur M, Garraghty P, Bruce C. (1985). Somatosensory cortex in macaque monkeys: laminar differences in receptive field size in BA3b and BA1. *Brain Research*. 342(2): 391-395.

Sur M, Merzenich M, Kaas J. (1980). Magnification, receptive-field area, and "hypercolumn" size in BA3b and BA1 of somatosensory cortex in owl monkeys. *Journal of Neurophysiology*. 44(2): 295-311.

Sur M, Nelson R, Kaas J. (1980). Representation of the body surface in somatic koniocortex in the prosimian Galago. *The Journal of Comparative Neurology*. 189(2): 381-402.

Sur M, Nelson R, Kaas J. (1982). Representations of the body surface in cortical BA3b and BA1 of squirrel monkeys: Comparisons with other primates. *The Journal of Comparative Neurology. 211(2): 177-192.*

Sur M, Wall J, Kaas J. (1981). Modular Segregation of Functional Cell Classes within the Postcentral Somatosensory Cortex of Monkeys. *Science*. 212(4498): 1059-1061.

Sur M, Weller R, Kaas, J. (1980). Representation of the body surface in somatosensory area I of tree shrews, Tupaia glis. *The Journal of Comparative Neurology*. 194(1): 71-95.

Szentágothai J. (1975). The ‘module-concept’ in cerebral cortex architecture. *Brain Research*. 95(2–3): 475-496.

Talbot W, Darian Smith I, Kornhuber H, Mountcastle V. (1968). The sense of flutter vibration: comparison of human capacity with response patterns of mechanoreceptive afferents from the monkey hand. *Journal of Neurophysiology*. 31: 301-334.

Tamamaki N, Tomioka R. (2010). Long-Range GABAergic Connections Distributed throughout the Neocortex and their Possible Function. *Frontiers in Neuroscience*. (4):202.

Taoka M, Toda T, Iriki A, Tanaka M, Iwamura Y. (2000). Bilateral receptive field neurons in the hindlimb region of the postcentral somatosensory cortex in awake macaque monkeys. *Experimental Brain Research*. 134(2): 139-146.

Thakur P, Fitzgerald P, Hsiao S. (2012). Second-order receptive fields reveal multidigit interactions in BA3b of the macaque monkey. *Journal of Neurophysiology.* 108*(1): 243-262.*

Tommerdahl M, Delemos K, Favorov O, Metz C, Vierck C, Whitsel B. (1998). Response of Anterior Parietal Cortex to Different Modes of Same-Site Skin Stimulation. *Journal of Neurophysiology*. 80(6): 3272-3283.

Tommerdahl M, Delemos K, Vierck C, Favorov O, Whitsel, B. (1996). Anterior parietal cortical response to tactile and skin-heating stimuli applied to the same skin site. *Journal of Neurophysiology*. 75(6): 2662-2670.

Tommerdahl M, Favorov O, Whitsel B, Nakhle B, Gonchar Y. (1993). Minicolumnar Activation Patterns in Cat and Monkey SI Cortex. *Cerebral Cortex*. 3(5): 399-411.

Torebjork H, Vallbo A, Ochoa J. (1987). Intra-neural microstimulation in man: Its relation to specificity of tactile sensations. *Brain*. 110: 1509-1529.

Toth K, Freund T, Miles R. (1997). Disinhibition of rat hippocampal pyramidal cells by GABAergic afferents from the septum. *Journal of Physiology*. (500): 463–474.

Ts’o D, Roe A, Gilbert C. (2001). A hierarchy of the functional organisation for colour, form and disparity in primate visual area V2. *Vision Research*. 41(10–11): 1333–1349.

Turing A. (1952). Philosophical Transactions of the Royal Society of London. Series B, Biological Sciences, Vol. 237, No. 641. pp. 37-72.

Ugolini G. (2010). Advances in viral transneuronal tracing. *Journal of Neuroscience Methods*. *194*(1): 2–20.

Vaden J, Gonzalez J, Tsai M, Niver A, Fusilier A, Griffith C, Kramer R, Wadiche J, Overstreet-Wadiche L. (2020). Parvalbumin interneurons provide spillover to newborn and mature dentate granule cells. *ELife*. (9): e54125.

Villringer K, Kurth R, Repenthin J, Stoll T, Curio G, Schwiemann J, Wolf K, Villringer A. (1998). fMRI Mapping of Digital and Facial Sites in Human Brodmann Area 3b. *NeuroImage*. 7(4): S403.

Voges N, Guijarro C, Aertsen A, Rotter S. (2010). Models of cortical networks with long-range patchy projections. *Journal of Computational Neuroscience*. *28*(1): 137–154.

Vogt B, Pandya, D. (1978). Cortico-cortical connections of somatic sensory cortex (areas 3, 1 and 2) in the rhesus monkey. *The Journal of Comparative Neurology*. 177(2): 179–191.

Vogt C, Vogt O. (1919). Aligeimeinere Ergebnieee unserer Hirnforschung. *J Psychol Neurol. Leipzig*. 25: 279-462.

Wang Z, Chen L, Négyessy L, Friedman R, Mishra A, Gore J, Roe A. (2013). The Relationship of Anatomical and Functional Connectivity to Resting-State Connectivity in Primate Somatosensory Cortex. *Neuron*. 78(6): 1116-1126.

Weber A, Saal H, Lieber J, Cheng J, Manfredi L, Dammann J, & Bensmaia S. (2013). Spatial and temporal codes mediate the tactile perception of natural textures. *Proceedings of the National Academy of Sciences*. 110(42), 17107-17112.

Wen Q, Chklovskii D. (2008). A Cost–Benefit Analysis of Neuronal Morphology. *Journal of Neurophysiology*. *99*(5): 2320–2328.

Westling G, Johansson R. (1987). Responses in glabrous skin mechanoreceptors during precision grip in humans. *Journal of Experimental Brain Research*. 66: 128-140

Witham C, Baker S. Modulation and transmission of peripheral inputs in monkey cuneate and external cuneate nuclei. *Journal of Neurophysiology*. 106: 2764-2775.

Womelsdorf T, Lima B, Vinck M, Oostenveld R, Singer W, Neuenschwander S, Fries P. (2012). Orientation selectivity and noise correlation in awake monkey area V1 are modulated by the gamma cycle. *Proceedings of the National Academy of Sciences*. 109(11): 4302–4307.

Wong R. (1999). Retinal Waves and Visual System Development. *Annual Review of Neuroscience*. 22(1):29-47.

Woolsey T, Van der Loos H. (1970). The structural organisation of layer IV in the somatosensory region (S1) of mouse cerebral cortex. *Brain Research*. 17(2): 205–242.

Xiao Y, Felleman D. (2004). Projections from primary visual cortex to cytochrome oxidase thin stripes and interstripes of macaque visual area2. *Proc. Natl. Acad. Sci*. USA 101: 7147–7151.

Xu A, Qian M, Tian F, Xu B, Friedman R, Wang J, Song, X, Sun Y, Chernov M, Cayce J, Jansen E, Mahadevan-Jansen A, Zhang X, Chen G, Roe A. (2019). Focal infrared neural stimulation with high-field functional MRI: A rapid way to map mesoscale brain connectomes. *Science Advances.* 5(4): eaau7046.

Xu J, & Wall J. (1999). Functional organisation of tactile inputs from the hand in the cuneate nucleus and its relationship to organisation in the somatosensory cortex. *The Journal of Comparative Neurology*. 411(3): 369-389.

Xu J, Wall J. (1996). Cutaneous Representations of the Hand and Other Body Parts in the Cuneate Nucleus of a Primate and Some Relationships to Previously Described Cortical Representations. *Somatosensory & Motor Research*. 13(3-4): 187-197.

Yan M, Yu W, Lv Q, Lv Q, Bo T, Chen X, Liu Y, Zhan Y, Yan S, Shen X, Yang B, Hu Q, Yu J, Qiu Z, Feng Y, Zhang X, Wang H, Xu F, Wang Z. (2022). Mapping brain-wide excitatory projectome of primate prefrontal cortex at submicron resolution and comparison with diffusion tractography. *ELife*. *11*: e72534.

Yau J, Kim S, Thakur P, Bensmaia S. (2016). Feeling form: the neural basis of haptic shape perception. *Journal of Neurophysiology*. 115(2): 631-642.

Yoshioka T, Blasdel G, Levitt J, Lund J. (1996). Relation between Patterns of Intrinsic Lateral Connectivity, Ocular Dominance, and Cytochrome Oxidase-Reactive Regions in Macaque Monkey Striate Cortex. *Cerebral Cortex*. 6(2): 297–310.

Yuan M, Meyer T, Benkowitz C, Savanthrapadian S, Ansel-Bollepalli L, Foggetti A, Wulff P, Alcami P, Elgueta C, Bartos M. (2017). Somatostatin-positive interneurons in the dentate gyrus of mice provide local- and long-range septal synaptic inhibition. *Elife*. (6) e21105.

Zeng H, Sanes J. (2017). Neuronal cell-type classification: challenges, opportunities and the path forward. *Nature Reviews Neuroscience*. 18(9): 530-546.

Zhou K, Zhu L, Hou G, Chen X, Chen B, Yang C, Zhu Y. (2021). The Contribution of Thalamic Nuclei in Salience Processing. *Frontiers in Behavioral Neuroscience*. *15*: 634618.

Zhou T, Zhu H, Fan Z, Wang F, Chen Y, Liang H, Yang Z, Zhang L, Lin L, Zhan Y, Wang Z, Hu H. (2017). History of winning remodels thalamo-PFC circuit to reinforce social dominance. *Science*. *357*(6347): 162–168.

Zohary E, Shadlen M, Newsome W. (1994). Correlated neuronal discharge rate and its implications for psychophysical performance. *Nature*. 370(6485): 140–143.

10. Publication List

11.1. Publications of the thesis

Mir et al. (2022). Modular Organisation of Signal Transmission in Primate Somatosensory Cortex. *Front Neuroanat*. Jul 8; 16:915238. doi: 10.3389/fnana.2022.915238. **IF: 3.267**

Ramos-Prats A, Paradiso E, Castaldi F, Sadeghi M, **Mir MY**, Hörtnagl H, Göbel G, Ferraguti F. (2022). VIP-expressing interneurons in the anterior insular cortex contribute to sensory processing to regulate adaptive behavior. *Cell reports*. *39*(9):1-24. doi.org/10.1016/j.celrep.2022.110893. **IF: 9.423**

11.3. Conference publications of the thesis

Mir Y, Pálfi E, Roe A, Friedman R, Négyessy L. (2019) Corrigendum to "Structural correlates of modular organisation of activity propagation in the primate somatosensory cortex" [IBROR 6S (2019) S540]. *IBRO Rep*.

Mir Y, Pálfi E, Roe A, Friedman R, Négyessy L. (2021) Structural correlates of modular organisation of signal transmission in the primate somatosensory cortex. *European Neuropsychopharmacology*.

11.4. Other publications

Baba, Abu Imran, **Mohd Yaqub Mir**, Riyazuddin, Ágnes Cséplő, Gábor Rigó, and Attila Fehér. 2022. "Plants in Microgravity: Molecular and Technological Perspectives *„International Journal of Molecular Sciences*. 23, no. 18: 10548. https://doi.org/10.3390/ijms231810548. **IF: 6.205**

DOI:10.14753/SE.2023.2830

1. Acknowledgements

Time flies so fast, after five years of PhD study in Hungary, Finally, I am able to defend and tell the story of my project. The scientific training and life experience I have gotten in Hungary, Austria and Sweden Laboratories during the past few years is my invaluable treasure, which will have big impact on my future scientific career and personal life.

Above all, I would like to express my special thanks to my supervisor, **László Négyessy**, who has given me great support and excellent guidance during this critical period of my career. I deeply appreciate your patient and motivating discussion of scientific issues with me, and the great opportunities you have provided for international scientific communication. The rigorous training you have provided during my PhD period gave me a solid foundation and good start to continue my scientific career. I am also very thankful to Dr Francesco Ferraguti and Dr Fahad Sultan for their enormous support during my stay in their laboratories for different projects.

My thanks must be given to all the members of my lab for their help whenever I needed. It is a great honour to have Emese Palfi who taught me how to use the Neurolucida Program and for taking care and handling all my administrative procedures which was a great help for my PhD project.

My thanks also go to all our USA collaborators especially to Dr Robert Friedman for his time and efforts to evaluate my manuscript. In addition, I am very grateful **to Péter Buzás and Gergely Zachar** for reviewing my thesis.

I would like to thank Wigner Research Centre for Physics, Tempus Public Foundation and Semmelweis University, for offering me this great PhD program opportunity to study in a beautiful city, Budapest, Hungary

I would also like to thank to my friends both in and out of Hungary: Owais Mujtaba, Aaqib Lone, Mir Ishtiyaq, Imran Abu Baba, Fanni Tanka, Krisztina Szabo and many others. Thanks for all the good moments you have shared with me, and your support and help when I encountered difficulties.

Last but not least, I would like to deeply thank all my family members. To my parents and my siblings for their strongest support and respect of my own choice. They always stand by my side and believe in me, and their encouragements have inspired me to overcome many difficulties during my stay in Hungary and other countries.